ANTICROSSING STUDIES OF He^+, n = 4

by

Galip Gültekin Tepehan

Thesis submitted to the University of Stirling

for the degree of Doctor of Philosophy

Institute of Atomic Physics
University of Stirling
STIRLING FK9 4LA

July 1980

ABSTRACT

Higher order, S-D and S-F, anticrossing signals induced by a static electric field were investigated to measure the fine structure splittings between magnetic sublevels from S and D and from S and F in the n=4 level He^+. The excited helium ions were produced by electron bombardment parallel to the magnetic field. The signal centres which are shifted by the electric field were extrapolated to the zero field. Effects of experimental parameters like current, excitation voltage and in particular the pressure were investigated.

The following fine structure values were derived from the crossing positions of the signals.

Intervals	Present Experiment (MH_z)	Theory (MH_z) Erickson (1977)
$^4F_{7/2}$-$^4S_{1/2}$	31100.7 ∓ 2.4	31103.84 ∓ 0.04
$^4F_{5/2}$-$^4S_{1/2}$	27438.1 ∓ 3.1	27446.06 ∓ 0.04
$^4D_{5/2}$-$^4S_{1/2}$	27455.8 ∓ 4.6	27459.02 ∓ 0.04
$^4D_{3/2}$-$^4S_{1/2}$	20143.2 ∓ 3.9	20143.27 ∓ 0.04

The electric field necessary to induce the signals causes a shift of the crossing centres and so allowed the measurement of the low field Stark effect of this hydrogenic system. The quadratic Stark effect dominates in most cases and the quadratic Stark constants obtained with about 2% accuracy are in agreement with the theoretical calculation based on the diagonalisation of the energy matrix in combined

electric and magnetic fields.

A theoretical study was made to calculate the signal shape on the basis of the full fine structure system to derive theoretical values of the crossing centres and Stark constant.

To my Mother

ACKNOWLEDGEMENT

I would like to thank Dr J Beyer for his invaluable help and guidance through the course of this work.

I am indebted to Professor H Kleinpoppen for his supervision, overall advice, and continuous interest in the progress of this research.

I would also like to thank all other members of the Institute of Atomic Physics and of the Department of Physics, particularly Dr A J Duncan and Dr A Zaidi for their assistance and useful discussion.

Many other people were involved with the preparation of this work. I would like to thank my fellow students S. M. Khalid, N.A. Malik and H. Seyflu for their useful cooperation; Mr A J Duncan, Mr A D Sherman and Mr T P Young for their excellent work in constructing the apparatus; Mr R Marshall of the University's computing service for his valuable advice; Mrs L North and Mr R Harrison for their assistance on drawings.

I would like to thank Mrs H Queen for the accurate typing of this work.

This research was supported by a study leave from the Science Faculty of Istanbul University and by a grant from the British Council.

TABLE OF CONTENTS

1. INTRODUCTION

The study of single electron atoms has played an important role in the development of quantum mechanics and quantum electrodynamics. Discrepancies between theoretical predictions and experimental results have helped the development and improvement of both experimental methods and theoretical models. The progress made in these works has focussed new interest on fine structure and Stark effect measurements. In the following two sections previous work on the fine structure and the Stark effect is outlined and the purpose of the present study is explained briefly.

1.1. Fine Structure

Until 1947 when Lamb & Retherford discovered that the states $2^2S_{\frac{1}{2}}$ and $2^2P_{\frac{1}{2}}$ in hydrogen were not degenerate but separated by the "Lamb shift", the Dirac theory, which predicts that these levels have the same energy, was widely accepted as a complete description of a one electron atom. Confirmation of the Lamb-Retherford result was obtained by several spectroscopists, but measurements have been carried out up to the present time in order to increase the accuracy to allow better comparison with the theory.

In parallel with the Lamb shift measurements, several experimental techniques have been developed over the past 30 years to measure the fine structure separation of excited atomic states. Precise measurements of fine and hyperfine splittings in short lived excited states of atoms

became possible with the development of the radio frequency (RF) technique by Lamb & Retherford (1947, 1950, 1951), the optical double resonance (ODR) technique by Brossel & Bitter (1952), the level crossing technique by Colegrove, Franken, Lewis & Sands (1959) and the anticrossing technique by Eck, Foldy & Wieder (1963). In all these techniques signals are seen as a result of a coupling between two Zeeman levels. For ODR and RF, this coupling is achieved when a resonant radio frequency field is applied between the two states while for an anticrossing the two crossing levels are coupled by a static interaction. In level crossing experiments on the other hand, coherent excitation of two states results in interference of coherently re-emitted radiation if the separation of the two states is comparable to or less than the natural width.

The He II ($n=4 \rightarrow n=3$, 4686 Å) line complex has undergone a considerable amount of study throughout the development of the understanding of one-electron atoms. Several experimental techniques have been employed, such as optical, radio frequency and anticrossing spectroscopy.

Among the recent optical spectroscopic studies are those of Roesler and Mack (1964), Larson & Stanley (1967) and Berry & Roesler (1970). The optical measurements have suffered from Doppler broadening. To reduce the Doppler width, Larson & Stanley used an atomic beam rather than the more common cooled hollow cathode discharge of Roesler & Mack, but still there was a considerable line width due to recoil from the electron bombardment excitation.

The radiofrequency technique was successfully employed in the experiments of Lea, Levental & Lamb (1966), Hatfield & Hughes (1967), Beyer & Kleinpoppen (1967), Jacobs, Lea & Lamb (1971) and Eibofner (1974, 1976a, 1976b) for the S-P intervals of n=4, He^+. Eibofner (1974) also measured the 4F-4D intervals in which the uncertainty was higher since the signals were weak and broad. All these methods were of $\Delta\ell=1$ electric dipole transitions which the RF method can easily produce but requires very high RF fields to produce $\Delta\ell>1$ multiquantum transitions.

The first observation of higher order signals, between magnetic sublevels of S and D and of S and F of He^+,n=4, were reported by Eck & Huff (1968). They employed anti-crossing technique which provides, in many cases, the same information as obtainable from the radiofrequency method while requiring less sophistication experimentally. Using the same technique Beyer & Kleinpoppen (1971, 1972) measured the intervals 4S-4D and 4S-4F of He^+. The excited states of the He^+ ion were produced by electron impact in a sealed glass system at a pressure of 10 mTorr. Since the system did not allow variation of the He pressure, the accuracy of the measurement was limited by the inability to assess possible pressure effects on the signals. In addition, a 5% uncertainty in the separation of the Stark plates added to the systematic uncertainty of the fine structure and Stark effect measurements.

In the present experiment, the previous system of Beyer & Kleinpoppen was modified by re-designing the vacuum system, including the electron gun and the Stark plates,

to give a better defined and more homogenous electric field over the interaction region and to allow variation of the pressure.

A theoretical study was also made to find the signal shape, the crossing centre and the Stark constant of the anticrossing signals. It was based on the calculation of the intensity of the observed spectral transitions as a function of magnetic field in the vicinity of a suitable crossing of two states when these states are perturbed by a static electric field.

1.2. Stark Effect

The splitting of a spectral line in an electric field was discovered independently by Stark and by Lo Surdo in 1913. Using the canal ray technique, Stark demonstrated considerable splitting of the Balmer lines of the hydrogen atom in electric fields of the order of 10^5 V/cm. When the field strength is reduced spectroscopic investigation becomes difficult to perform, but most recently this method has been used by Gebauer & Selhofer (1970a, 1970b) to observe the Stark effect in the Hβ and Hγ lines of hydrogen with an accuracy of 1%. They have measured the linear Stark effect down to 1.7 kV/cm.

In recent years, the interest has turned to the low field Stark effect encouraged by the development of high resolution spectroscopic methods and by the development of techniques for calculating atomic wave functions and oscillator strengths (by means of computer) which makes it possible to calculate theoretical Stark constants and

compare them with experiments. A detailed discussion of several experimental techniques and theoretical methods may be found in the article by Kollath & Standage (1978).

More recently, the techniques of level crossing, quantum beat and anticrossing have been applied to measure the low field Stark effect of hydrogenic systems. Level crossings have been employed by Kollath & Kleinpoppen (1974) to observe the low field Stark effect in the level n=2 of hydrogen over the electric field range 0-250 kV/m.

Some Stark effect measurements have been carried out by the quantum beat technique. Andrä (1970) used this method to investigate the Stark effect in n=2 of H in an electric field range from 100 to 400 V/cm and obtained agreement with theory. Employing the same technique, Bourgey, Denis & Desesquelles (1977) have more recently observed the Stark effect in He^+, n=4, for an electric field range between 300 V/cm and 900 V/cm. They compared the results with the calculation of the first order Stark perturbation taking the fine structure and the Lamb shift into account and agreement was reached within the limits of 5% experimental accuracy.

Another way to study the low field Stark effect is the anticrossing technique. A static electric field, either used to induce the signals or applied in addition where the signal is induced by another perturbation, causes a Stark shift of the crossing position. For the hydrogenic system, the observed Stark shifts can be compared with theoretical values obtained by numerical diagonalisation of the energy matrix with combined Zeeman

and Stark effect. Beyer, Kleinpoppen & Woolsey (1973) have used the S-D and S-F anticrossing signals to measure the Stark effect in the level n=4 of He^+ in the electric field range 0-215 V/cm. Experimental results and theory agreed in most cases within the experimental errors of between 10-15%. Since the experiments were carried out in a sealed glass system at a fixed pressure of 10 mTorr, no pressure effect on the Stark constant could be observed. Together with the 5% uncertainty of the separation of the Stark plates, the error of the observation increases by a considerable amount.

The design of the present system made it possible to investigate the Stark effect at various pressures with a more precise set of Stark plates.

2. THE EXPERIMENTAL METHOD

In the present experiment, higher order ($\Delta\ell>1$) electric field induced anticrossing signals have been detected from the n=4 states of He^+. Such anticrossing signals are observed as an intensity or polarisation change in the transition line complex from n=4 to n=3 at 4686 Å, when the magnetic field is varied through appropriate crossings with a static electric field applied perpendicular to the magnetic field. The excited states of n=4 are produced by electron impact excitation, and a monochromator or an interference filter is used to isolate the lines. The data have been collected as a function of the electric field (0-210 V/cm), the gas pressure (2-15 mTorr), the excitation energy (250-350V) and the excitation current (150-500 μA).

Fig.1 shows the fine structure and the Zeeman splitting of the n=4 state of He^+ in a magnetic field alone. Some of the states are prevented from crossing when a suitable electric field is applied perpendicular to the magnetic field. As illustrated in fig.2, the levels repel one another and the wave function of two states interchange their identities as the magnetic field is varied through the region of close approach. At the magnetic field strength corresponding to closest approach the wave function of each state is a 50-50 mixture of the wave functions of the uncoupled states. If the uncoupled states have different population, a change in the light emission is observed due to this state mixing.

2. THE EXPERIMENTAL METHOD

In the present experiment, higher order ($\Delta\ell>1$) electric field induced anticrossing signals have been detected from the n=4 states of He^+. Such anticrossing signals are observed as an intensity or polarisation change in the transition line complex from n=4 to n=3 at 4686 Å, when the magnetic field is varied through appropriate crossings with a static electric field applied perpendicular to the magnetic field. The excited states of n=4 are produced by electron impact excitation, and a monochromator or an interference filter is used to isolate the lines. The data have been collected as a function of the electric field (0-210 V/cm), the gas pressure (2-15 mTorr), the excitation energy (250-350V) and the excitation current (150-500 μA).

Fig.1 shows the fine structure and the Zeeman splitting of the n=4 state of He^+ in a magnetic field alone. Some of the states are prevented from crossing when a suitable electric field is applied perpendicular to the magnetic field. As illustrated in fig.2, the levels repel one another and the wave function of two states interchange their identities as the magnetic field is varied through the region of close approach. At the magnetic field strength corresponding to closest approach the wave function of each state is a 50-50 mixture of the wave functions of the uncoupled states. If the uncoupled states have different population, a change in the light emission is observed due to this state mixing.

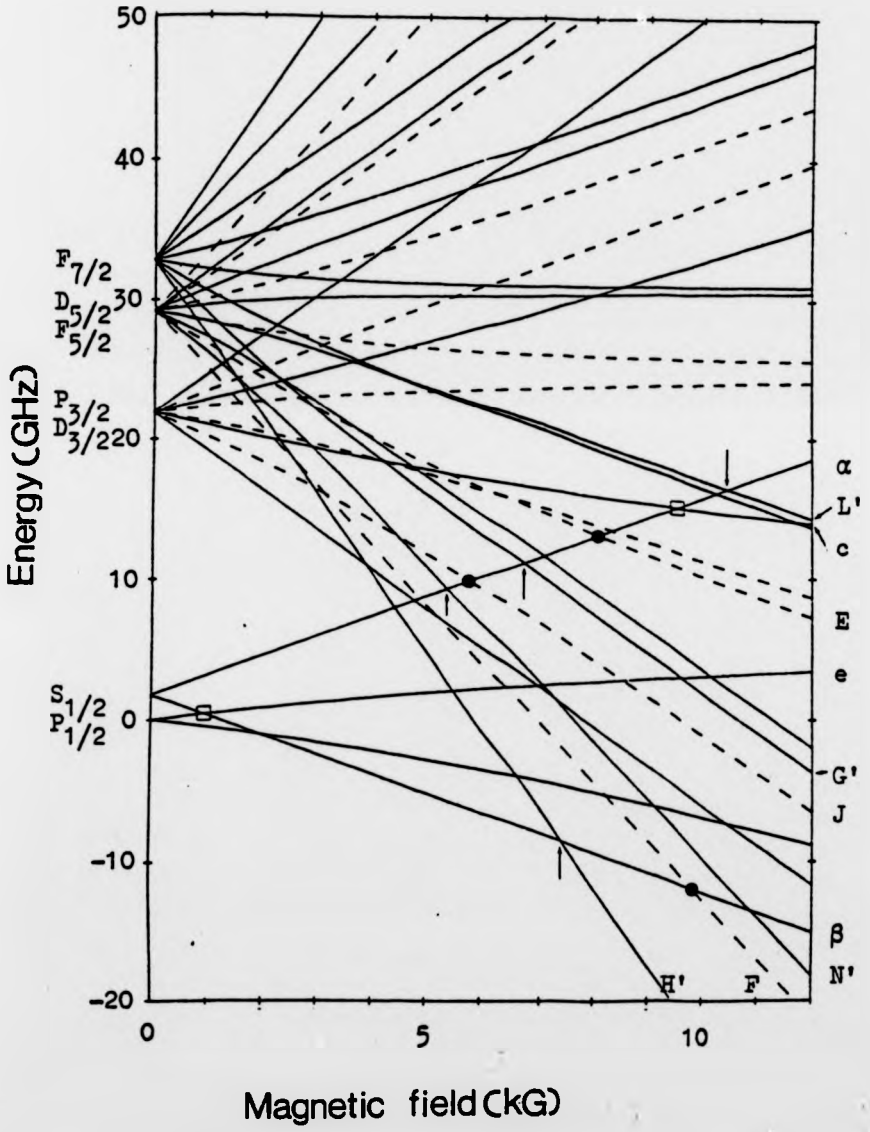

Fig.1: (Fig.3 of Eck & Huff 1967): The fine-structure and Zeeman effect of the n=4 term of He^+. The D sublevels are shown as dashed lines and the S,P, and F sublevels as solid lines. The anticrossings occurring between S and P, S and D, and S and F are marked by squares, circles and arrows respectively.

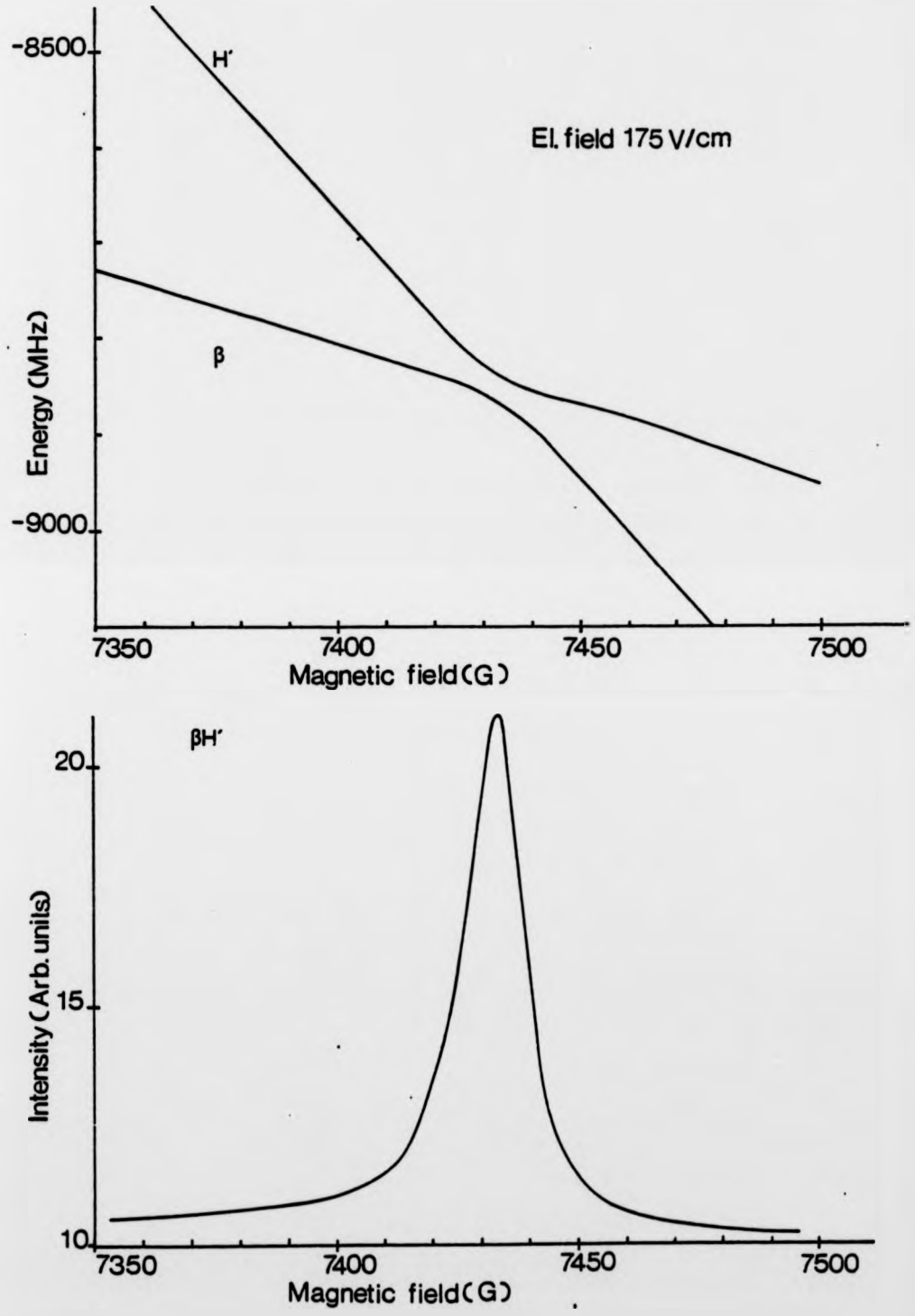

Fig.2: The anticrossing of the states β and H' and the corresponding βH' signal as a function of magnetic field at the electric field of 175 V/cm ($E \perp H$). The $P_{\frac{1}{2}}$ state is taken as the zero point of the energy in the top diagram. The signal in the bottom diagram is calculated using equation 3.16 of sec.3.2.4. Lamb's notation of the sublevels is used. See Appendix 3 for the explanation.

The S,P,D and F states of He^+, n=4, are unequally populated because of different lifetimes (Roesler & Mack 1964) and different production cross sections (Sutton & Kay 1974). Thus the populations of these states are re-adjusted due to the electric field induced state mixing in the vicinity of appropriate crossings. The population of the S states is much higher than that of the P,D and F states, therefore any anticrossing between S and the other states will result in less decay through S states and more decay through the other states. Only the 4686Å (n=4 → n=3) line is detected, and according to the branching ratios shown in fig.3 such a change in the decay results in a net transition gain or loss of this line when the state mixing occurs.

The electric field necessary to induce the signals also affects the crossing positions by Stark interaction, and therefore the measured crossing positions are extra-polated to zero electric field for an accurate determination of the fine structure separation. This also made it possible to investigate the low field Stark effect.

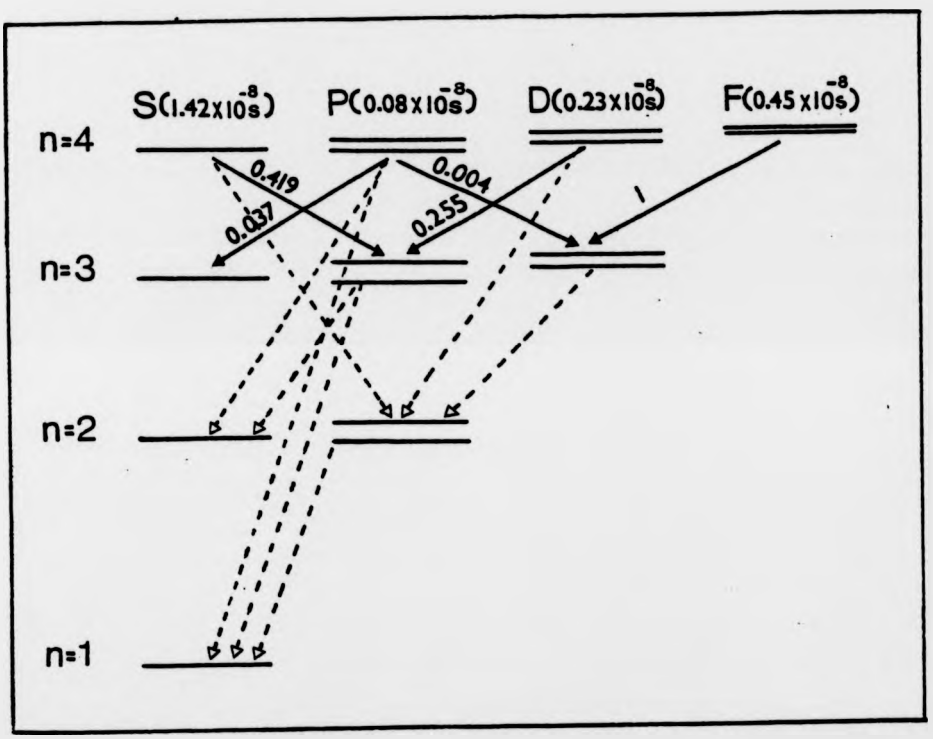

Fig.3: The levels and branching ratios for singly ionised helium up through n=4. The arrows with a solid line show the observation line 4686Å. The numbers on them are the relative probability for an excited state to decay through this channel (Bethe & Salpeter 1968). Note that the diagram is not drawn to scale.

3. THEORY

The energies of sublevels of atomic excited states, in an external magnetic field, depend on the strength of this field. At certain values of the field sublevels may cross, and some of these crossings can be located by measuring the intensity of the fluorescent radiation emitted in a particular direction as a function of magnetic field. These measurements are referred to as the crossing (Colegrove, Franken, Lewis & Sands 1959) and anti-crossing technique (Eck et al 1963). In both methods the spectroscopic resolution is determined by the natural width of the emitting states. In the level crossing technique the observed signal is the result of interference in the decay from the two crossing Zeeman levels. In the anticrossing technique, on the other hand, a static internal or external perturbation is required to induce a signal. Since no coherence is required in the excitation or decay channels, anticrossing signals occur in many experimental situations for which there would be no signals from a normal level crossing. Anticrossing signals were first observed by Eck, Foldy and Wieder (1963) during a level crossing investigation of the fine and hyperfine structure of the 2^2P term of Lithium. Later a theory was developed by Wieder & Eck (1967) describing level crossings and anticrossing signals in a combined equation. Glass-Maujean & Descoubes (1978) derived an equivalent equation

using the density matrix formalism. The signals, in both calculations, are the result of direct coupling between the two sublevels. Beyer (1973) calculated the crossing positions independently of the theory of the anticrossing signal (Wieder & Eck (1967), using two different methods. In the first method the Zeeman and Stark effects were treated independently. It was based on the assumption that a small electric field has little influence on the energy of the magnetic substates. Only such substates, which couple directly with either of the crossing substates by dipole interaction, were considered. This reduced the number of substates contributing to the shift of each anticrossing signal. This approach represented a good approximation for electric fields below 150 V/cm (See fig.32b). At larger electric fields when the Stark energies become comparable with the Zeeman energies, this method was considered to be less adequate.

A second calculation was made with a combined treatment of the Zeeman and Stark effect. Using the time independent approach, the energy matrix of the full fine structure system of n=4 was diagonalised applying electric and magnetic fields simultaneously. This method does not give the exact position of the energy eigenvalue of the intersecting Zeeman substates near their closest approach, especially when the interaction energy, V, is less than or equal to the energy corresponding to one quarter of the differences between the line widths (i.e. $V = \frac{1}{4}|\gamma_a - \gamma_b|$ where γ_a, γ_b are the widths of the corresponding substates)(Lamb 1952). Below this

critical energy the sublevels, which are supposed to cross in the time dependent approach, do not cross in this approach. Nevertheless, using the time independent matrix diagonalisation, the Stark shift and the crossing centres of the signals can be derived very accurately by finding the closest distance of the two anticrossing states. Moreover, the interaction element V_{ab}, derived from this calculation can be used in Wieder & Eck's theory to calculate the width and the degree of saturation of the signals.

Since in the time independent diagonalisation of the energy matrix the eigenvalues do not contain information about the lifetimes of the states, the full line shape of the anticrossing signals could not be calculated by this method.

In the present work, the energy matrix of the full fine structure system was diagonalised using the time dependent approach. Since the imaginary parts of the energy eigenvalues represent the lifetimes of the states at the corresponding electric and magnetic fields, this method made it possible to calculate not only the crossing centre and the Stark shift but also the shape of the anti-crossing signal. For a better approximation of the Stark shift all 32 substates of the fine structure system were again included since a number of substates, having little or no effect on the crossing centre, may still contribute to the Stark shift of the crossing position.

In the following section the anticrossing signals derived by Wieder & Eck and the present derivation using

the full fine structure system are described.

3.1. Theory of Crossing Signals Based on a Two Level System

The theory presented in this section follows that given by Wieder & Eck (1967).

Consider the resonance fluorescence intensity of two states $|a\rangle$ and $|b\rangle$ in the vicinity of their crossing. The states $|a\rangle$ and $|b\rangle$ are eigenstates of the Hamiltonian H_o with eigenvalues $\hbar w_a$ and $\hbar w_b$. Let H' be the time independent perturbation Hamiltonian coupling the states $|a\rangle$ and $|b\rangle$. The damping of the states is taken into account by introducing an operator H_D whose matrix is diagonal with elements $-i\hbar \frac{\Gamma_a}{2}$ for $|a\rangle$ and $-i\hbar \frac{\Gamma_b}{2}$ for $|b\rangle$ ($\Gamma = \frac{1}{\tau}$, where τ is the mean lifetime of the state).

Let $|t\rangle$ be the state of the atom at time t. The wave function of the atom can be found by solving the Schrödinger equation of motion.

$$i\hbar \, (d|t\rangle/dt) = (H_o + H_D + H')|t\rangle \qquad (3.1)$$

Equation 3.1 was solved by Eck & Wider (1967) and the following steady state anticrossing signal, expressed as a function of $\Delta\nu$ (the frequency separation between levels a and b) was found:

$$S = \underbrace{(1/\gamma_a) \; \Sigma \, \{ |f_a|^2 |g_a|^2 \}}_{1} + \underbrace{(1/\gamma_b) \; \Sigma \, \{ |f_b|^2 |g_b|^2 \}}_{2} + \underbrace{(\gamma_a\gamma_b/\gamma D) \; \Sigma \{ f_a f_b^* g_a g_b^* + f_a^* f_b g_a^* g_b \}}_{3}$$

$$- \underbrace{(i\gamma_a\gamma_b\Delta\nu/\bar{\gamma}^2 D)\ \Sigma\ \{f_a f_b^* g_a g_b^* - f_a^* f_b g_a^* g_b\}}_{4}$$

$$- \underbrace{(2|V|^2\gamma_a\gamma_b/\bar{\gamma}D)\ \Sigma\ \{fg\}}_{5}$$

$$+ \underbrace{(2/\bar{\gamma}D)\ \Sigma\ \{(V^* f_a f_b^* + V f_a^* f_b)(V g_a g_b^* + V^* g_a^* g_b)\}}_{6}$$

$$+ \underbrace{(\Delta\nu\gamma_a\gamma_b/\bar{\gamma}^2 D)\ \Sigma\ \{f(V g_a g_b^* + V^* g_a^* g_b) + g(V^* f_a f_b^* + V f_a^* f_b)\}}_{7}$$

$$+ \underbrace{(i\gamma_a\gamma_b/\bar{\gamma}D)\ \Sigma\ \{f(V g_a g_b^* - V^* g_a^* g_b) + g(V^* f_a f_b^* - V f_a^* f_b)\}}_{8} \qquad (3.2.)$$

where

$$D = \gamma_a\gamma_b + |2V|^2 + (\gamma_a\gamma_b/\bar{\gamma}^2)\Delta\nu^2,\ \omega = \omega_a - \omega_b = 2\pi\ \Delta\nu$$

$$\Delta\nu = \frac{1}{2\pi}(\omega_a - \omega_b) \qquad \gamma_a = \frac{\Gamma_a}{2\pi} = \frac{1}{2\pi\tau_a},$$

$$\Gamma_a = 2\pi\gamma_a, \Gamma_b = 2\pi\gamma_b,\ \bar{\gamma} = \tfrac{1}{2}(\gamma_a + \gamma_b)$$

$$f = (|f_a|^2/\gamma_a) - (|f_b|^2/\gamma_b),\ g = (|g_a|^2/\gamma_a) - (|g_b|^2/\gamma_b)$$

V is the matrix element of the state interaction which couples states a and b. γ_a and γ_b are the natural widths in frequency units. The summation symbol Σ means that the quantity within the bracket is to be summed over all relevant levels m of the initial state and m' of the final state. The symbol f_a is an abbreviated notation for $f_{am} \equiv \langle a|\vec{f}.\vec{r}|m\rangle$, the electric dipole matrix element for excitation to state a from state m, and $g_a = g_{m'a} \equiv \langle m'|\vec{g}.\vec{r}|a\rangle$, is the matrix element for spontaneous decay from state a to state m', $\vec{f}$ and $\vec{g}$ is the polarisation vector of the exciting and emitted light respectively.

The first two terms in the expression (3.2) represent the non-resonant background scattering from the states |a> and |b>. The third and fourth terms describe the level crossing signal corrected for the perturbation V. The observation of a signal based on these terms requires coherence in both the excitation and detection channels of the experiment.

The fifth term of equation (3.2) represents the pure anticrossing signal which does not require coherence in either the excitation or detection processes.
If the excited sublevels are equally excited and populated or $\Gamma_a = \Gamma_b$ then the anticrossing signal vanishes. It vanishes also when the sublevels have equal radiation rates, i.e. $\sum_m |g_a|^2/\gamma_a = \sum_m |g_b|^2/\gamma_b$. The last three terms of equation (3.2) represent mixed level crossing and anticrossing signals. Term 6 requires coherence in both excitation and decay, and terms 7 and 8 require coherence at least in one step.

If $\gamma_a = 0$ or $\gamma_b = 0$, i.e. if one of the sublevels is non-radiative, no level crossing or anticrossing occurs. When there is no perturbation the last four terms vanish and only the level crossing signal with the non-resonant background remains.

3.1.1. The Anticrossing Signal

When coherence is absent in both the excitation and the detection processes, only the anticrossing (term 5) and the background signals are left.

The anticrossing signal, as a function of separation

$\Delta\nu$ of the undisturbed sublevels $|a\rangle$ and $|b\rangle$, based on the equation (3.2) is represented by an absorption Lorentzian curve centered at $\Delta\nu = 0$ (Beyer & Kleinpoppen 1978)

$$S(\Delta\nu) = d \frac{A}{1 + \Delta\nu^2/B^2} \quad \ldots \quad (3.3)$$

where d takes account of instrumental parameters for intensity and spectral distribution of the resonance lamp, aperture of light detector etc. A is the amplitude and 2B is the full width at half-maximum:

$$A = \frac{(\Sigma_m, |g_a|^2/\gamma_a - \Sigma_m, |g_b|^2/\gamma_b)(\Sigma_m |f_a|^2/\gamma_a - \Sigma_m |f_b|^2/\gamma_b)|2V_{ab}|^2}{(\gamma_a+\gamma_b)(1+|2V_{ab}|^2/\gamma_a\gamma_b)} \quad \ldots \quad (3.4)$$

$$2B = (\gamma_a+\gamma_b)(1+|2V_{ab}|^2/\gamma_a\gamma_b)^{\frac{1}{2}} \quad \ldots \quad (3.5)$$

where V_{ab} is the matrix element of the static interaction which couples states $|a\rangle$ and $|b\rangle$; $\sum_m, |g_a|^2/\gamma_a = \sum_m, |\langle m'|\vec{g}.\vec{r}|a\rangle|^2/\gamma_a$ is the branching ratio of the state $|a\rangle$ in the decay to the selected states m'; $\sum_m |f_a|^2/\gamma_a = \sum_m |\langle a|\vec{f}.\vec{r}|m\rangle|^2/\gamma_a$ is the steady state population of the state $|a\rangle$ excited from the states m. In the present experiment atoms are excited by electron impact excitation and $\Sigma|f_a|^2$ and $\Sigma|f_b|^2$ are replaced by the excitation rates r_a and r_b respectively.

3.1.2. Mixed Level Crossing-anticrossing Signals

As pointed out in 3.1, terms 7 and 8 of equation (3.2) require coherence at least in one of the steps, either in excitation or decay. Some S and D sublevels of the hydrogenic system can decay to common lower nP sublevels and

interference may thus take place if S and D substates are brought into coincidence by the application of magnetic and electric fields. This was observed for the S-D anticrossings of the present study (See sec.5.4). The interference part can be excluded if the observation condition is chosen in such a way that decay can take place to a common sublevel.

3.2. Theory of Crossing Signals Based on the Full Fine Structure System

The calculation of anticrossing signals using the diagonalised energy matrix of the full fine structure system is essentially an evaluation of the strength of the transition line complex from a higher state to a lower state when the excited states are perturbed by external magnetic and electric fields. In the following sections the setting up of the working Hamiltonian, the result of the diagonalisation of the time dependent energy matrix and the derivation of the anticrossing signal will be discussed.

3.2.1. Working Hamiltonian

The high field n,ℓ,mℓ,ms-representation (Condon & Shortley 1970) was used to set up the energy matrix of the full fine structure system (32 x 32 for n=4). The spin orbit interaction, magnetic field and electric field were treated simultaneously and a damping Hamiltonian H_D, whose matrix is diagonal with elements $-i\hbar\Gamma_{j/2}$ (where $\Gamma_j = \frac{1}{\tau_j}$ is the lifetime of the $_j$th state), was introduced to treat radiative decay. The effective Hamiltonian is written as

$$H = H_{s.o} + H_M + H_E + H_D \qquad (3.6)$$

where $H_{s.o}$, H_M, H_E and H_D are the spin orbit, the magnetic field and the electric field interaction and H_D is the damping Hamiltonian.

3.2.1.1. Spin Orbit and Magnetic Field Interaction

The spin orbit interaction arises from the fact that the spin magnetic moment interacts with the magnetic field produced by the motion of a charged particle. In the high field representation, the Hamiltonian of the spin orbit interaction contains diagonal and off diagonal elements. Off diagonal elements cause the mixing of the basis vectors. The matrix was set up in such a way that diagonalisation in zero field gives the fine structure of the atomic system. Since the Lamb shift is not included in the $H_{s.o}$, the fine structure energy values, taken from Erickson (1977), were incorporated into the matrix.

The Hamiltonian, H_M, in the high field representation is based on the assumption that the spin orbit coupling is small compared to the magnetic field splitting (Paschen-Back effect). The Hamiltonian is diagonal in the high field representation.

A correction was applied to g_ℓ, to account for the effect of the motion of the nucleus. Lamb (1952) showed that the electrons' contribution to the angular momentum, and hence to the orbital term in the Zeeman effect is reduced by the factor $\frac{M}{m+M} \approx 1 - \frac{m}{M}$, where M is the nuclear

mass and m the electron mass. The relativistic effect and the quadratic Zeeman effect are less then 0.2 MHz at around 7 kG (Bethe & Salpeter 1977) and are thus too small to require a correction.

The matrix elements corresponding to $H_{s.o}$ and H_M are (Condon & Shortley 1970, Beyer 1973):

$$\langle n\ell m_\ell m_s | H_{s.o} + H_M | n\ell m'_\ell m'_s \rangle = \langle n\ell m'_\ell m'_s | H_{s.o}+H_M | n\ell m_\ell m_s \rangle$$

$$= \{W_{j=\ell-\frac{1}{2}} + \frac{\Delta W}{2\ell+1}(\ell+1+2m_\ell m_s) + \mu_B H(g_\ell m_\ell + g_s m_s)\}\delta_{m\ell\, m'_\ell}\delta_{m_s\, m'_s}$$

$$+ \frac{\Delta W}{2\ell+1}\sqrt{(\ell-m+1/2)(\ell+m+1/2)}\,\delta_{m'_\ell\, m\ell\pm1}\delta_{m_s\, m_s\pm1} \qquad (3.7)$$

where $m = m_s + m_\ell$, W is the energy of the fine structure level at zero magnetic field corresponding to $j = \ell - \frac{1}{2}$. ΔW is the fine structure separation between the sublevels corresponding to $j = \ell + \frac{1}{2}$ and $j = \ell - \frac{1}{2}$. H is the magnetic field in z-direction and μ_B is the Bohr magneton. $g_\ell = 1 - \frac{m}{M}$ and $g_s = 2\frac{\mu_e}{\mu_B}$ (μ_e is the magnetic moment of the electron).

3.2.1.2. Electric Field Interaction

The presence of an electric field gives rise to displacements of the fine structure energy levels (Stark effect). When a uniform electric field of strength E is applied, an additional term

$$H_E = \vec{E}.\vec{er} \qquad (3.8)$$

occurs in the Hamiltonian where $\vec{er}$ is the operator of the electric dipole moment. Using equation 60.11 and 63.5 in Bethe & Salpeter (1977), the matrix elements are obtained as:

$$\langle n\ell m_\ell m_s | \vec{E}.\vec{er} | n\ell+1 m'_\ell m_s \rangle = \langle n\ell+1 m'_\ell m_s | \vec{E}.\vec{er} | n\ell m_\ell m_s \rangle$$

$$= \frac{3}{2}\frac{n}{Z}\sqrt{n^2 - (\ell+1)^2}\sqrt{\frac{(\ell+1)^2 - m_\ell^2}{(2\ell+3)(2\ell+1)}}\,\delta_{m'_\ell\, m_\ell} ea_o Ez$$

$$\mp \frac{3}{4}\frac{n}{Z}\sqrt{n^2 - (\ell+1)^2}\sqrt{\frac{(\ell\pm m_\ell+2)(\ell\pm m_\ell+1)}{(2\ell+3)(2\ell+1)}}\,\delta_{m'_\ell m_\ell \mp 1} ea_o Ex$$

where a_o is the Bohr radius.

3.2.3. Matrix Diagonalisation

A computer subroutine (NAG.F02AKF) was used to diagonalise the non-Hermitian complex matrix described above. These time dependent results may be compared with the time independent results obtained from diagonalisation of the real part of the matrix (excluding the damping elements). A comparison of the time dependent and time independent eigenvalues of α and G' substates near the αG' crossing is shown in fig. 4 for an electric field of 50 V/cm perpendicular to the magnetic field. It can be seen from the figure that the sublevels do cross in the time dependent but not in the time independent approach. Lamb (1952) had shown for a two level system that, in the time dependent treatment the crossing of the sublevels is not removed until the electric field interaction energy is greater than the energy corresponding to a quarter of the difference between the line widths ($|V_{ab}| < \frac{1}{4}|\gamma_a - \gamma_b|$). This may not hold exactly for the crossings considered in the present work, since the substates contain some admixture from the other substates. For example, a small amount of P admixture in S states causes a considerable lifetime decrease of the S states.

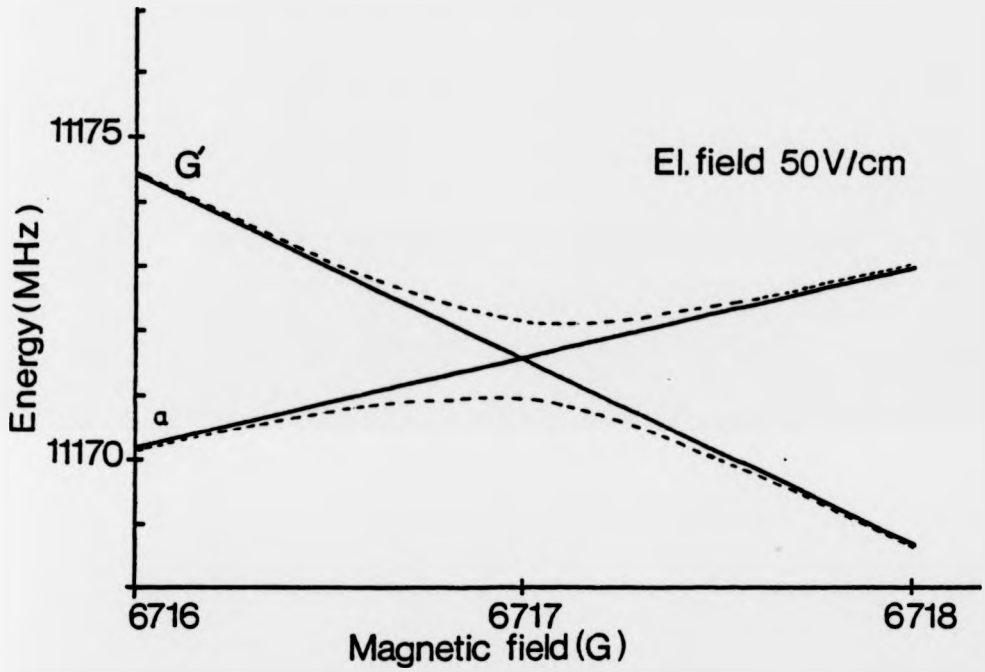

Fig. 4: Energy eigenvalues of the states α and G' of He^+, n=4 as a function of magnetic field. The solid line represents the values in the time dependent, the dashed lines those in the time independent approach. The $P_{\frac{1}{2}}$ state is taken as the zero point of the energy scale.

Fig.5 shows the energies of the βH' crossing at and near their crossing points for various electric field values. The crossing of the sublevels is removed at around 130 V/cm which is slightly less than the calculated value of 132.5 V/cm.

Since only the electric dipole interaction elements were included in the energy matrix, the results of the diagonalisation show that states differing in ℓ by more than 1 can be coupled through one or more intermediate states, each step being governed by the appropriate dipole selection rules. The admixture of these intermediate states can be seen in the eigenvector components of the coupled states.

As stated earlier, the imaginary part of the energy eigenvalue gives the lifetime of the eigenstate. Fig.6 and 7 shows the two anticrossing levels β and H' and their lifetimes as a function of magnetic field at electric fields of 175 V/cm and 50 V/cm. At 175 V/cm, the lifetimes of the two anticrossing states become equal when the separation of the two sublevels are minimum. At 50 V/cm, on the other hand, the lifetimes have a minimum at the crossing point of the sublevel but do not become equal.

3.2.4. Calculation of the Anticrossing Signal

The anticrossing signals depend on the population of the states and for the mixed level-crossing-anticrossing signal also on the coherence induced by the static perturbation between the crossing states. The shape of the signal can be obtained if the intensity of the observed

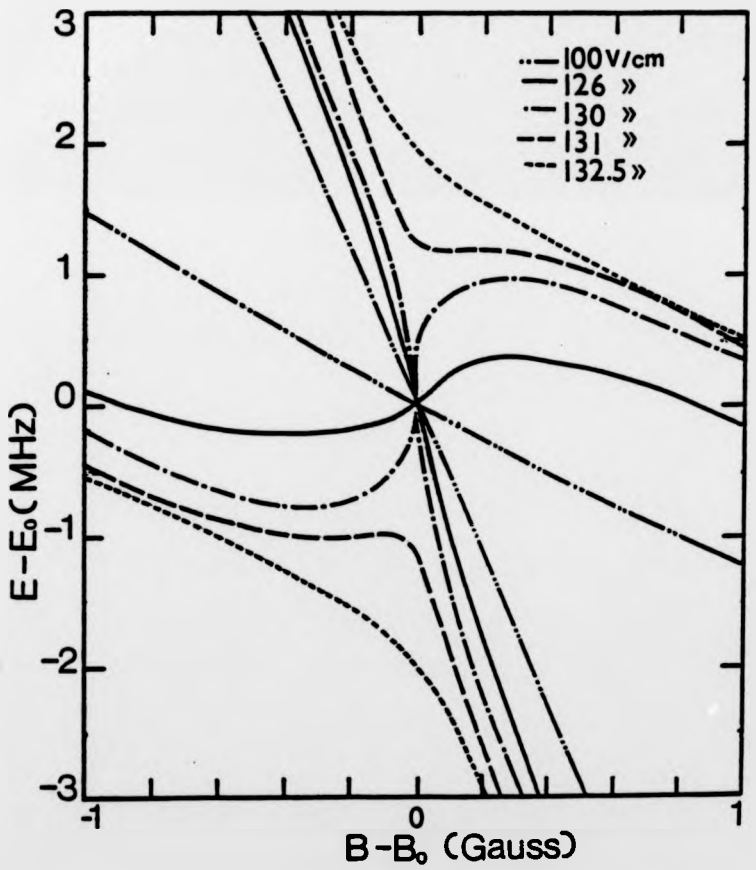

Fig. 5: Energy eigenvalues of the states β and H' of He^+, n=4 near their crossing for various values of electric field strength. The crossing centres which would be shifted by the electric field are normalised to B_o. The calculation was made by diagonalising the time dependent energy matrix of the full fine structure system with combined electric and magnetic fields.

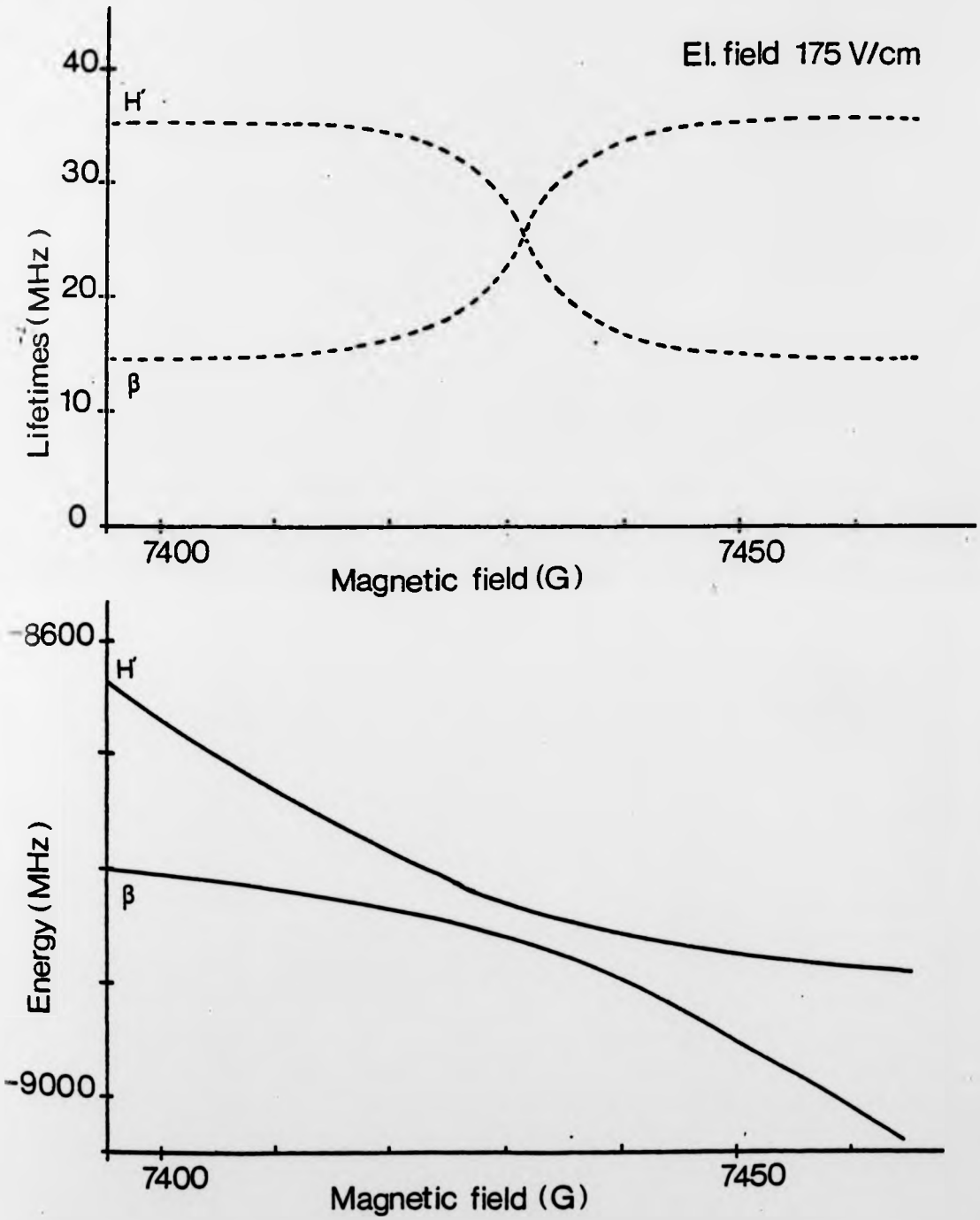

Fig. 6: The lifetimes and the energy eigenvalues of the two anti-crossing states β and H' as a function of the magnetic field at an electric field of 175 V/cm. The lifetimes of the states are equal at the minimum separation of the sublevel. The $P_{\frac{1}{2}}$ state is taken as the zero point of the energy scale.

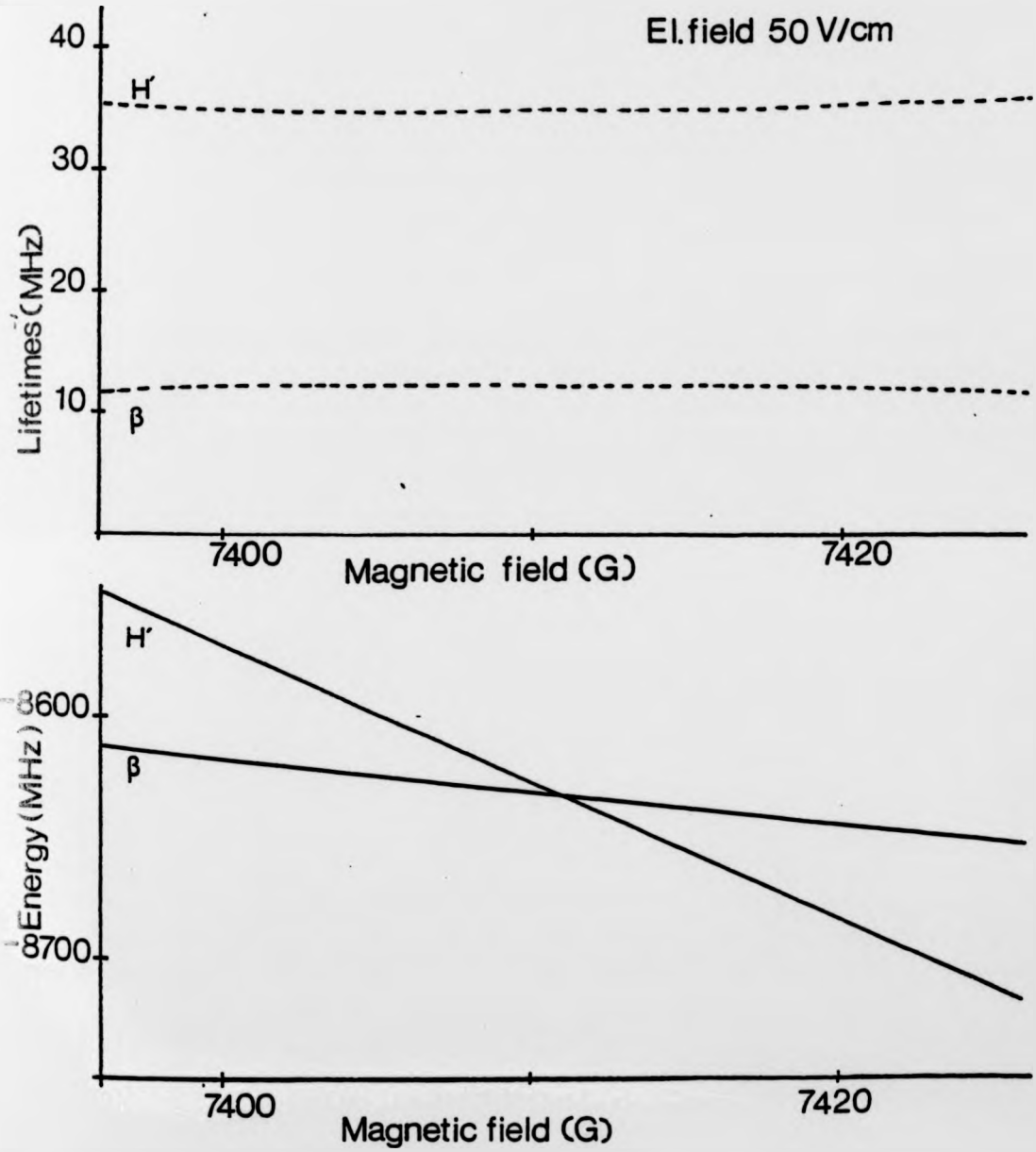

Fig. 7: The lifetimes and the energy eigenvalues of the β and H' as a function of the magnetic field at an electric field of 50 V/cm. The difference of the lifetimes has a minimum at the magnetic field value where the energies cross. The $P_{\frac{1}{2}}$ state is taken as the zero point of the energy scale.

spectral transitions is calculated as a function of magnetic field in the vicinity of a suitable crossing of two substates, when these substates are perturbed by a static electric field.

The emitted light intensity from state $|a\rangle$ to state $|b\rangle$ is proportional to

$$|\vec{e}_o\langle a|\vec{er}|b\rangle|^2 \qquad (3.10)$$

where $\vec{er}$ is the operator of the electric dipole moment of the atom and $\vec{e}_o$ is the unit vector of the polarisation of the photon.

Usually either of two directions of the propagation are chosen for the observation when the Zeeman components of spectral lines are investigated; one along the magnetic field direction (z-axis) and the other perpendicular to the field direction. In the first case the propagation vector, $\vec{k}$, is directed along the z-axis and the polarisation vector, $\vec{e}$, lies in the x-y-plane. The light is propagated with a right (transition $\Delta m=1$) and left circular polarisation ($\Delta m=-1$).

The intensity of right-and left-polarised circular (σ) light, in general, is respectively proportional to (Condon & Shortley 1970, p97):

$$\sum_{m_\ell} \tfrac{1}{2}|\langle n\ell m_\ell m_s|\vec{er}|n'\ell' m_\ell+1\ m_s\rangle|^2(1+\cos^2\theta), \quad (\Delta m=1) \qquad (3.11)$$

$$\sum_{m_\ell} \tfrac{1}{2}|\langle n\ell m_\ell m_s|\vec{er}|n'\ell' m_\ell-1\ m_s\rangle|^2(1+\cos^2\theta), \quad (\Delta m=-1) \qquad (3.12)$$

where θ is the angle between the z-axis and the direction of observation.

The π light is polarised along the z-axis but also observed in the direction perpendicular to $\vec{H}$. The general equation for the intensity of this component is proportional

to

$$\sum_{m_\ell} |\langle n\ell m_\ell m_s|\vec{er}|n'\ell' m_\ell m_s\rangle|^2 \sin^2\theta, \quad (\Delta m=o) \qquad (3.13)$$

The eigenstates, which specify the energy eigenvalues of the system when the electric and magnetic fields are on, are superpositions of the basis states ($n\ell m_\ell m_s$ in the present case). Hence, to obtain the decay amplitude of a transition from any of these composite states, one has to calculate the dipole transition element for each basis state in the mixture and multiply it with the normalised eigenvector components corresponding to the composite state. Therefore the decay amplitude is equal to

$$\sum_{\substack{jk \\ m}} \langle m|\vec{er}|j\rangle\langle j|U|k\rangle \qquad (3.14)$$

where j is the basis state in $n\ell m_\ell m_s$ representation, k is the superposition state after the interaction with the fields, m the lower state to which the atom decays and $U = e^{iE_k t - \frac{\gamma_k t}{2}}$ is the energy operator.

In the intensity calculation, first the coherence between the crossing states will be neglected so that the population of each state can be defined separately.* To find the population of the eigenstate, the excitation cross-section of the pure state, f_ℓ^2, should be multiplied by the modulus squared of the corresponding eigenvector components of the superposition state, as was done in the case of the decay amplitudes. Therefore, the steady state population is equal

---

*Although there is still coherence between components within each superposition state.

to

$$P_k = \sum_j \frac{f_j^2 |\langle k|U|j\rangle|^2}{\gamma_k} \qquad (3.15)$$

where j is the basis state, k is the composite state and γ_k is the lifetime of the composite state.

The intensity is then proportional to

$$I \propto \sum_k P_k \left| \sum_m \sum_j a_j^k \langle m|e\vec{r}|j\rangle \right|^2 \qquad (3.16)$$

where k is the superposition state, j is the basis state, m is the lower state and a_j^k is the eigenvector component ($\langle k|U|j\rangle$).

The anticrossing signals of He^+,n=4 were calculated by using formula (3.16). Fig. 8 and 9 show the calculated signals for the αG' and βF crossings. In both cases, the intensity is calculated for the direction of light emission used in the experimental observation (i.e. $E \perp H_\perp$ observation). The shapes of the signals for σ, π and unpolarised light are in agreement with the experiment (see fig. 9 and 18 for a comparison of the experimental and the theoretical shapes of βF signal). The signals were computer fitted to a Lorentzian function (also used for the experimental results) in which the crossing centre, the width and the relative amplitude were calculated. The results are compared with the calculation of Beyer (1973) and with the present experimental work. As stated before, Beyer used the time independent approach for the calculation. In that calculation, the point of closest approach of the two anticrossing states represented the crossing centre of the signal and the state separation at this point the interaction matrix element of the coupling state. This matrix element was used in formulas 3.4 and 3.5

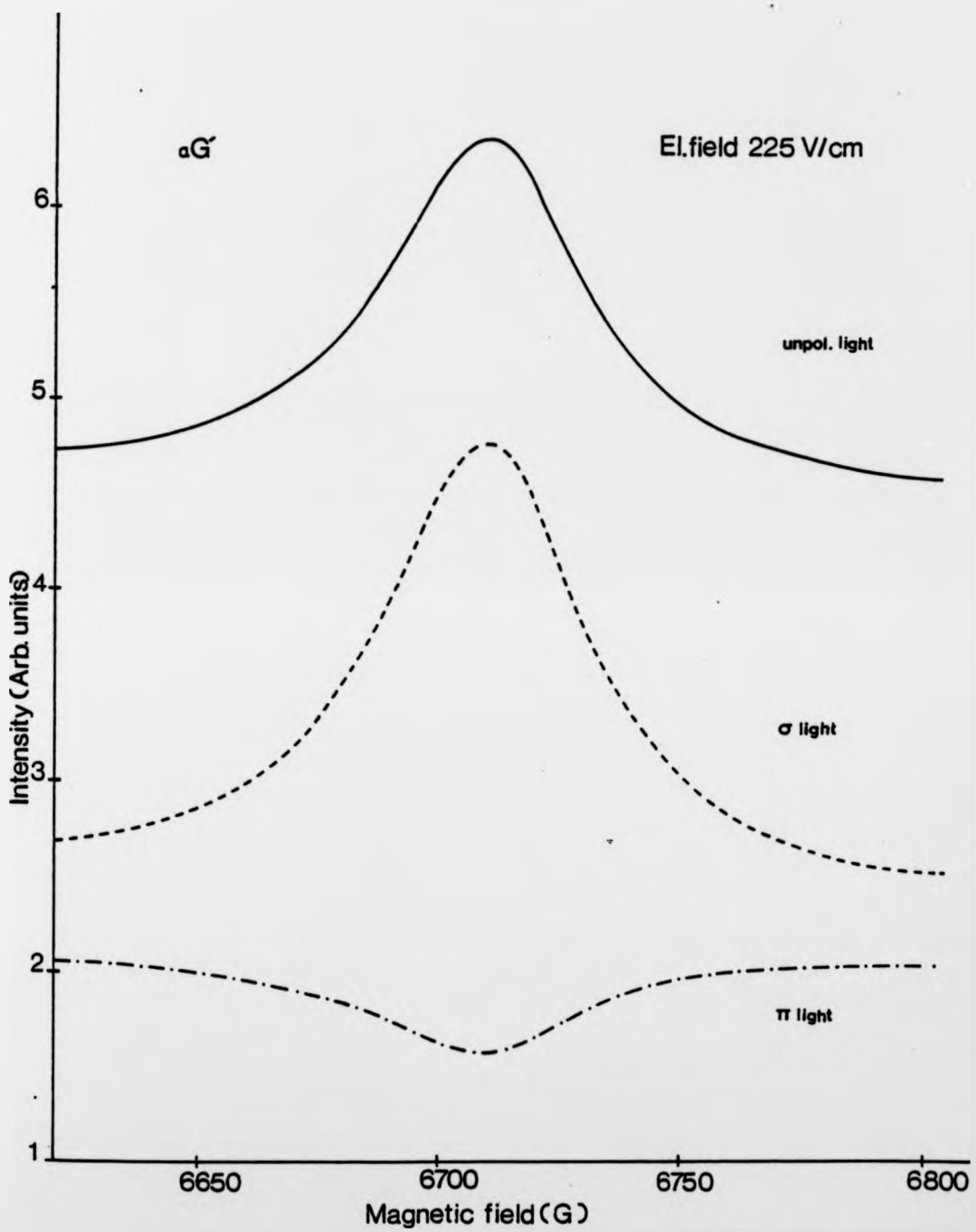

Fig. 8: The S-F anticrossing signal αG' calculated with the formula 3.16 using σ, π and unpolarised light. The following cross sections in ($10^{-21}cm^2$) were used for simultaneous electron impact ionisation and excitation of He to He^+; 4S:8.1 4P:2.9, 4D:0.68 and 4F:0.01 (Sutton & Kay 1973).

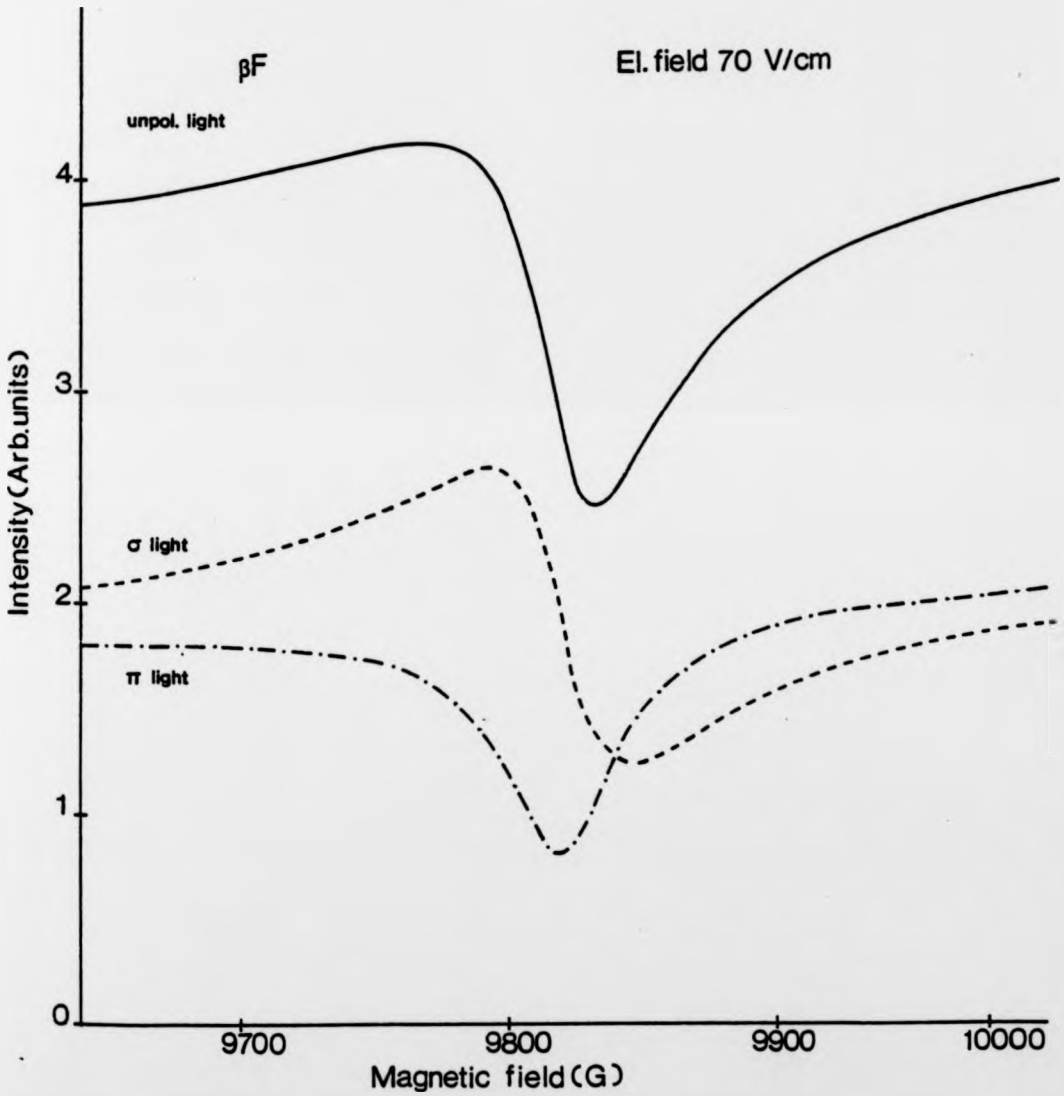

Fig. 9: The S-D anticrossing signal βF calculated according to the formula 3.16 using σ, π and unpolarised light. See fig.18, for a comparison with the experimental observation.

to find the degree of saturation and the width of the signals as a function of the electric field.

The crossing centres and the Stark shifts of the present calculation are in good agreement with the calculation of Beyer. Only the Stark constant of the αG' signal differed slightly from Beyer's calculation, as shown in fig.32b, resulting in a better agreement with the present experimental work. The comparison of the theoretical and experimental crossing centres and Stark constants will be given in section 7.

The signal amplitudes with respect to the background (relative amplitudes) were about three times higher than the experimental results. This was probably due to the lack of actual experimental data for the differential cross section of the substates used in the intensity calculation. Fig.10b shows the relative amplitude of the αG' signal as a function of electric field. As also observed in the experiment, the signal showed a quenching effect at high electric field due to non-resonant Stark mixing of the states (see sec.5.6).

In fig.10a, the width of the αG' signal is shown as a function of the electric field. Above 200 V/cm, the present calculation is in good agreement with the present experiment and with the calculation of Beyer. At low electric field, the present calculated value becomes smaller than the sum of the natural widths. The cross terms between the substates, which were not included in the approximation, may be the cause of this difference.

In general, the results of this calculation showed that the anticrossing signals calculated without the inclusion of the interference between the crossing states approximate the

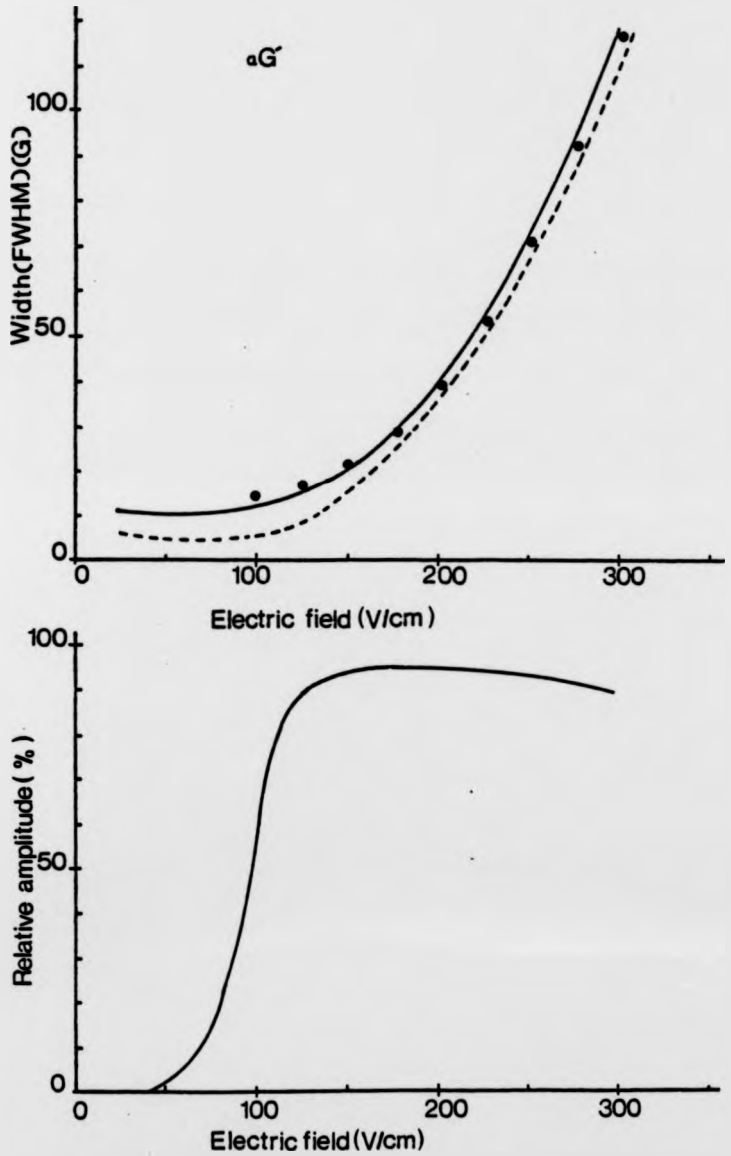

Fig.10: The width and the relative amplitude of the αG' signal as a function of the electric field.

a) The dashed line represents the values derived from the signal calculated using the equation 3.16. The solid line is the calculation based on the time independent diagonalisation and the theory (sec. 3.1). The points are the measured values.

b) The relative amplitude calculated from the signals based on the equation 3.16. See fig.26a for a comparison of the experimental work.

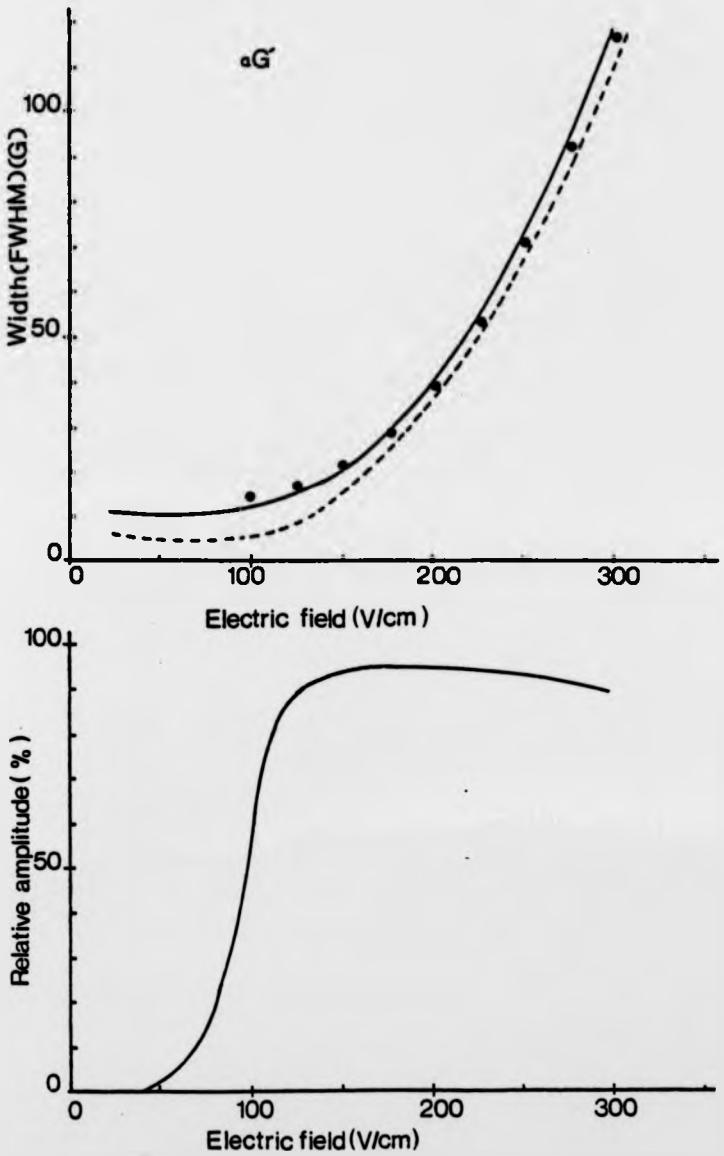

Fig.10: The width and the relative amplitude of the αG' signal as a function of the electric field.

a) The dashed line represents the values derived from the signal calculated using the equation 3.16. The solid line is the calculation based on the time independent diagonalisation and the theory (sec. 3.1). The points are the measured values.

b) The relative amplitude calculated from the signals based on the equation 3.16. See fig.26a for a comparison of the experimental work.

crossing centres and the Stark constants at least consistently with Beyer's calculation. Besides that, the shapes of the signals for different polarisation were in good agreement with the experimental results. Since the width at low electric field did not agree with the experimental results, nor with the previous calculation, a second calculation was needed to look at the effect of interference between the crossing states.

In the second calculation, the population in formula 3.16 is replaced by the excitation amplitudes and the time integration is explicitly introduced in the decay amplitude. The expression becomes

$$I \propto \Big|\sum_{\substack{jkk' \\ m}} f_k \langle j|U|k\rangle\langle m|er|k'\rangle\langle k'|U|j\rangle \int_{-\infty}^{0} e^{iE_{\hbar}t - \frac{\Gamma_j}{2}t} dt\Big|^2 \qquad (3.17)$$

where $f_k\langle j|u|k\rangle$ is the excitation amplitude, k and k' are basis states, j is an eigenstate and m is a lower state to which the transition takes place.

Using $\langle j|U|k\rangle = a_k^j$, $\frac{E}{\hbar} = \omega$

and

$$\int_{-\infty}^{0} \left(e^{i\omega_j t - \frac{\Gamma_j}{2}t}\right)\left(e^{i\omega_{j'} t - \frac{\Gamma_{j'}}{2}}\right)^* dt = \underbrace{\frac{\frac{1}{2}(\Gamma_j+\Gamma_{j'}) + i(\omega_j-\omega_{j'})}{(\omega_j-\omega_{j'})^2 + \frac{1}{4}(\Gamma_j+\Gamma_{j'})^2}}_{A_{jj'}}$$

Thus the expression becomes

$$I \propto \sum_m \sum_{jj'} \{(\Sigma f_k^2 a_k^j (a_k^{j'})^*) \sum_{k'k''} |\langle m|\vec{er}|k'\rangle\langle m|er|k''\rangle| a_{k'}^j (a_{k''}^{j'})^* A_{jj'}\} \qquad (3.18)$$

The anticrossing signals of He^+,n=4 were calculated using the formula (3.18) which showed that the interference between the crossing states reduced the amplitude of the signals resulting in a wider width. Fig.11 shows a comparison

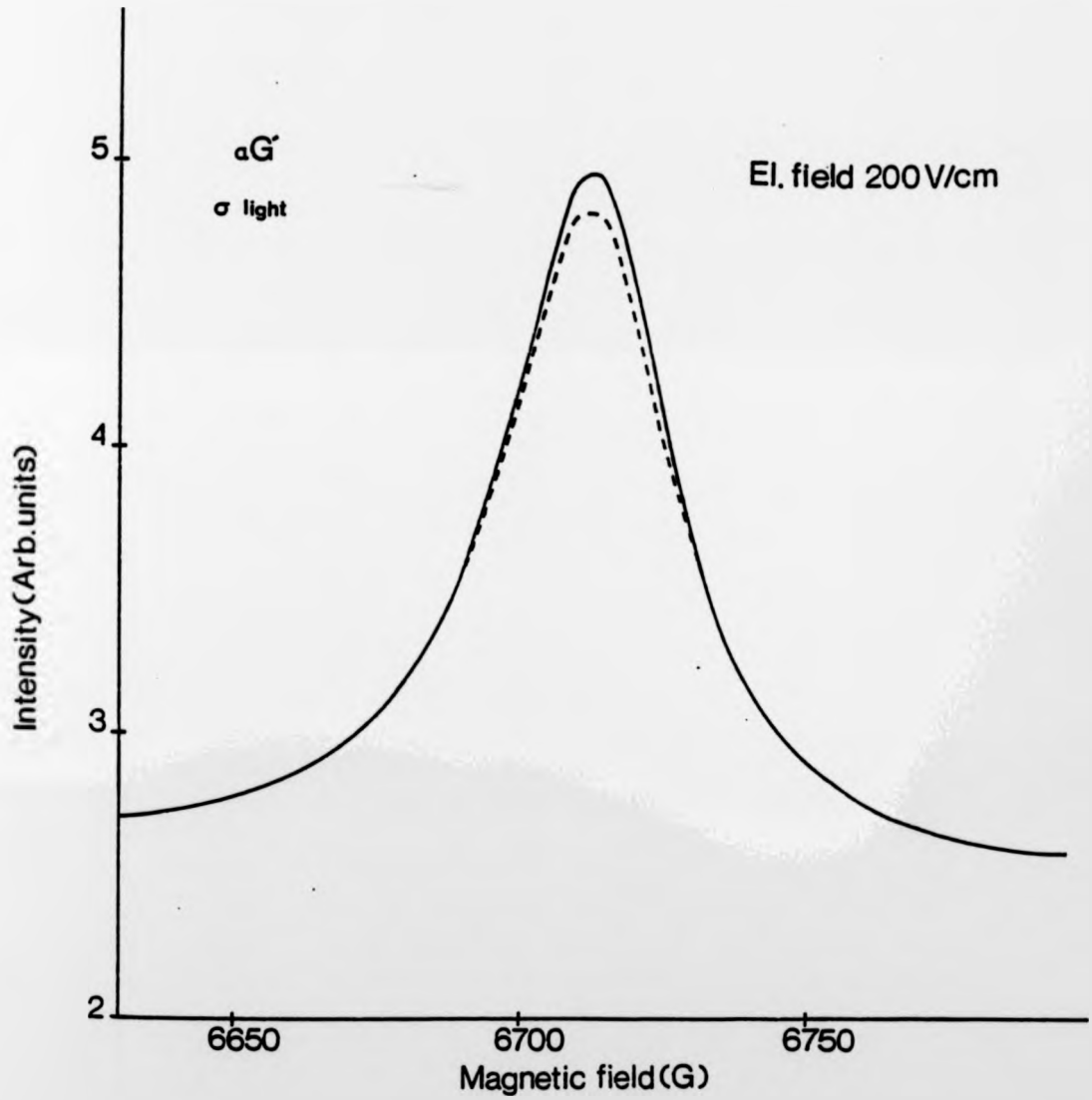

Fig. 11: The calculated signal of the anticrossing αG' in He^+, n=4 using σ light. The solid and the dashed line represents the calculated values using the quation 3.16 and 3.18 respectively.

of the $\alpha G'$ signals calculated using equations 3.16 and 3.18 at the electric field of 200 V/cm. The figure shows that the inclusion of the interference between the crossing states did not affect the background but decreased the amplitude of the signals while the crossing centres remained the same. Formula 3.18 gave the same results as formula 3.16 when the interference was excluded from the calculation.

A problem arose when the signals were calculated at low electric field. As shown in fig. 12 an oscillation appeared near the crossing centre which made the extraction of the width and the crossing centre difficult. With the present experimental set up, observation in this electric field region is difficult because of the low degree of signal saturation, but there was no indication of an oscillation at the smallest electric field (90 V/cm) used in the experiment. No final conclusion regarding the origin of this oscillation can be made until some experimental data with good signal to noise ratio can be obtained at lower electric field.

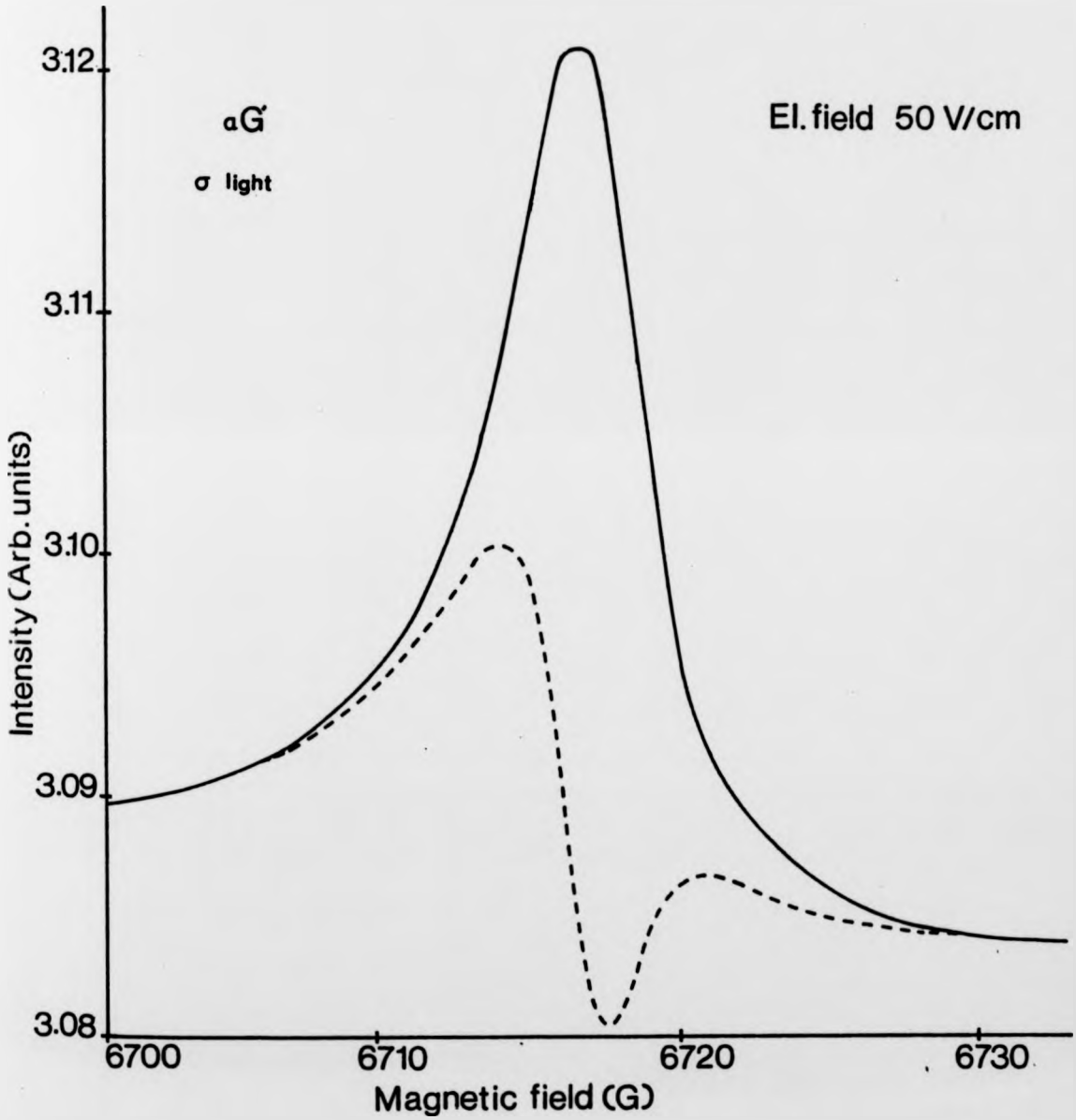

Fig. 12: The calculated αG' signal using σ light with an electric field of 50 V/cm. The solid and the dashed line show the signal calculated using the equation 3.16 and 3.18 respectively.

4. APPARATUS

A schematic diagram of the system used in the present work is shown in fig.13. A vacuum system, containing the electron gun and of the order of 1 to 15 mTorr of the gas to be studied, was placed in a magnetic field parallel to the electron beam. Either a monochromator or an interference filter was used to isolate the spectral lines. The intensity of the line, measured by a photomultiplier, was recorded as a function of the magnetic field.

The equipment used in the measurement will be discussed under the following headings:

1. Vacuum system and electron gun
2. Magnetic field and its measurement
3. Light detection and data collection

4.1. Vacuum System and Electron Gun

A glass tube, 18 cm long and 5 cm in diameter, which contains the electron gun and the Stark plates was used as a vacuum system (fig.14). Glass is non-magnetic and after baking has a very low outgassing rate. The tube can easily be filled with helium by diffusion through the heated walls since the He diffusion rate is high and increases steeply with temperature (Altemose 1961). The expansion coefficient of the glass used is $50.10^{-7}/C^{\circ}$ which allowed the ultraviolet transmitting front window (Schott glass 8337) to be joined directly to the body. Molybdenum feedthroughs were used to make the electrical connections to the electron gun. The vacuum tube, sealed to a flanged glass, is connected to

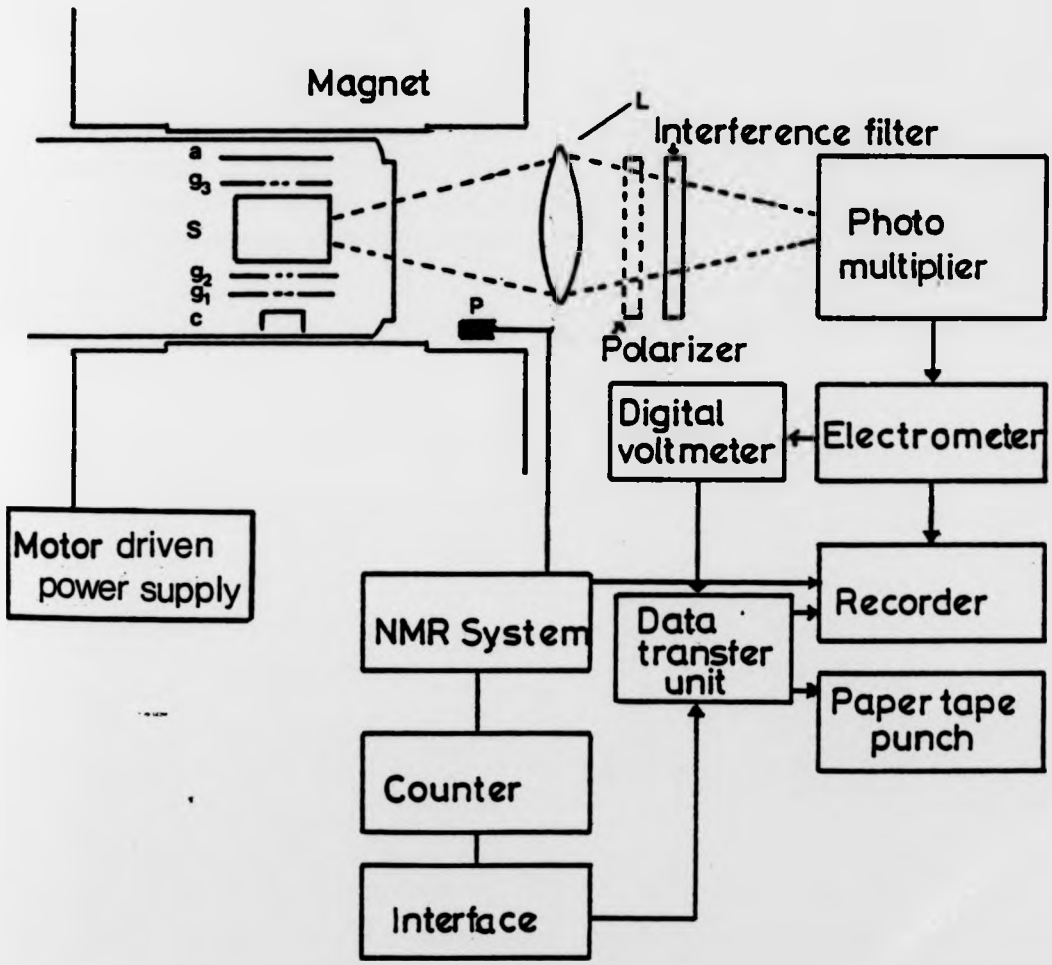

Fig.13: Schematic diagram of the apparatus, S: Stark plates, P: NMR probe, L: lense, g1: grid 1, g2: grid 2, g3: grid 3, a: anode, c: cathode.

the pump and to a quartz tube by means of a stainless steel adaptor as shown in fig.14. The quartz tube, used for the helium diffusion, is enclosed in an oven which contained helium gas at atmospheric pressure. A valve separated the pump from the vacuum system, which could thus be evacuated, and be filled to any desired He pressure.

For the construction of suitable Stark plates, various alternatives were tested to obtain optimum homogeneity of the electric field. In the first place gold coated glass plates were baked at a temperature of 500°C for one day to simulate the annealing and vacuum baking processes. At

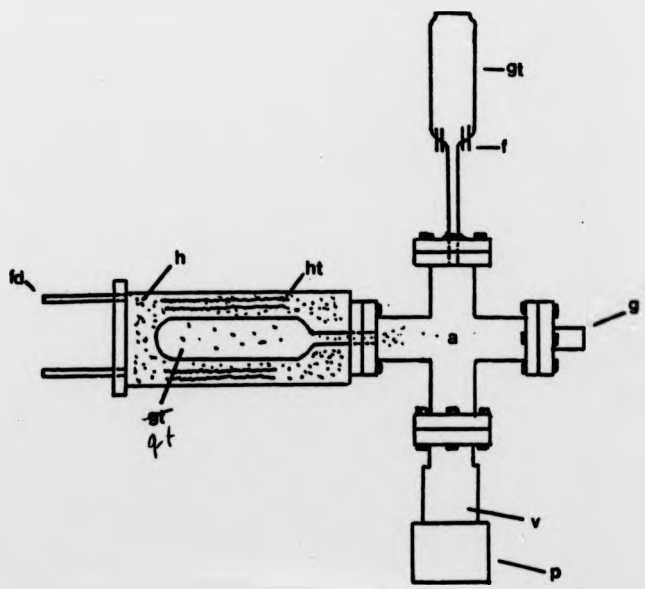

Fig.14: Top view of the vacuum system. f: feed throughs, gt: glass tube, g: gauge head, a: adaptor, v: valve, p: pumps (below paper plane), ht: heater, h: helium gas, fd: feeding hole, qt: quartz tube.

the end of this operation it was found that much of the gold had disappeared from the plates. Moreover, there were problems in drilling mounting holes through the plates and it was difficult to ensure secure electrical contacts to the coatings. Therefore the idea of using gold coated glass plates was abandoned. Secondly, a set of 4 mm thick Al plates was tested in the oven as an alternative to the glass plates. In the high temperature of the oven (500^{o}C) they bent probably due to release of tension from the machining. Finally, 1 mm thick commercial molybdenum plates were adopted. The electrocleaning technique (electro-polishing) (Rosebury 1965) was used to remove any oxide layers and to remove any possible irregularities on the surface.

A solution of 20% NaOH in water was put in a glass container as a solution for the electrocleaning process. A carbon rod and the molybdenum plate were used as positive and negative electrodes respectively. About 5 volt and 5 amp D.C. was applied for two minutes. The voltage and current values were found by experience and also applied for the polishing of the plates.

The first test of the plates in the oven resulted in oxidisation of the molybdenum. The second test was thus carried out by sending a continuous flow of argon gas through the glass container during the baking process. The result was successful as no visible oxide or insulating layer was formed on the surface of the plate. This latter technique was, therefore, adopted for the sealing and the annealing of the glass tube to avoid the oxidisation of the

Stark plates and other molybdenum pieces (washers, nuts and screws) inside the glass system.

Alumina tubes were used between the Stark plates as spacers and insulators. The outside of the spacers was painted with aquadag dry film lubricant to make them slightly conductive. The insulators should not affect the field distribution if the conductive layer is homogeneous. Considerable difficulties arose from the drastic drop in the resistance of the painted surface material after it had been heated. The ideal thickness of the layer for the desired resistance was found by trial and error. The current between the Stark plates through the spacers was 2 mA at 150 V of Stark voltage (i.e. 75 kΩ).

The glass tube must be placed in the air gap between the poles of the magnet, thus putting a restriction on the size of the tube. The Stark plates were made as large as compatible with this limitation. The size adopted was 25 x 35 cm with 7.030 ± 0.015 mm separation. An internal micrometer with a sensitivity of 1/1000 mm was used to measure the separation at various points between the plates after they were mounted and the uncertainty was found to be 0.2% of 7 mm.

The electron gun and the Stark plates were mounted on a 35 x 45 mm glass plate by 1 mm diameter molybdenum rods (fig.15). The nearer Stark plate is kept about 7 mm away from the mounting plate to protect the interaction region from possible charging up effects of the glass.

The electron gun consisted of a commercial oxide coated cathode of 4 mm diameter emitting surface (M-O Valve

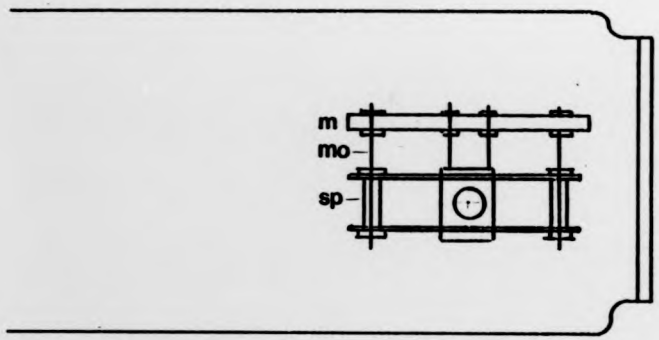

A

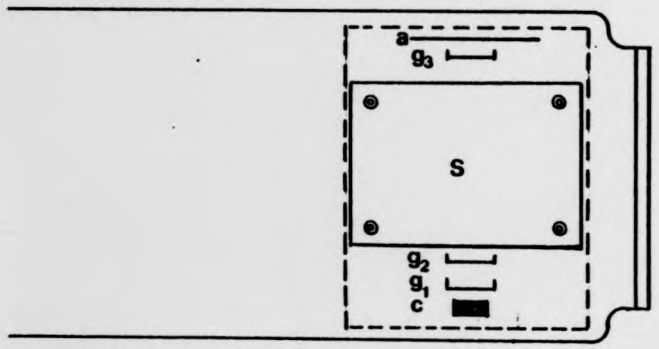

B

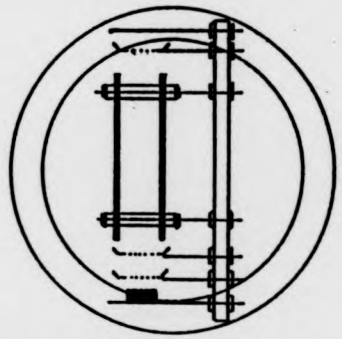

C

Fig.15: Electron gun system. A: Top view, B: Side view, C: Front view, a: anode, g_i: grid 1, g_2: grid 2, g_3: grid 3, c: cathode, m: mounting glass plate, S: Stark plates, sp: spacers, mo: molybdenum rods.

Co.Ltd., type DGL 4A) and an anode. The first grid, g1, (see fig.15) controls the electron current and the second, g2, accelerates the electrons to the desired energy. The third grid, g3, near to the anode was designed to prevent secondary electrons from re-entering the interaction region, but no effect was observed and it was therefore connected to the anode. The voltage between cathode and g1 is controlled by an electronic regulation circuit sensing the anode current. This stabilises the current against the variation of electron energy and the magnetic field. The anode, made from tantalum was earthed to keep the observation region near earth potential. (The potential on the second grid was about -3V with respect to anode).

A sorption pump (Vacuum Generator) and an 8 ℓ/s ion getter pump were used to evacuate the vacuum system. The glass system was baked at 400°C for one day in a temperature controlled furnace. Heating tapes were used for the metal parts. The pressure was 2.10^{-8} Torr when the system cooled down to room temperature. The oxide cathode was activated by heating slowly (over a period of several hours) to about 900°C. The valve was then closed and the system filled with helium by diffusion through the heated walls of the helium container (see fig.14). When a different helium pressure was required the system was evacuated and refilled by the same method.

4.2. Magnetic Field and Its Measurement

A commercial (Bruker, B-E25B8) electromagnet was used to generate the magnetic field. The magnet has 25 cm diameter movable pole pieces, so that the air gap can be adjusted at will from 0 to 70 mm with a precision spindle (an additional screw on the two nuts of the threaded spindle fixes the pole pieces at any air gap value). The ring shims around the pole faces of the magnet were properly adjusted at 6 kG to improve the homogeneity of the field. The inhomogeneity of the field over the interaction region was about 7 ppm which had negligible effect on the results. A motor driven potentiometer incorporated into the 6 kW power supply (Bruker, 150/40 Si 6 ng) allows the magnetic field to be swept. The field had to be measured 4 cm away from the interaction region outside the vacuum system. The glass system together with the vacuum pump were mounted on a movable trolley which helped to remove the system from the centre of magnet to make a field correction after each experimental run. It was found that the field difference between the probable position and the centre of the magnet was not the same when the magnet was stopped from upward or downward sweep. The hysteresis effect was considered to be the reason and thus the corrections were measured for both sweep directions. The mean of these two values was taken for the final correction to the field.

The nuclear magnetic resonance (NMR) (AEG-NMR Cabinet) allowed very accurate measurements of magnetic fields and

the NMR frequency is registered with an 8-digit counter (Hewlet Packard 5245L).

The actual field measuring system (NMR probe) consists of a small water sample surrounded by a high frequency coil. In the static magnetic field the magnetic dipoles of the protons in the sample precess around the direction of the magnetic field vector. The frequency ν of this precession is proportional to the magnetic field strength:

$$\nu = (\frac{\gamma}{2\pi})H \qquad \frac{\gamma}{2\pi} = 4.257602(12)\text{kHz/G} \text{ (Cohen \& Taylor 1973)}$$

where H is the magnetic field (in Gauss) and $\frac{\gamma}{2\pi}$ is the gyromagnetic ratio of protons in water.

The magnetic field value was directly read from the counter in Gauss. This was made possible by controlling the counter gate externally by the quartz of the NMR system which has an internal frequency equal to the numerical factor of the proton gyromagnetic ratio ($\gamma/2\pi$). Therefore, the value displayed on the counter becomes numerically equal to the magnetic field strength at the probe position. The NMR signal may be locked for automatic and continuous frequency adjustment of the oscillator. The magnetic field value as displayed by the counter can be obtained as calibration mark at every full 1 or 10 G.

The preset value of the gyromagnetic ratio of protons in water in this system was measured as 4.257682 kHz/G at the beginning and 4.257694 kHz/G at the end of the research. The difference of 2 ppm has a negligible effect on the uncertainty of the measurement. These values are to be compared with the recently measured value of 4.257602(12)kHz/G

(Cohen & Taylor). The difference of 20 ppm gives about +0.15 G correction to the measured value of the magnetic field at 8 kG. The internal standard of the counter was checked against the frequency standard of 200 kHz emitted from Droitwich transmitter using a standard frequency receiver (Rohde und Schwartz, type XKD).

4.3. Light Detection and Data Collecting

The spectral line 4686Å was isolated either by using a monochromator (McPherson, model 218) or an interference filter. The monochromator was selected for high light power but the narrow entrance slit still caused a reduction of the detected light intensity by a factor of 15 as compared to the interference filter used.

The light coming from the interaction region was focussed on the plane of the entrance slit of the monochromator by a lens which created an image of ∿1:1. For the interference filter, an image enlarged by 2:1 was produced on an aperture near the plane of interference filter so that the range of angles at which the light was transmitted through the filter was reduced. Position and size of the slit or the aperture were arranged in such a way that only light from the interaction region between the Stark plates was accepted. A linear polariser was used when only the π or the σ component of the light was to be selected.

A highly sensitive 13-stage photomultiplier (EMI, 9635QA) was used to detect the light. The output of a photomultiplier is severely affected by the environmental

magnetic field. The effect is particularly important in the region between the cathode and first dynode. It is also very important that nothing should touch the tube envelope which will disturb its potential stabilisation. Any material in contact with the envelope should be at cathode potential. A mu-metal cylinder connected to cathode potential performed the dual function of an electrostatic and a magnetic shield. The photomultiplier was operated about 60 cm away from the centre of the magnetic field and partially shielded from stray magnetic fields by the yoke of the electromagnet.

A picoammeter (Keithley 417) was used to measure the anode current of the photomultiplier. The output was connected simultaneously to a digital voltmeter (Solartron, LM 1426) and a x-t recorder (Bryans, 27000). At preselected time intervals (usually 5 s) during the runs, readings were taken of the light intensity through the digital voltmeter and of the magnetic field through the frequency counter, and transferred on to paper tape. The signals were also recorded on the chart recorder.

5. OBSERVATIONS AND DATA ANALYSIS

5.1. Investigation of Impurities

The glass system was filled with helium gas through diffusion and initial measurements were made to check for impurities inside the system. Using a monochromator, the spectrum of the tube was recorded between 2500 Å and 5050 Å. The analysis showed the existence of several strong impurity lines in the spectrum. These were identified as molecular bands of the CO^+ Comet-Tail system (Pearse & Gaydon 1965), arising probably from the oxide cathode and the stainless steel part of the vacuum system connecting the pump to the glass system. One of the bands overlapped with the 4686 Å line (see fig.16), so that it was necessary to investigate ways to eliminate the impurities, if possible without re-opening the glass system.

Refilling and baking the tube did not help, but it was found, as shown in fig.16, that the impurity bands near the observation line disappeared when electric fields in excess of about 30 V/cm, perpendicular to the magnetic field, were applied to the Stark plates. Since most of the measurements would be taken above this electric field value, no further attempt was necessary to eliminate the impurities completely.

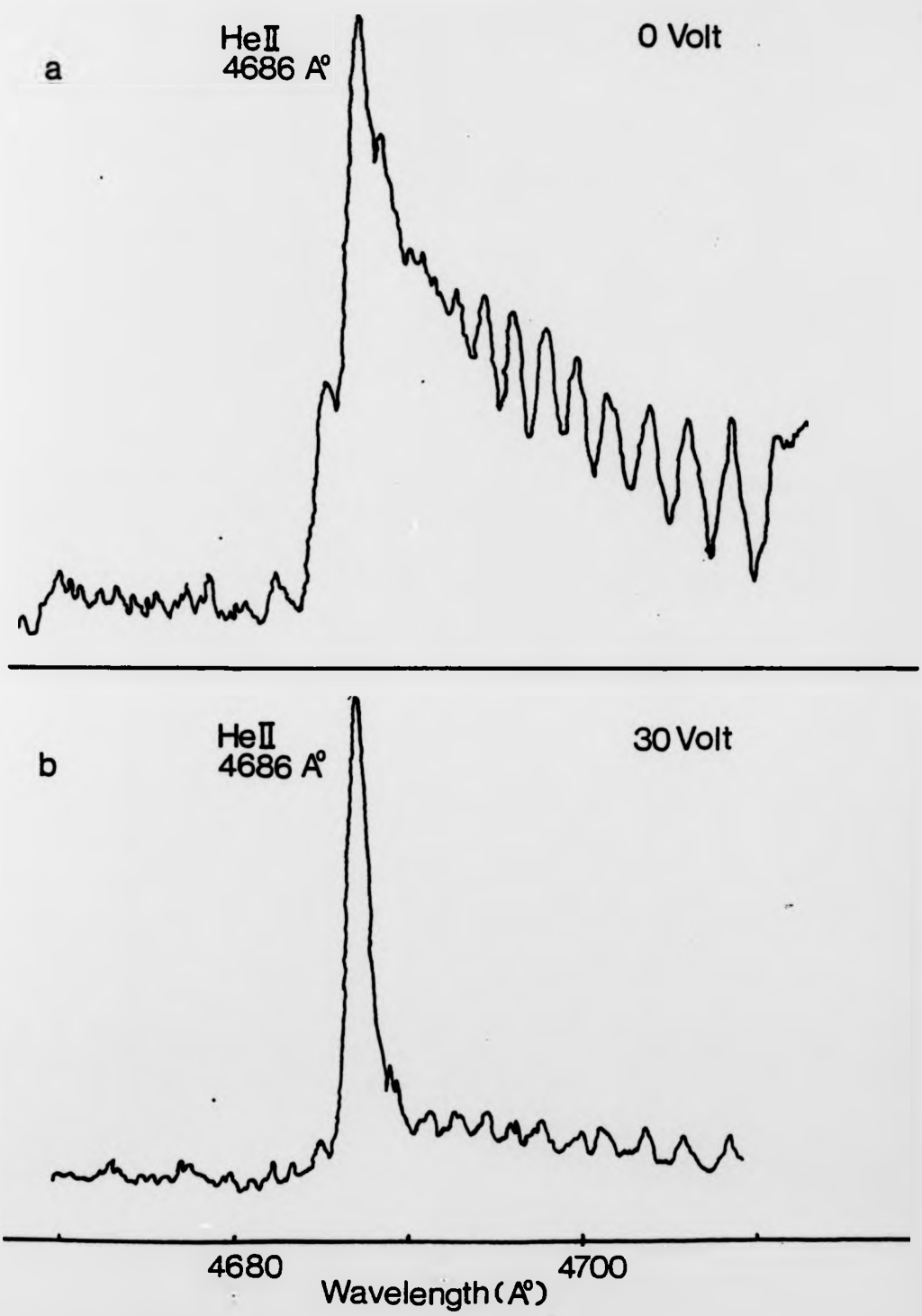

Fig.16: The helium ion line of 4686 Å (n=4 → n=3), excited in a magnetic field of 6600 G with an electron beam current of 300μA, and an excitation energy of 300 V.
a) The impurity lines of a CO^+ band are shown at the tail of the 4686 Å line when there is no Stark voltage.
b) The impurity lines mostly disappear at a Stark voltage of 30 V.

5.2. Excitation Function of the Line He II-4686 Å

The excitation function in Fig.17a for the He II line 4686 Å was obtained at a gas pressure of 12.3 mTorr and at an electron beam current of 300 μA. The energy of the electron beam was varied from 0 to 325 eV. The measurement was carried out at 7300 G, i.e. outside any anticrossing signal of n=4 and at an electric field of 190 V/cm.

It should be noted that the electron energy is affected by the Stark field. This effect arises in the present experimental set up since one of the plates is connected directly to the second grid of the electron gun so that the potential of the second plate is negative with respect to anode and grid 2. Thus the energy of the electrons along the trajectory between the plates is reduced because of the potential drop caused by this arrangement. Previously an attenpt was made to keep the observation region at zero potential by applying equal but opposite voltages on the Stark plates. This arrangement, however, was not successful as the intensity of the observed line fluctuated throughout the experimental run.†

After the correction of the electron energy, the present result is in good agreement with the previous measurements of Anderson, Lee & Lin (1967) and Beyer (1973). The small peak at around 130 Volt is possibly another

---

† Effects of the electron energy variation on the crossing centre and and on the intensity of the observed line were checked and no change was observed. Therefore it was not necessary to adjust the acceleration voltage with each electric field variation to keep the electron energy constant.

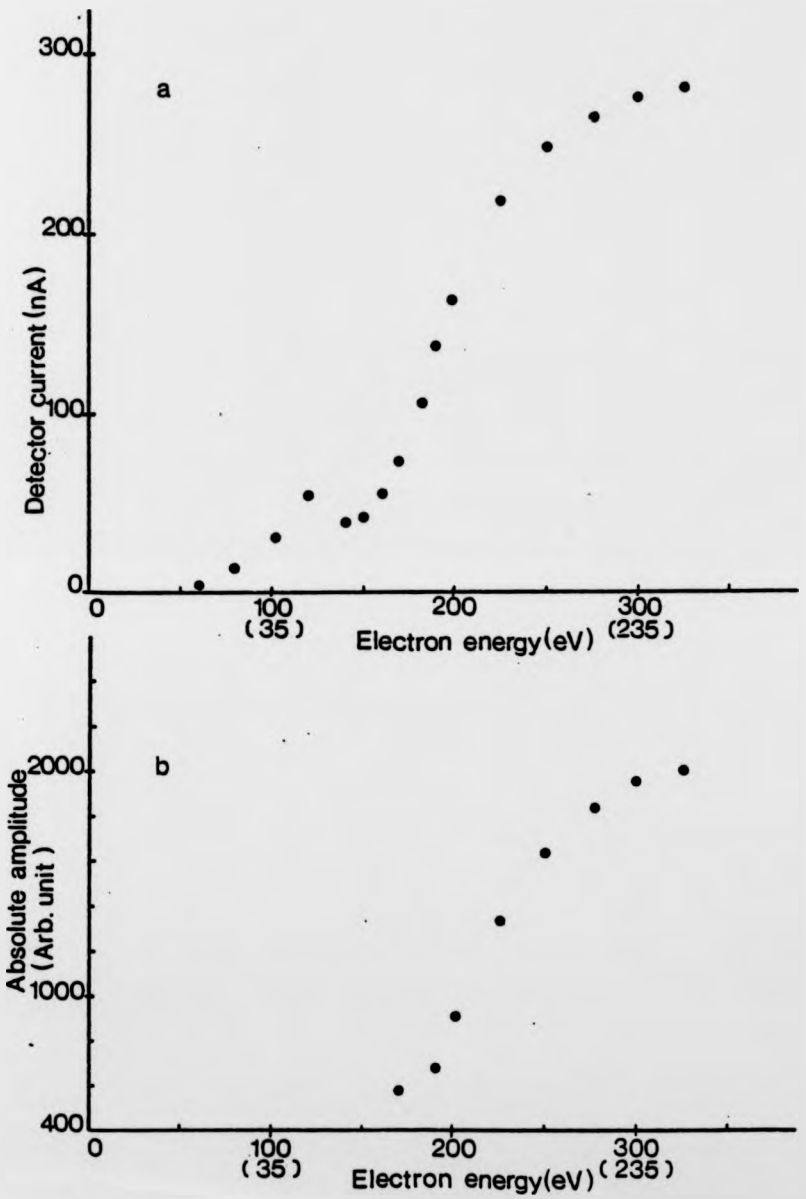

Fig 17: The excitation function of the HeII transitions 4686 Å at a gas pressure of 12 mTorr and an electron beam current of 300μA. The numbers in paranthesis show the value of electron energy after correction according to sec. 5.2.

a) The intensity as a function of electron energy outside any anticrossing signal at a magnetic field of 7300 G and an electric field of 190 V/cm.

b) The amplitude of the anticrossing βH' as a function of the electron energy at an electric field of 190 V/cm.

result of the present experimental set up, since at this voltage the cathode potential happens to be the same as the lower potential Stark plate.

The dependence of the amplitude of the βH' signal on the excitation voltage of an electric field of 190 V/cm is shown in fig.17b. The comparison of fig.17a and fig.17b shows that the amplitude of the anticrossing signal is proportional to the strength of the observed line.

5.3. General Survey of Anticrossings in n=4

Typical experimental conditions for the observation of the anticrossing signals were: excitation voltage, 300 V; bombarding current, 300 μA; helium pressure, 1-15 mTorr; Stark voltage, 20-147 Volt $\hat{=}$ 29-210 V/cm.

Using unpolarised and linearly polarised π and σ light for the detection, a general survey of the signals was first carried out in order to find the best experimental conditions. The anticrossing signals listed in table 1 were found to be the most suitable for fine structure and Stark effect measurements. From these, the signals βH', αG', αN' and αJ were selected† for the detailed study of pressure effect. Their differing Stark constants and good signal to noise ratios would also give the necessary data for the analysis of various other pressure related effects such as electron and ion space charges.

---

† For the identification of the signals, Lamb's notation of the magnetic substates is used throughout the text. A full list, up to n=5, is given in appendix 3.

Normally the anticrossing signals are of absorption Lorentzian shape (see fig.20) but the S-D signals have also dispersion admixture. As explained in sec.3.1.2, a mixed level-crossing-anticrossing signal is possible if there is coherence in either the excitation or the decay channel or in both. Since the 4S and 4D substates of the crossings αJ, αE and βF can decay to common substates of 3P, coherence between the anticrossing substates introduced by the static electric field applied perpendicular to the magnetic field, can result in interference in the decay. In the present experimental set up, the interference part can be avoided by choosing π light for the observation at which there is no decay to a common substate (see fig.18). This was done for the βF crossing, but the αJ and αE signals were observed under σ and unpolarised light respectively, since

Anti Crossing	Lamb Notation	Crossing sublevels	Polarisation chosen for the observation
S-F	αN'	$4S_{1/2},m_j=\frac{1}{2}$ - $4F_{5/2},m_j=-5/2$	un pol
	αG'	$4S_{1/2},m_j=\frac{1}{2}$ - $4F_{7/2},m_j=-5/2$	σ pol
	βH'	$4S_{1/2},m_j=-\frac{1}{2}$ $4F_{7/2},m_j=-7/2$	σ pol
S-D	αJ	$4S_{1/2},m_j=\frac{1}{2}$ - $4D_{3/2},m_j=-3/2$	σ pol
	αE	$4S_{1/2},m_j=\frac{1}{2}$ - $4D_{5/2},m_j=-3/2$	un pol
	βF	$4S_{1/2},m_j=-\frac{1}{2}$ - $4D_{5/2},m_j=-5/2$	π pol
P-F	fN'	$4P_{1/2},m_j=-\frac{1}{2}$ - $4F_{5/2},m_j=-5/2$	un pol

Table 1: Anticrossing signals in n=4 of He^+ selected for the fine structure and Stark effect measurements. See appendix 3 for Lamb's notation.

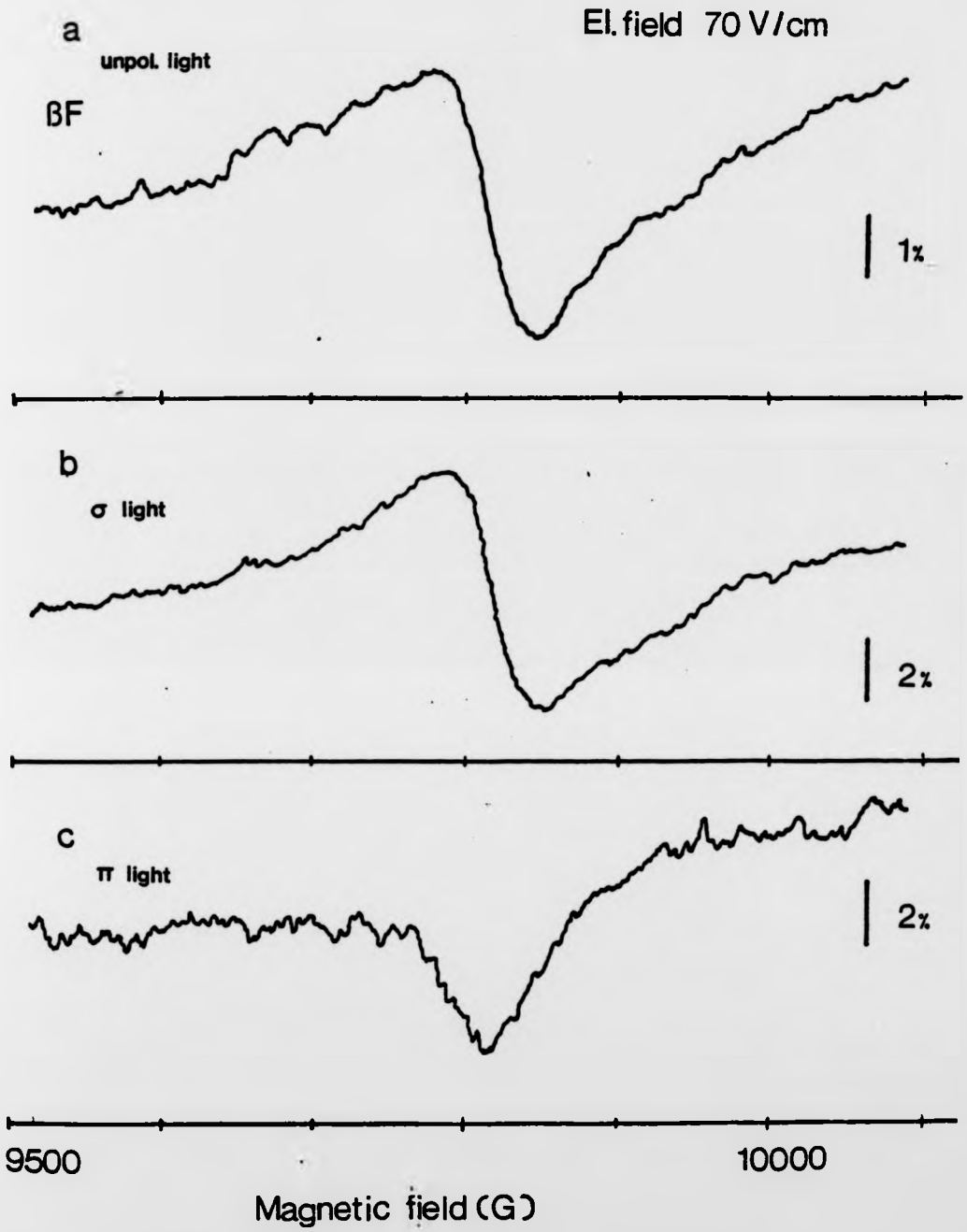

Fig.18: Recorder traces showing the S-D anticrossing βF in n=4 of He^+.
a) Unpolarised light; b) σ-light; c) π light.

The experimental condition for these signals is: Helium pressure, 13 mTorr; electron current 300 μA; Stark voltage, 50 Volt ≙ 70 V/cm; time constant, 4.5s; anode at 300 V, grid 1 at 10 V and grid 2 at 297 V with respect to cathode. The bar represents the percentage of the total light intensity.

the signals under π light were found to be very weak.

The fitting function for the signals included a dispersion part and thus allowed the analysis of both mixed S-D signals and absorption signals.

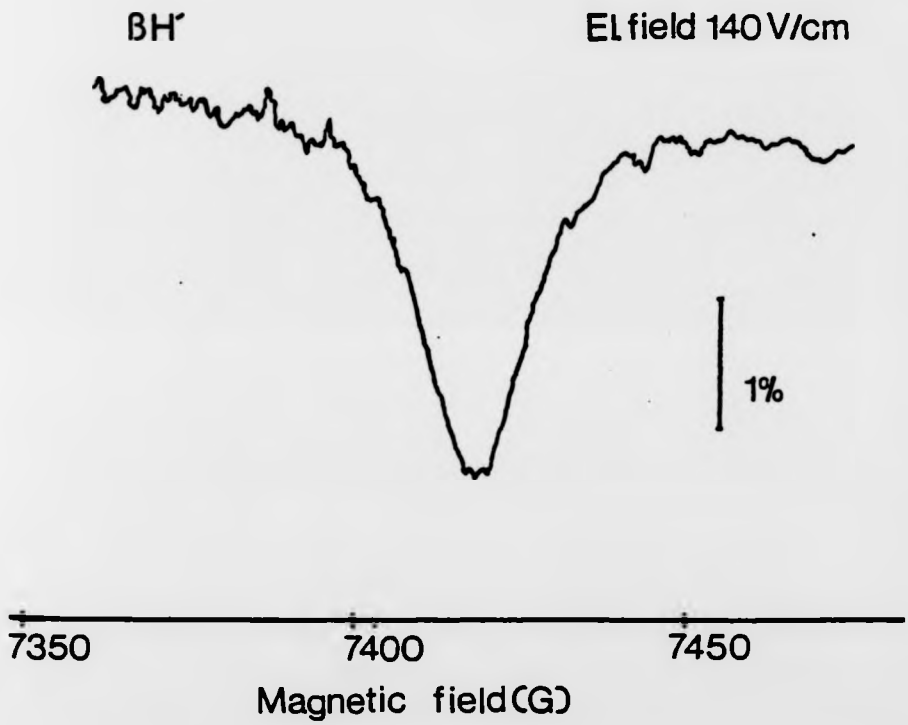

Fig.19: **Recorder trace showing the S-F anticrossing βH' in singly ionised helium, n=4, using π light. The sublevels H' cannot decay with π-light, hence the negative anticrossing signal observed in π-light results only from the population reduction of the S-sublevel. (The same signal in unpolarised light is positive and much stronger).**

The experimental condition for this signal is: Helium pressure, 11 mTorr; electron current, 300 μA; Stark voltage, 119 V; time constant 3s; anode at 300 V, grid 1 at 10 V and grid 2 at 297 V with respect to cathode. The bar represents 1% of the total light intensity.

5.4. Data Taking Procedures

At preselected time intervals, the light intensity and the magnetic field are measured by a digital voltmeter and a frequency counter, respectively, and the data transferred on to paper tape. The signals are also recorded on a chart recorder, and some typical examples are shown in figs. 20-24. The other parameters that were manually recorded for each run included the time constant, the pressure of helium gas, the electron current, the range and suppression of the multiplier current and Stark voltage.

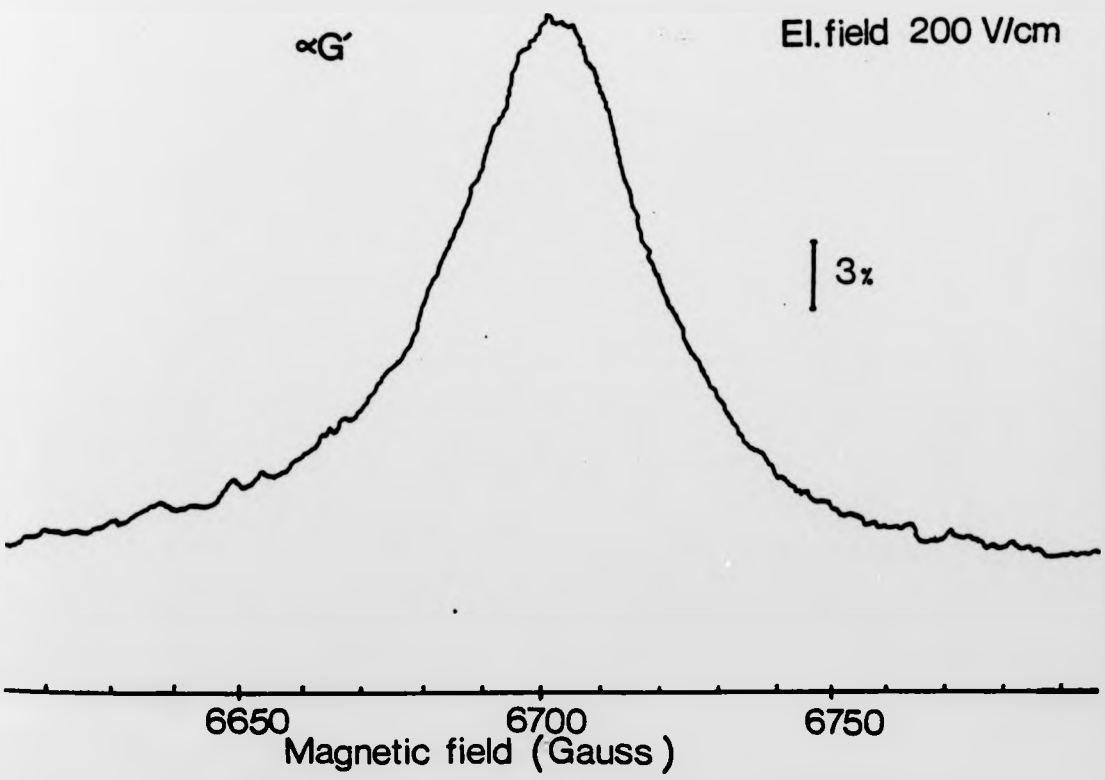

Fig.20: Recorder trace showing the S-F anticrossing αG' in singly ionised helium, n=4, using σ light. The experimental condition for this signal is: Helium pressure, 8 mTorr; electron current 300 μA; Stark voltage, 140 Volt; time constant 4.5s; anode at 300 V, grid 1 at 10 V and grid 2 at 297 V with respect to cathode; The bar represents 3% of the total light intensity.

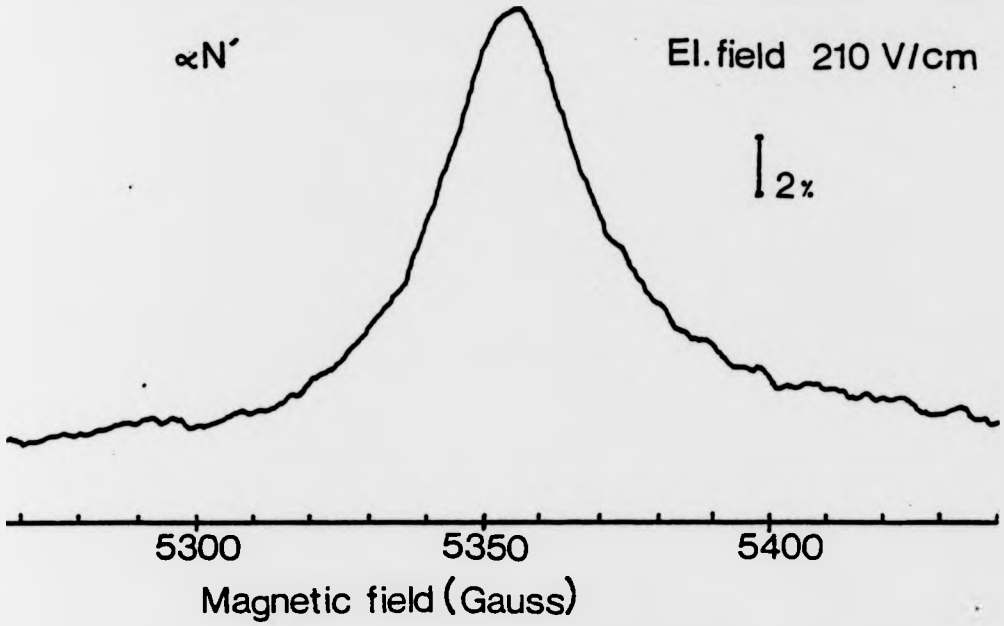

Fig.21: Recorder trace of the anticrossing αN' in singly ionised helium, with n=4, using unpolarised light. Helium pressure, 11.5 mTorr; electron current, 300 μA; Stark voltage, 147 V; time constant, 4.5s; anode at 300 V, grid 1 at 10 V and grid 2 at 297 V with respect to cathode. The bar represents 2% of the total light intensity.

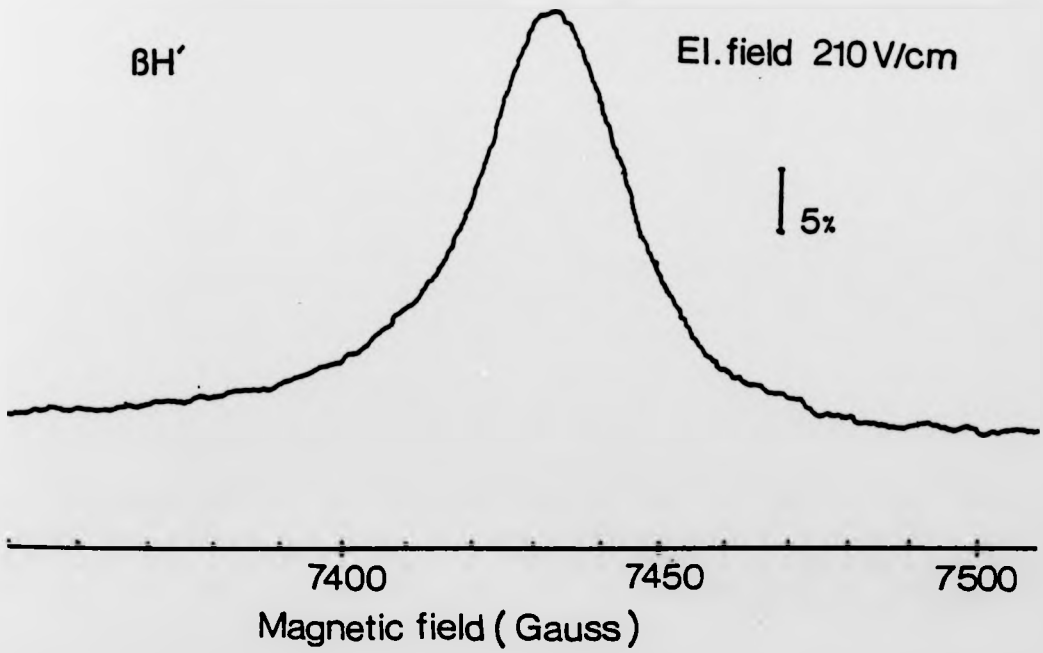

Fig.22: Recorder trace of the anticrossing βH' in singly ionised helium, with n=4, using σ light. Helium Pressure, 11.5 mTorr; electron current, 300 μA; Stark voltage, 147 V; time constant 4.5s; anode at 300 V, grid 1 at 10 V and grid 2 at 297 V with respect to cathode. The bar shows 5% of the total light intensity.

The S-F signals show an absorption Lorentzian shape (fig.20) whereas the S-D signals consist of a mixture of absorption and dispersion character in σ light or a pure absorption character when π light is chosen for the observation (fig.18).

The magnetic field was swept continuously through the crossing, so that the time constant of the detector circuit had to be considered carefully. A large time constant provides a good signal to noise ratio, but requires a low sweep rate of the magnetic field to avoid undue distortions of the signals. On the other hand if the sweep rate is too low, long term drifts may influence the signals. A sweep rate of less than 0.1 line widths (FWHM) per time constant was aimed at (Isler 1969) to obtain a minimum distortion of the line shape. All signals were recorded in pairs by sweeping the magnetic field in upward and downward direction thus eliminating the shifts and minor distortions caused by the time constant effect.

The parameters and the values on the paper tape were handled by a computer fitting programme which calculates the crossing centre, width, relative and absolute amplitudes and standard deviation for each signal.

A six parameter Lorentzian function, consisting of absorption and dispersion parts with common centres and widths on a sloping background, was used as a fitting function to the measured data. The function is:

$$Y = \frac{A}{1+(X-Z)^2/B^2}\,(1 + C(X-Z)) + D(X-Z) + E$$

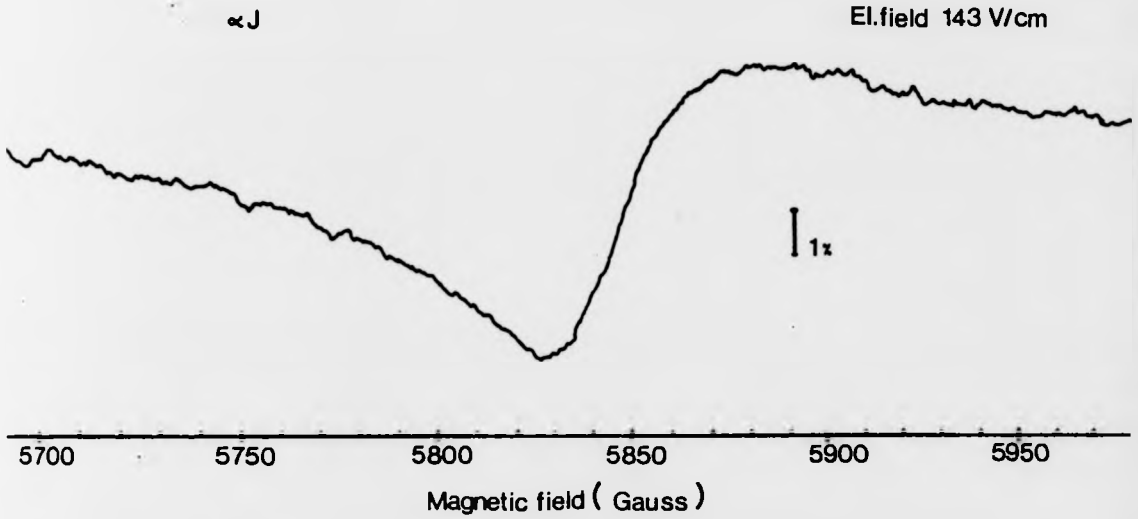

Fig.23: Recorder trace of the anticrossing αJ in singly ionised helium, n=4, using σ light. Helium pressure, 15 mTorr; Electron current, 300 μA; Stark voltage, 100 V; Time constant, 6s; Anode at 300 V grid 1 at 10 V and grid 2 at 297 V with respect to cathode. The bar shows 1% of the light intensity.

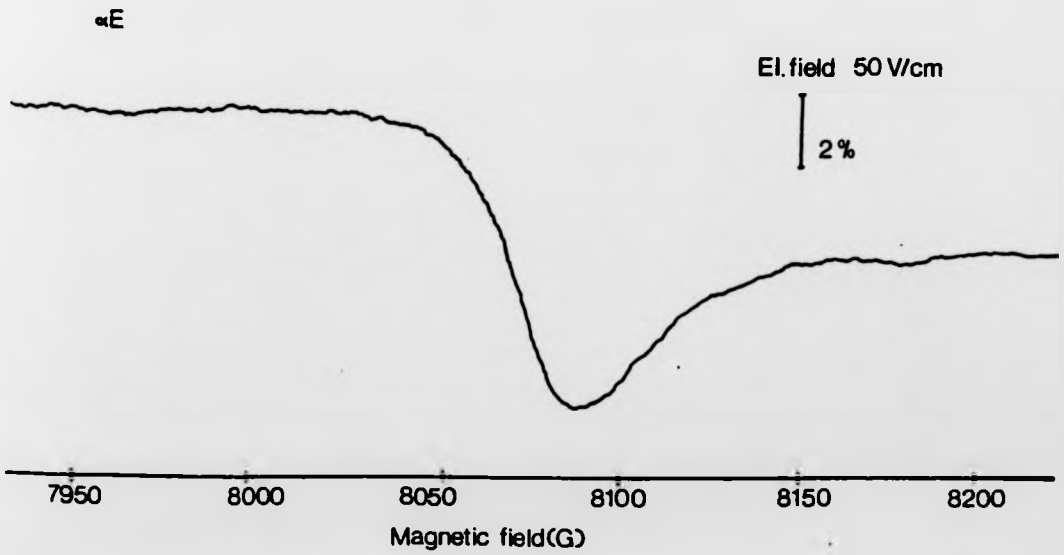

Fig.24: Recorder trace of the anticrossing αE in singly ionised helium of n=4, using unpolarised light. Helium pressure 10 mTorr; Electron current, 300 μA; El. field 50 V/cm; Time constant, 6s; Stark voltage, 35 volt; Anode at 300 V, grid 1 at 10 V and grid 2 at 297 V with respect to cathode. The bar represents 2% of the total light intensity.

where A: Absorption amplitude, 2B: full width at half maximum (FWHM), C: dispersion amplitude parameter, D: slope of the baseline, E: background at X=Z, Z: magnetic field at the centre. The function is explained elsewhere (Beyer 1973) in detail.

Between 30-100 readings were stored on paper tape for each signal and fitted to the function described above. The comparison of the experimental points and the fitted function will be discussed in sec. 5.6.

5.5. Cascading Anticrossing from $n \geq 5$

In the same way as the excitation of higher n states can affect the population of n=4 through cascades, population changes of high n states due to anticrossings can also influence the population of the n=4 states. This may cause a distortion of the observed signal.

The excitation cross sections and the proportion of the cascading light decaying through n=4 decrease as n increases. In addition the cascading anticrossings have their own electric and magnetic field dependence, such that most of them saturate at low electric field so that the signals will be very broad at electric fields high enough to induce the high order signals in n=4. Therefore no considerable effect is observed on the detected signals of n=4 except that there may be a small contribution to the signal asymmetry.

In some cases, as Mader et al (1971) observed, the cascading from the higher states may cause a slight shift

in the observed resonance curves. Besides that Beyer et al (1972) have shown that, in certain circumstances, the cascading signals can be strong enough to derive fine structure separations of a higher level. They have measured the separations $5S_{1/2}$-$5G_{7/2}$(αE") and $5S_{1/2}$-$5G_{9/2}$(αI") from the cascade effects observed in the line 4686 Å of n=4.

As in the lower n states, the S states should be the most strongly populated state of n=5. Thus 5S-5G coupling should result in less decay from 5S and more decay from 5G But due to the branching ratios of the respective states only 1% of the population change of 5S will be observed in the line n=4 → n=3, whereas all the change in 5G can be observed.

In the present work, a measurement similar to Beyer et al (1972) was done to find the zero electric field crossing positions corresponding to the cascading anticrossing αI". Good agreement is reached with the previous measure-

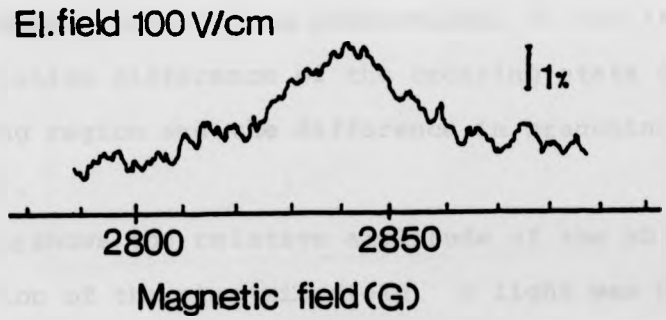

Fig.25: Recorder trace of the cascading anticrossing αI" in singly ionised helium, n=5, observed in the line n=4 → n=3. The experimental condition for this signal is: Helium pressure, 6.1 mTorr; electron current, 300 μA; Stark voltage, 70 Volt; time constant, 3s; anode at 300 V, grid 1 at 10 V and grid 2 at 297 V with respect to cathode. The bar represents 1% of the total light intensity.

ment and the theory as shown in Table 2. The recorder trace of one of the αI" signals is shown in fig.25. The signals are much weaker than the anticrossing signals of n=4. The shapes are Lorentzian with amplitudes 1-2% of the total 4686 Å light

Interval	Lamb Notation	Present Exp. (Gauss)	Beyer et al(1972) (Gauss)	Theory (Gauss)
$S_{1/2}-G_{9/7}$	αI"	2872.98(0.59)	2872.73 (0.29)	2873.29

Table 2: Cascading anticrossing αI" of n=5 detected in the line 4686 Å. The value in parenthesis is the standard deviation of the extrapolated crossing position.

5.6. Strength of the Signals

An electric field, the strength of which depends on the coupling and lifetimes of the crossing states, is required to induce anticrossing signals. The amplitudes of the signals, which rise with increasing electric field until saturation occurs, are proportional to the steady state population difference of the crossing state outside the crossing region and the difference in branching ratios (see sec.2).

Fig.26a shows the relative amplitude of the αG' signal as a function of the electric field. σ light was chosen for the observation and the helium pressure was set at 10 mTorr, the bombardment current at 300 μA and the excitation voltage at 300 V. As seen in fig.26a a quenching effect was observed in which the signal weakened when the electric field was further increased. A possible explanation

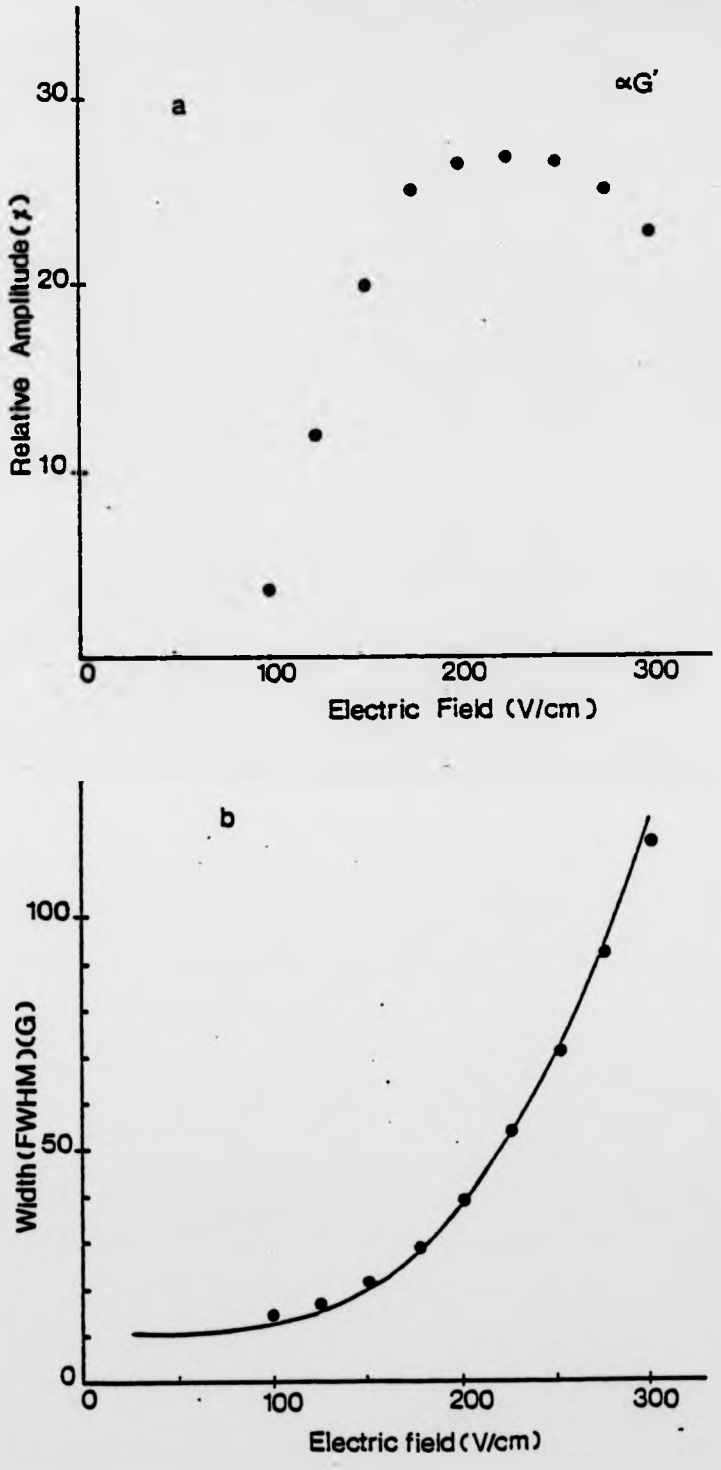

Fig. 26: a) Signal strength, and b) Signal width of the anticrossing αG' as a function of the electric field. Helium pressure 10 mTorr, bombardment current 300 μA and excitation voltage 300 V. σ light is chosen for the observation. The point size approximately represents the estimated experimental uncertainty. The solid line in b) represents the theory (time independent approach).

for this is that the population difference between the crossing states (outside the crossing region) is altered by non-resonant Stark mixing of the crossing substates with other substates. Since the lifetime of the 4S states is about twenty times larger than that of the 4P states, a small amount of S-P mixing may lead to a decrease of the S state lifetime and a considerable amount of decay through P will eventually affect the signal amplitude. Thus a theoretical study was made to look into the non-resonant Stark mixing of the crossing states as a function of the electric field. It was based on the eigenvector components of the crossing states obtained from the matrix diagonalisation of the full fine structure time dependent energy matrix in combined electric and magnetic fields. The result shows that the population of S states decreases with increasing electric field through non-resonant admixture of P states. Therefore the amplitude of the $\alpha G'$ should weaken with increasing electric field as was observed in the experiment. However, this effect was observable only at an electric field around 200 V/cm when the signal was nearly saturated and the decrease was no longer masked by the steep rise of the signal amplitude due to the increased coupling between the crossing states.

5.7. Shape of the Signals

The experimental and theoretical results have shown that the shapes of the signals are generally Lorentzian although recordings of S-F signals (see figs. 20 and 22) show

slight distortions from a pure absorption shape. As stated in sec. 5.4, a parameter for the slope of the background intensity is included in the fitting function. Comparisons of a S-F signal and a S-D signal with their fitted Lorentzian function are illustrated in figs. 27 and 28. The difference between the experimental and fitted points, in units of σ, are shown beneath each graph. There is no obvious systematic deviation of the experimental values from the fitted function.

The internal electric fields created by the ion and electron space charge (see sec. 5.8) and the motional fields experienced by the ions cause an inhomogeneous distribution of the overall electric field over the interaction region. The extent of this field variation depends also on the helium pressure (the effect of pressure on the width will be discussed in sec. 5.8).

The influence of the internal fields depends on the Stark shift and the degree of saturation of the signal. A typical example of the width and the amplitude as functions of the electric field is shown in fig. 26a-b. Below saturation, the amplitude rises strongly with the electric field. Near saturation, on the other hand, the amplitude variation is small butthe width increases rapidly with the field. Thus, considering the observed signal to be the superposition of signals induced by a field distribution, we have to expect a distorted signal shape, if the range of the field distribution in conjunction with the Stark constant causes a noticeable signal spread.

Further contributions to the signal asymmetries may

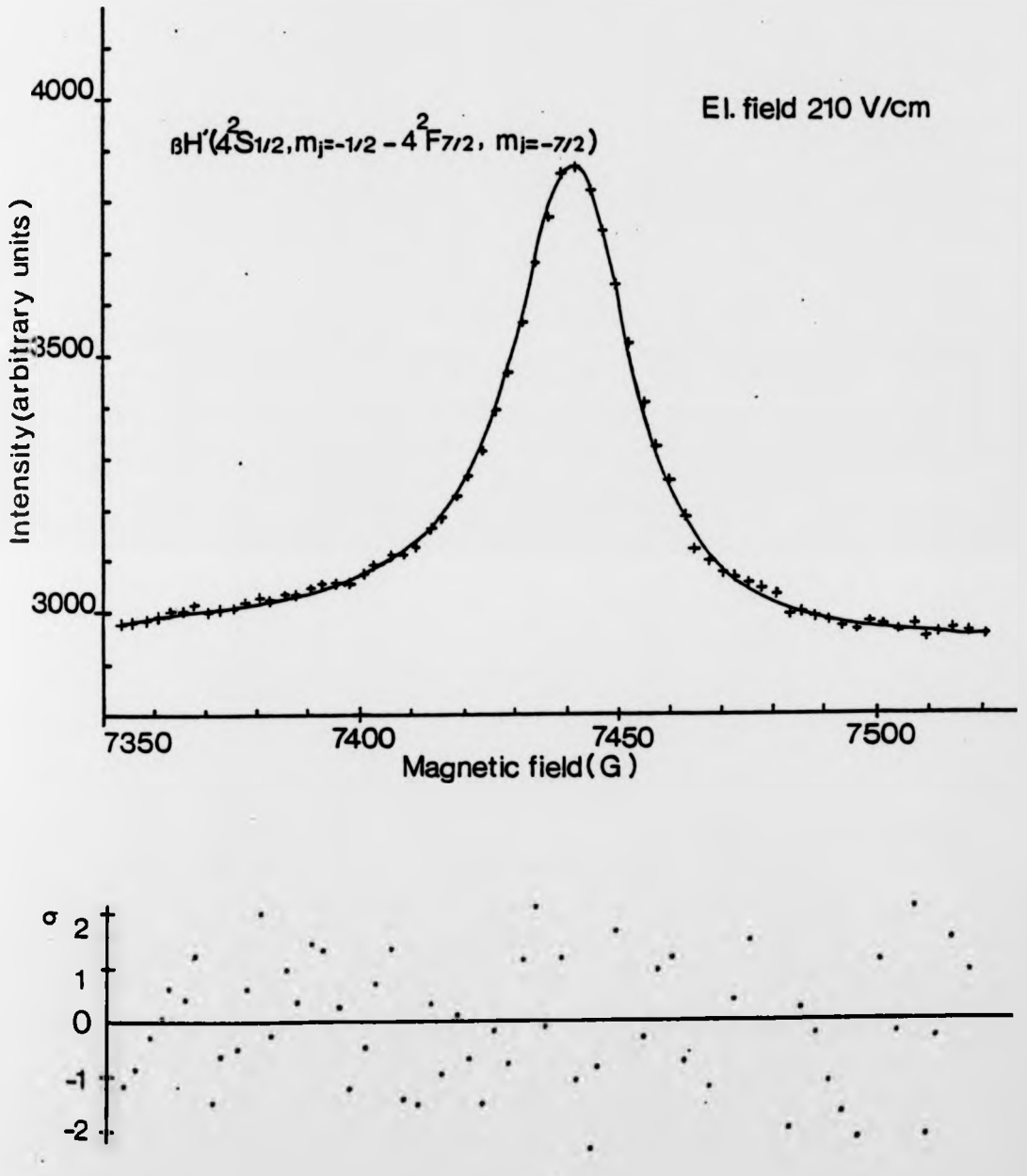

Fig. 27: Resonance line shape of the anticrossing βH' with its fitted Lorentzian function. The crosses are the experimental points which are read from the paper tape. The solid line represents the fitted function. The dots at the lower portion show the deviation of the experimental points from the fitted function in units of σ.

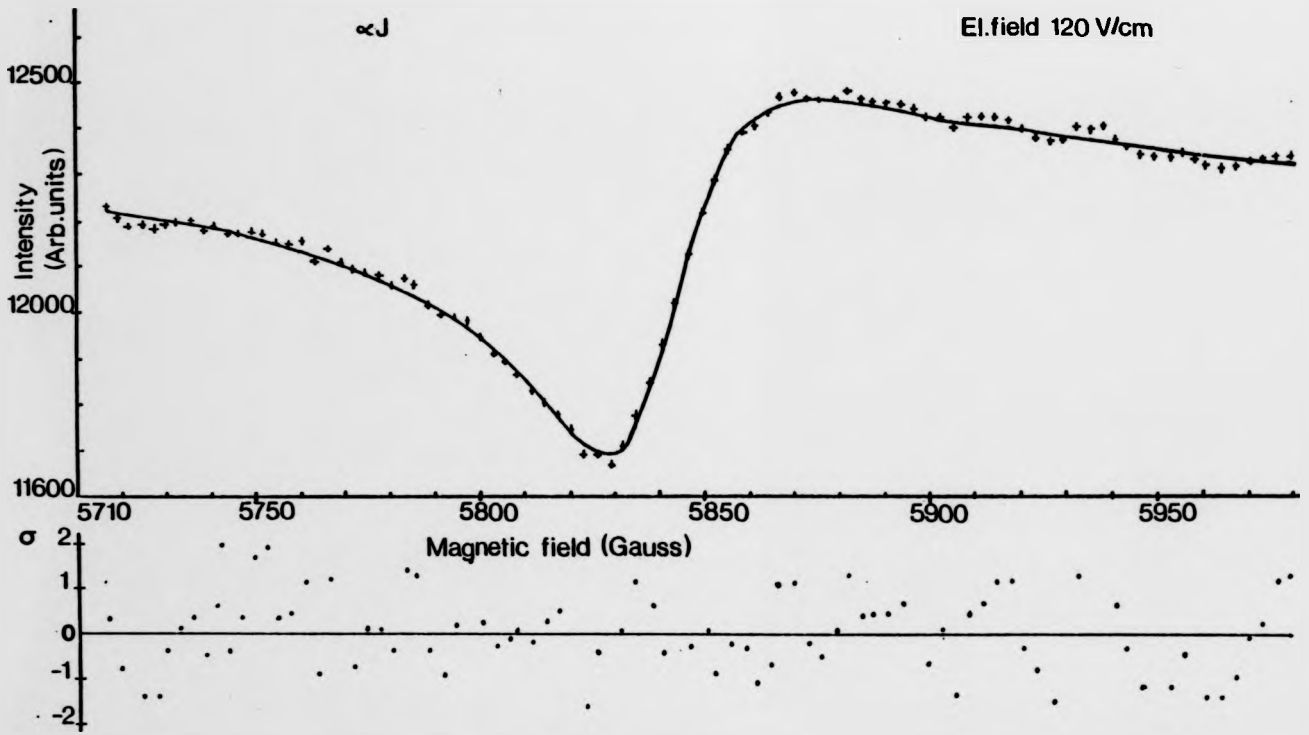

Fig. 28: Resonance line shape of the anticrossing αJ with its fittted Lorentzian function. The crosses are the experimental points which are read from the paper tape. The solid line represents the fitted function. The dots at the lower portion show the deviation of the experimental points from the fitted function in units of σ.

come from the overlap with other anticrossing signals, the cascading effects from n>4 and the population change due to variation of magnetic field.

Since the low order ($\Delta\ell=1$) signals of n=4 saturate at very low electric field, they should be very broad for the strong electric field required for the observed high order S-F and S-D signals. Therefore, even though the observed signals may be disturbed by such overlapping signals, it should be possible to approximate the distortion reasonably well by a linear variation of the background with the magnetic field.

As discussed in sec.5.5 the cascading anticrossing signals, in some cases, are strong enough to be used for fine structure measurements (Beyer et al 1972). In other cases, as observed by Mader et al (1971), they might have considerable influence on the detected signal. Since the cascading anticrossings have their own magnetic and electric field dependence, different types of distortion would be expected for each signal depending on the crossing position and the electric field if there was any effect from them.

The majority of the effects described above are assumed either to have negligibly small influence on the signal asymmetries or to contribute mainly to the slope of the signals background. In any case the fit seems to work well.

5.8. Pressure Effects

5.8.1. Effect of the He Pressure on the Signal Amplitudes and Widths

The relative amplitude and the width of the signals, $\alpha G'$, $\beta H'$ and αJ have been investigated as a function of the pressure. Keeping the electric field constant the amplitude showed a broad maximum and the width a broad minimum at around 7 mTorr. A typical example is illustrated in fig.29a and b.

The change observed below the maximum is attributed to the electron space charge fields. It is considered that the electron beam, confined by the magnetic field, fills a long circular cylinder of the cathode radius 2 mm along the interaction region. The average radial electric field, due to an electron beam of 300 μA with 300 eV energy, is 2.6 V/cm. (The velocity of such electrons is 10.3×10^8 cm/sec the number per second is 1.8×10^{15} corresponding to a flux density of 15.0×10^{15} cm^{-2}sec. The density of the primary electron beam is 1.5×10^7 cm^{-3}). The electron space charge may be larger than estimated above because of secondary electrons, both those emitted from the anode and those generated in the bombardment region. Since the actual space charge field is smaller inside the beam than on the surface and since the direction of the field, being radial, is different at each point inside the beam, the overall electric field is distributed over a certain field range. The amplitude and width of the observed signal will be the result of a superposition of signals relating to different internal field values and

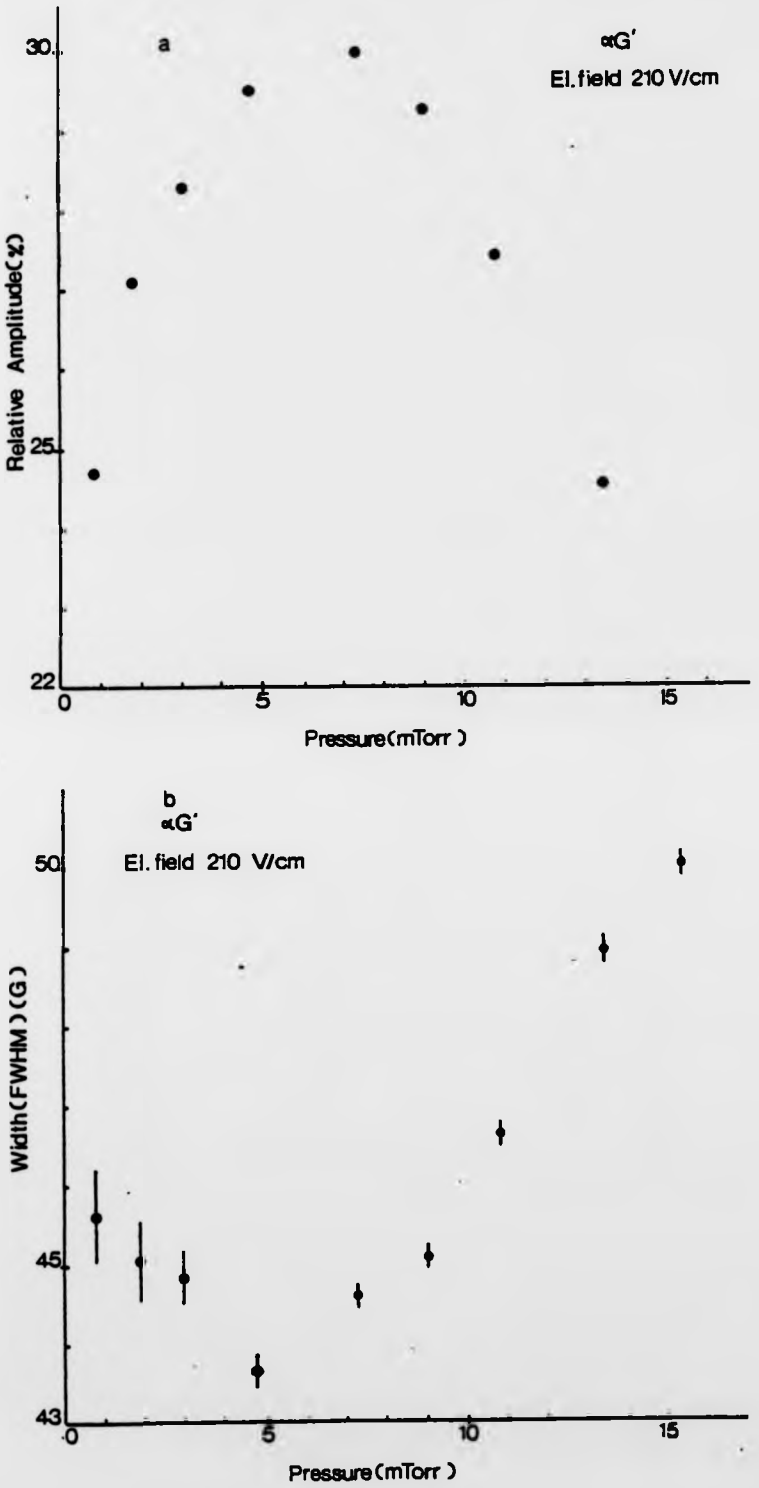

Fig. 29: a) Signal amplitude, and b) signal width of the anti-crossing αG' as a function of the pressure.

directions in the observation region. The resulting signals are wider and weaker than they would be in a homogenous field, depending on the field dependence of amplitude, width, and Stark shift. Since the electron space charge field decreases as the density of neutralising ions (i.e. the pressure) increases, the inhomogenous field range will be reduced accordingly and result in a stronger amplitude and a smaller width of the signal. As seen in fig.29athe amplitude of the signal reaches a broad maximum at around 7 mTorr where there may be sufficient ions to neutralise the electrons in the observation region. There will still be an electric field distribution due to motional fields, even if all space charges are neutralised.

The decrease of the intensity above a pressure of 7 mTorr may be attributed to the following effects.

(1) The time varying electric fields, due to collisions involving ions, atoms and electrons, may cause transitions between the excited states of ions resulting in a change of the lifetimes of the states. This may decrease the amplitude and widen the width as the pressure increases.

(2) The increasing density of the ions may, as the pressure rises, cause positive ion space charges. Using the formula III.10 given in Wilcox & Lamb (1960), the ion density at a pressure of 15 mTorr is calculated as $5.8 \times 10^8 ions/cm^3$, considering only primary electrons for the excitation. This is to be compared with the

electron density of $1.4 \times 10^{7} cm^{-3}$ which is about factor of 40 less than the ion concentration. The secondary electrons in the observation region should have a considerable effect on the neutralisation of positive ions, but there may still be more ions than can be neutralised. Hence, an inhomogeneous space charge electric field, created by unneutralised ions, may again cause the electric field to be distributed over a certain field range. (As explained for the electron space charge, the observed signal will be the result of a superposition of signals corresponding to different electric fields). This field strength will increase as the pressure increases, resulting in the detection of a broader signal of smaller amplitude.

5.8.2. The Effect of Pressure and Current on the Crossing Centre

Three signals, αG', αJ and βH', were investigated for the pressure effect. Two of them, βH' and αJ showed systematic changes in their signal centre. As shown in fig.30, the shift was particularly large for the αJ signal, which also has the largest Stark constant of all signals. However, even though there is a considerable shift at higher electric fields, this has little effect on the extrapolated crossing positions, since the Stark constant changes as well and balances most of the effect (see fig.31).

The different pressure dependence of the signals can be explained qualitatively if the experimental conditions

and the Stark constant of each signal are studied carefully.

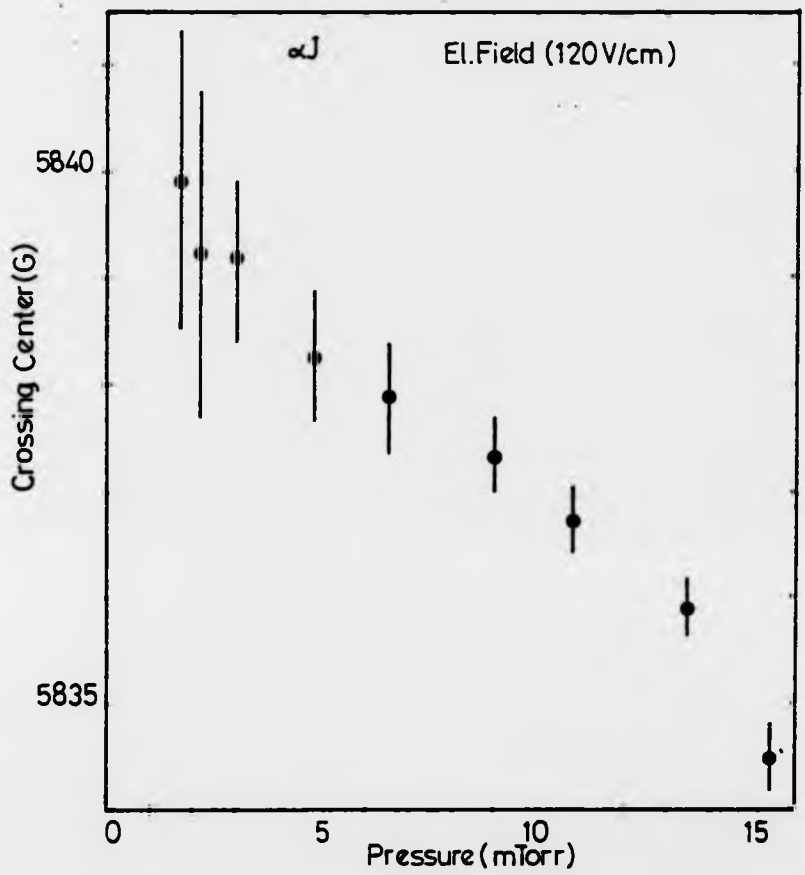

Fig. 30: Crossing centre of the αJ signal as a function of pressure at an electric field of 120 V/cm.

There are many electrons and positive helium ions in the observation region which are confined by the strong magnetic field and form a plasma column in the region. The magnetic field has a considerable effect on the dielectric properties of a plasma (Arzimovich 1965). The electric field applied perpendicular to the magnetic field results in the formation of an excess positive charge on

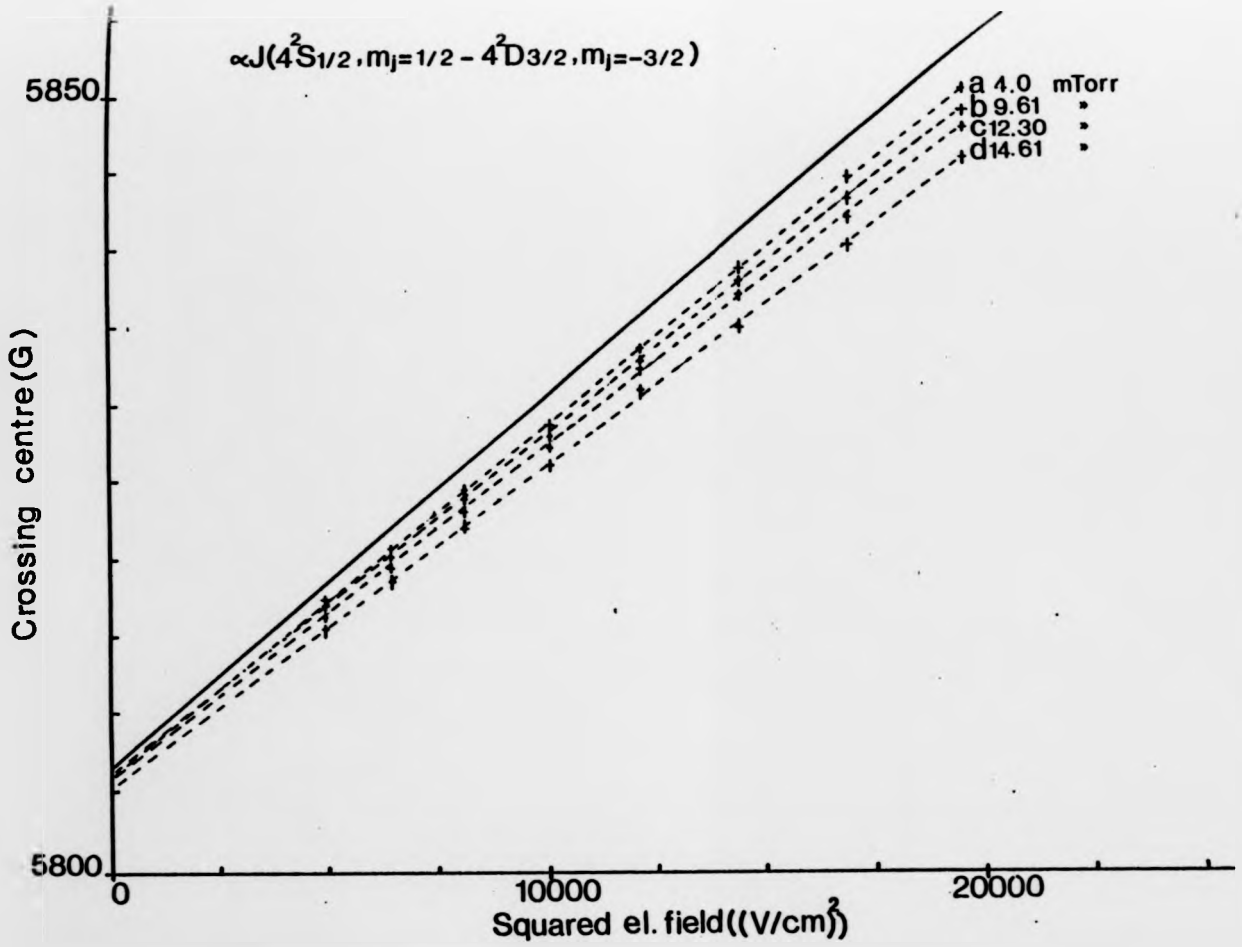

Fig. 31: Crossing centre of the αJ signal as a function of the squared electric field at various values of the helium pressure. The solid line represents the theoretical shift and the dashed lines are the fitted functions of the experimental points (crosses) for different pressures.

one side and negative on the other. These charges produce an electric field which is in opposite direction to the external electric field. The strength of this electric field not only depends on the applied magnetic and electric fields but also on the electron current and helium pressure. The reduction of the electric field for the anticrossing signals will result in a lower degree of saturation and less Stark shift depending on the Stark constant of each signal.

The Stark constant of the αG' signal is very small and thus the crossing centre is little affected even by much higher electric field variations. The αJ signal, on the other hand, has a large Stark constant and therefore very sensitive to any electric field change, has shown the largest pressure shift.

An investigation of the effect of the electron current on the signal position was made for the αG' and βH' signals. The βH' signal showed systematic but small effects with current. All crossing positions increased slightly with decreasing current. The αG' signal however showed no systematic effect which indicates that the current change again acts through an electric field effect.

5.8.3. Summary

The existence of other fields, such as ion and electron space charge and motional fields cause an inhomogenous field distribution in the observation region. As seen in sec.5.8.1., their influences are reduced to a minimum in the pressure

region of 4-10 mTorr where the signal to noise ratio, as observed in the experiment, is also good. Since the extrapolated crossing points are little affected by the pressure change, to obtain better and less distorted signal shapes the anticrossing measurements are best performed in this pressure region. For the Stark effect measurement, if the signal is very sensitive to electric field change, the Stark constant must be extrapolated to zero pressure, since the field created by the plasma can only disappear completely at zero pressure.

5.9. Stark Effect Measurement

Electric fields between 60-210 V/cm were applied to induce the anticrossing signals. Any electric field in the interaction region causes Stark shifts of the energy levels of the excited helium ions. The crossing positions are therefore, extrapolated to zero electric field for the fine structure measurement. Thus the anticrossing signals can also be used to investigate low field Stark effect.

The electric field dependence of the various anticrossing signals is illustrated in figs.32 a-e and compared with the theoretical values obtained from matrix diagonalisation (sec.3.2). The error bars represent the estimated uncertainty of the crossing centres. (The different effects contributing to the error and the effect of pressure on the Stark shifts is discussed in secs. 6.2 and 5.8.2 respectively.

Since it is difficult to determine the signal centre at low fields where the signal is weak and at high fields

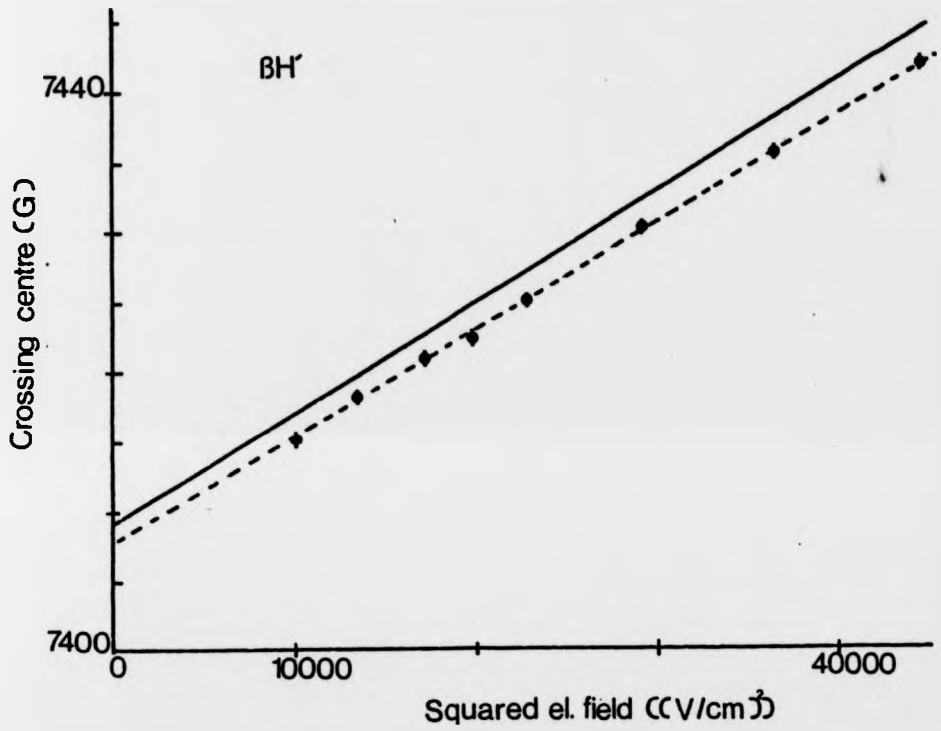

Fig.32: a-e: Crossing centres of the observed anticrossings in n=4 of He^+ as a function of the squared electric field. The solid line represents the shift of the theoretical crossing centre and the dashed line is fitted to the experimental points. The intersection of the fitted function at zero electric field determines the measured fine structure interval. The point size covers the uncertainty of the electric field.

Fig.32: a: Crossing centre of the βH' signal as a function of the squared electric field strength. The He pressure 13.8 mTorr.

where the signal is broad, the range which can be used for the Stark effect measurement is restricted. The values of

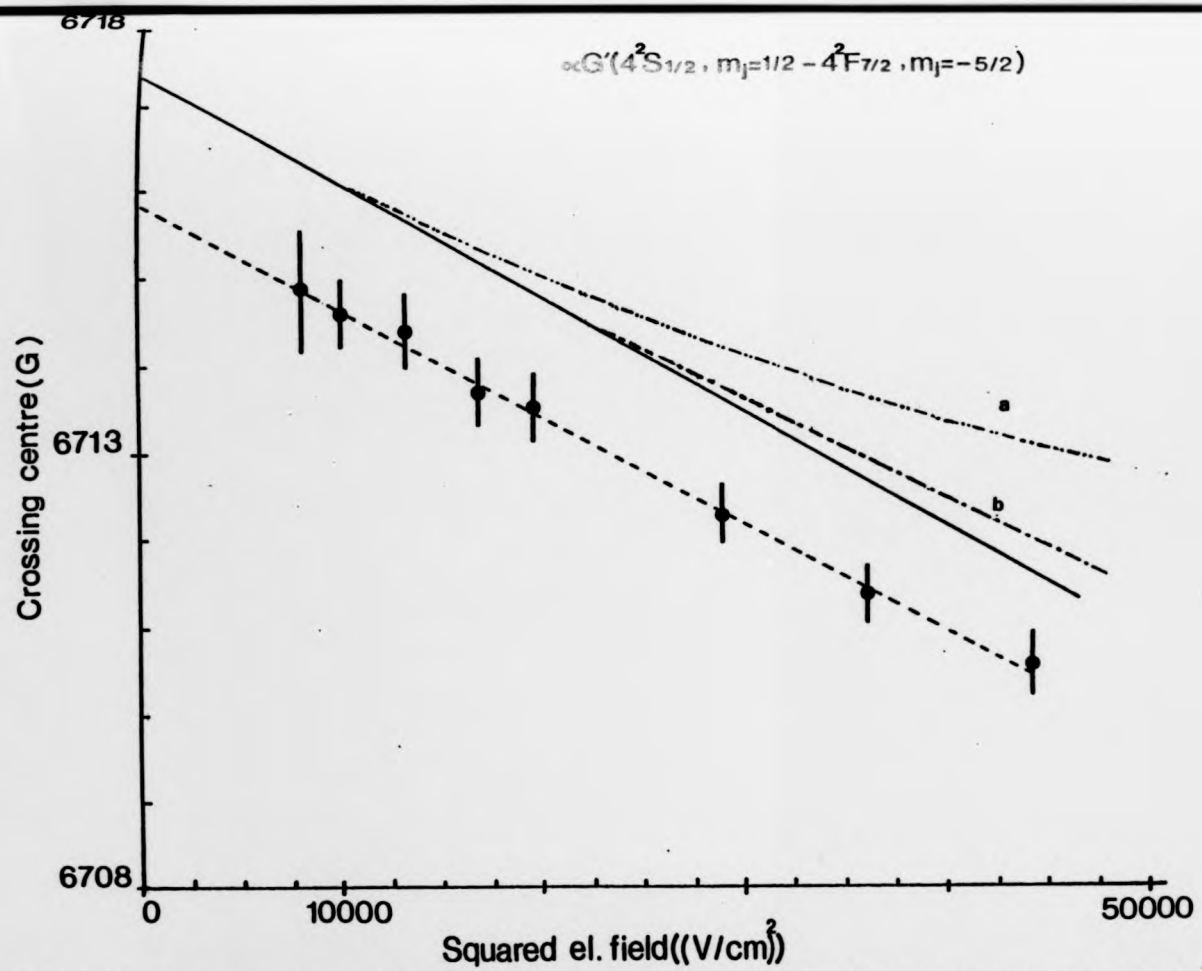

Fig.32b): Crossing centre of the αG' signal versus the squared field strength. The helium pressure is 12.3 mTorr. The solid line represents the theoretical calculation based on the time independent matrix diagonalisation. The dashed line a) shows the calculation based on the independent treatment of the Zeeman and Stark effect. The dashed line b) is the present calculation (see sec. 3.2.4).

low and high depend on the order of the anticrossing and are about 90 and 210 V/cm respectively for 4S-4F and about 35 and 140 V/cm respectively for 4S-4D signals.

All observed Stark shifts, except that of αN', show mainly a quadratic dependence in electric field strength, i.e. they show up as almost straight lines when the crossing positions are plotted against the square of the electric field strength, where the slope of the line is a measure of the quadratic Stark constant. Only the αN' signal deviates noticeably from the quadratic dependence as a result of two of the interacting substates being close enough for the Stark shift to become comparable with their separation even at the low electric field used. Therefore the beginning transition to the linear Stark effect is observed as shown in fig.32c.

For the extrapolation and the determination of the Stark constant, a fit based on a pure quadratic Stark effect was used with the exception of the αN' signal. The measured points were weighted according to their statistical uncertainties obtained from the Lorentzian fit of the crossing centres. The uncertainty of the electric field is negligibly small on the graphical scale, therefore it is not shown in the figures. A three parameter function ($F(E) = AE^2 + BE^3 + C$ where E is the electric field) was used to fit the αN' signal as a function of the electric field. The numerical results of the Stark constants will be given in sec. 7.2.

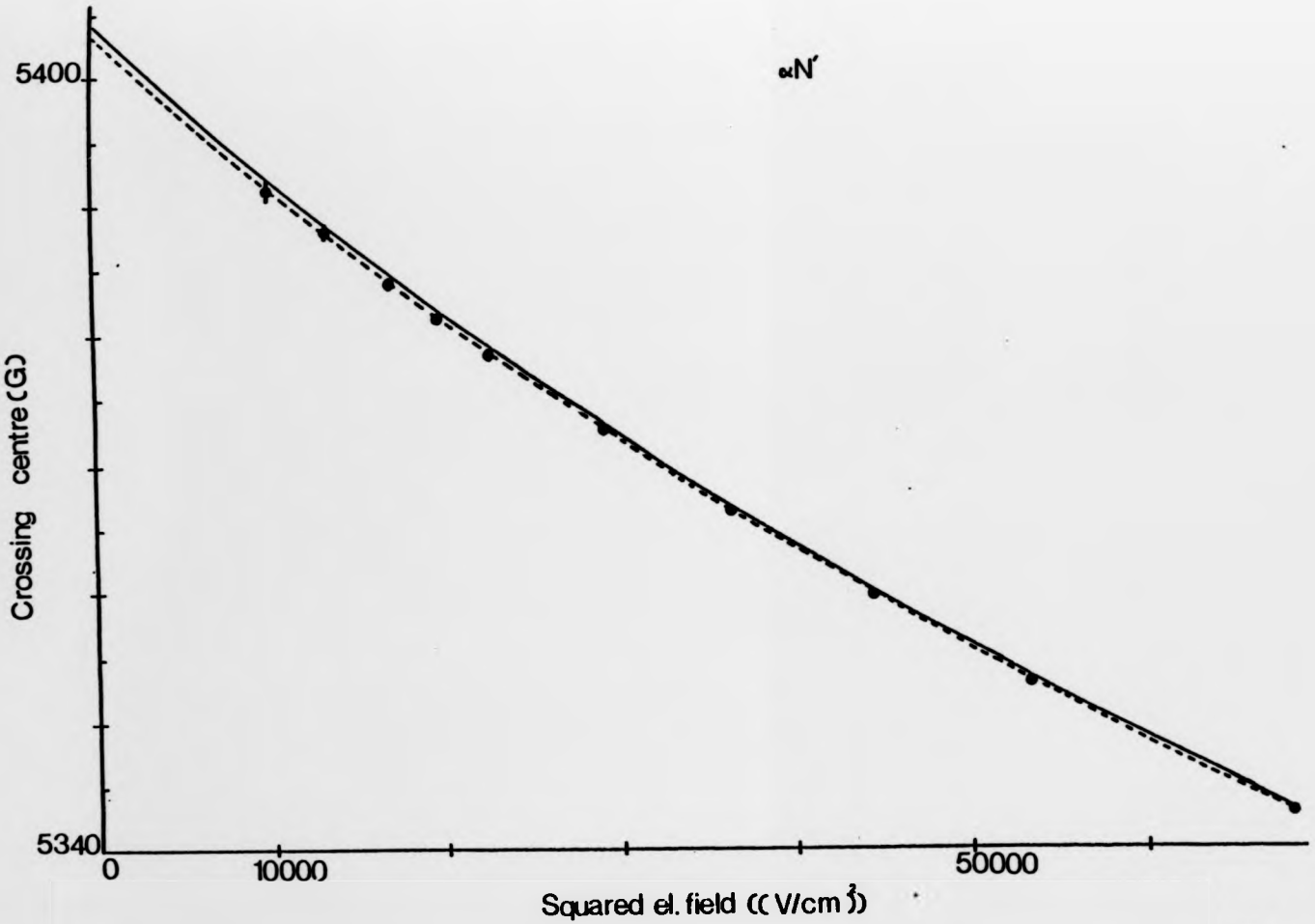

Fig.32c): Crossing centre of the αN' signal versus the squared electric field strength. The helium pressure is 6 mTorr.

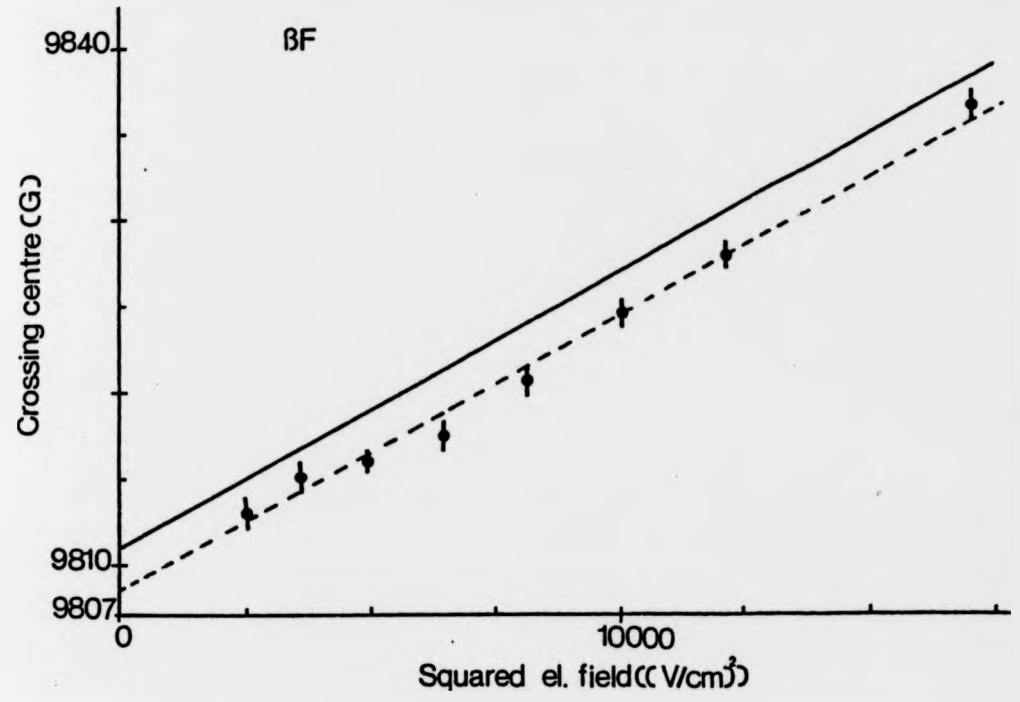

Fig.32d): Crossing centre of the βF signal versus the squared electric field strength. The helium pressure vs 10.7 mTorr

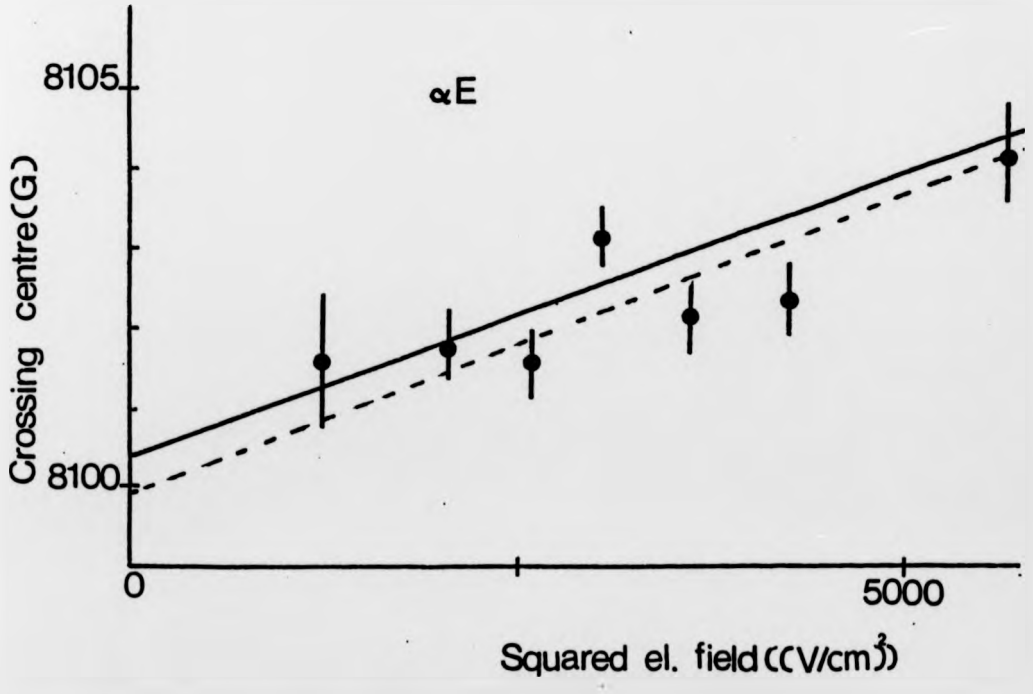

Fig.32e): Crossing centre of the αE signal versus the squared electric field strength. The helium pressure is 6.3 mTorr.

6. SOURCES OF ERROR

The systematic errors in the measurements, arising from the apparatus and from the uncertainty of the readings can be classified into two groups. Those with direct and those with little effect on the crossing centres and Stark constant of the signals. For example, the absolute accuracy of the electrometer reading does not affect the crossing centre as long as the reading is a linear function of the input. On the other hand, any error in the reading of the magnetic field will result in the same uncertainty on the crossing centres.

6.1. The Uncertainties of the Crossing Centres

The following sources of error were considered for the crossing positions of the signals: 1) Magnetic field, 2) Electric field, 3) Asymmetries of the Signals, 4) Statistical Uncertainties of the Extrapolated Crossing Positions.

6.1.1. Magnetic Field

The value of the crossing centre was corrected for the difference between the magnetic field measured at the probe position and the actual field at the interaction region. For the crossings below 8 kG, it was of the order of 0.10 - 0.15 G, and its uncertainty, including the field inhomogeneity, was estimated to be ±0.05 G.

Depending on the sweep rate of the magnetic field, there is a difference between the field displayed on the

counter and the actual field. In the present experiment, this difference is less than 100 mG with approximately 5 readings/s and a sweep rate of less than 0.5 G/s. This effect together with the effect of the time constant of the signal recording circuit was mostly eliminated by recording the signals in both sweep directions.

The difference between the currently adopted value of the gyromagnetic ratio and the preset value of the present system is about 20 ppm. A correction (about 0.15 G for 8 kG) was included in the measured value of the magnetic field due to this difference. The change of the preset value of the gyromagnetic ratios from the beginning to the end of the experiment is about 2 ppm, which is included in the estimate of magnetic field uncertainty.

6.1.2. Electric Field

As explained in sec.5.8, several mechanisms can create electric fields in the observation region resulting in changes and in a non-uniform distribution of the applied field. The sources of such fields are: a) Unneutralised space charge, b) The motion of the excited ions through the magnetic field which gives rise to a motional field $\vec{E} = (\vec{v}/c) \times \vec{H}$, c) The plasma screening, d) Electric stray fields from charged insulators, mostly those between the Stark plates, e) Any misalignment of the plates, f) Contact potential, g) Fringe fields.

a) The space charge effect on the crossing centres, due to unneutralised ions or the electron beam, will vary

depending on the Stark constant of each signal. For example, the Stark constant of the αG' signal is very small, therefore the crossing centre is not expected to be influenced by the space charge. As seen in sec.5.8.1. the space charge effect is reduced to a minimum in the 4-10 mTorr pressure region. Therefore, the measurements in this pressure region should have smaller uncertainties from space charge effects. The error estimate will be given together with the signal asymmetries.

b) For T=300 K the thermal velocity of helium ions is $\sqrt{\bar{v}_i^2} = 1.1 \times 10^5$ cm/sec. Excluding the acceleration of the ions during their lifetime, the magnitude of the motional field for $\vec{v}$ perpendicular to the magnetic field at 7400 G is 8.2 V/cm. Therefore, the motional field will contribute to the inhomogeneity of the field distribution in the observation region. The shift of the crossing centres caused by the motional field for the signals is negligibly small. The contribution to the asymmetry of the signal is discussed in the separate section 6.1.3 below.

c) The plasma field, depending on the gas pressure and the applied electric field, creates an internal field in the opposite direction to the applied field (see sec.5.8.2). The result of this effect is less on the extrapolated crossing centres than on the Stark constants of the signals. To include any small pressure dependence, the extrapolated crossing centres of the various runs were fitted linearly as a function of the gas pressure. For

the signals which showed no change in the observed pressure range, the mean of the extrapolated crossing centres was calculated.

d) For the insulators between the Stark plates, a dry lubricant was used to make them slightly conductive to avoid charging up. The mounting glass plate was far from the observation region and thus no effect is expected from it. The overall uncertainty caused by the insulators was assumed to be negligible.

e) Before sealing the system the uncertainty of the separation of the plates was measured to be ±0.2%. Its effect will be ±0.4% on the squared electric field strength and on the Stark constants of the crossings.

f) The plates were carefully mounted in such a way that the electric field is to be perpendicular to the magnetic field. A possible misalignment would cause a small field component in the direction of the magnetic field (z-direction) resulting in a reduction of the applied electric field $\perp$ H. If the misalignment of the plates is about 4^{o} in the direction of the magnetic field, this results in less than 0.2% reduction on the field in the x-direction which has negligible effect on the measured crossing centres.

g) Since copper wire is used to make the electrical connections of the Stark plates, contact potentials may arise due to the differences between the work functions of the metals. The contact potential may also be effective if the surfaces of the Stark plates show different conductivity. This was checked by applying the Stark

voltage in -x and +x-direction. No considerable differences were observed during the research period, therefore the measurements were carried on in one direction of the electric field only, and ±0.20 G was included in the error estimate.

h) The error in the electric field because of fringe field effects (A. Khadjavi 1966) is estimated to be in the order of 0.05% which is negligible for the crossing centres.

6.1.3. Asymmetries of the Signals

The shape of the signals and the possible cause of the asymmetries has been discussed in sec.5.7. It was shown that most contributions to the asymmetries of the signals can probably be approximated reasonably well by a slope of the background light intensity. The large amount of data taken at different helium pressures indicated that the change of the inhomogeneous electric fields over the interaction region did not cause any considerable shift of the extrapolated crossing centres.

The electric field caused by the plasma screening is assumed to be homogenous and is not expected to contribute to the asymmetries of the signals. The distribution of the motional field, on the other hand, is inhomogenous and affects signals at all pressures. Therefore it can contribute to the asymmetries of the signals resulting in an uncertainty of the crossing centres. It could also shift the signals if the fitting function is not absolutely

correct. The asymmetries attributed to the slope of the background are mostly taken into account by the inclusion of a dispersion admixture and a slope to the baseline of the fitting Lorentzian function. The remaining uncertainty is estimated to be ±0.30 G.

6.1.4. The Statistical Uncertainty

The statistical uncertainty of the zero field crossing points is calculated from the least square fittings of the crossings measured as a function of the electric field.

6.2. Uncertainties of the Stark Constants

The uncertainty of the magnetic field will not affect the Stark constants, since only the shift and not the absolute position of the anticrossing is important. Therefore all uncertainties of the magnetic field discussed in sec.6.1, have no effect on the Stark constant.

As pointed out in sec.6.1.2, the ±0.2% uncertainty of the separation of the plates gives a ±0.4% error on the Stark constant. A possible small component of the electric field in the direction of the magnetic field (misalignment of Stark plates with respect to the magnetic field) also gives about ±0.4% uncertainty on the Stark shift in the measured range of the electric field.

The asymmetries of the signals caused by space charge effects and by motional electric fields may add a small uncertainty to the Stark constant. This is estimated to be ±0.5%.

It was shown in sec. 5.8.2, that the plasma screening, particularly for the αJ signal, caused a systematic change of the Stark constant as a function of the pressure. This was corrected by extrapolating the Stark constant to zero pressure.

The contact potential and the fringe field effect, as described in sec. 6.1.2, give about ±0.2% and ±0.1% uncertainty, respectively, to the Stark constant.

The statistical uncertainties of the Stark constants are calculated from the least squares fits of the crossing centres as a function of the electric field.

7. RESULTS AND DISCUSSION

7.1. Fine Structure Results

7.1.1. Crossing Positions

The results of the crossing positions, extrapolated to zero electric field, are listed in Table 3 and compared with the previous measurements (Beyer & Kleinpoppen 1971, 1972 and Billy et al 1977) and with the theoretical values. The results for the various pressures

Ionised helium, n=4 anticrossing position (Gauss)				
Anti-Crossings	Lamb Notation	Present Experiment	Other Measurements	Theory
$^4S_{1/2}-^4F_{7/2}$	$\alpha G'$	6715.73±0.38	6715.2±2.5* 6710.5±4.5**	6717.335
	$\beta H'$	7407.94±0.42	7408.2±2.5*	7408.735
$^4S_{1/2}-^4F_{5/2}$	$\alpha N'$	5403.42±0.57	5402.4±2.5*	5404.271
$^4S_{1/2}-^4D_{5/2}$	αE	8099.90±1.18	8099.1±2.5* 8098.1±1.5**	8100.358
	βF	9809.38±0.53	9811.7±1.5**	9810.938
$^4S_{1/2}-^4D_{3/2}$	αJ	5805.87±0.72	5806.7±2.5* 5810.5±5. **	5806.253
$^4P_{1/2}-^4F_{5/2}$	fN'	9114.58± 6.	-	9119.261

Table 3: **The values of the crossing positions extrapolated to zero electric field. They are compared with the previous measurements (Beyer, Kleinpoppen & Billy et al) and the theory. The errors in the theory are less than the last digit, therefore they are not shown in the table. The quoted errors in the present results are overall uncertainties estimated according to sec. 6.1. The statistical uncertainties representing 68% confidence limit.**
***Beyer & Kleinpoppen (1971, 1972)**
****Billy Lhuillier & Faroux (1977)**

were extrapolated to zero pressure by a least squares fit using a linear pressure dependence. In cases where no pressure dependence was observed, the mean values were taken. The statistical uncertainties of the present results were obtained wherever possible from the repeated measurements using statistical techniques. The systematic errors estimated in sec.6.1, have been added quadratically to find the total error estimate.

The results of the previous measurements (Beyer & Kleinpoppen & Billy et al) and of the present experiments are in agreement within their respective error limits. Beyer & Kleinpoppen carried out their measurements at a fixed helium pressure of 10 mTorr. The errors were therefore kept large to allow for possible pressure dependences. In the present experiment, this uncertainty is reduced substantially as a result of the large number of data taken at various pressure values.

The theoretical values are based on Erickson's (1977) fine structure energies and the theory of Zeeman effect. The differences between the present experiment and the theory are mostly larger than the error limits. The discrepancy is slightly larger for the $\alpha G'$ signal, but all the differences lie in between 0.5 and 2 part in 10^4. (4σ for the $\alpha G'$ and about 2σ for the others).

The fine structure separations derived from the above crossings and possible contributions to the discrepancies will be explained in the following sections.

7.1.2. Calculation of Fine Structure Intervals

The fine structure intervals are derived by an analysis similar to that of Beyer & Kleinpoppen (1975). It is based on the fact that the LS coupling is partially broken up at the magnetic field value of the crossing positions. The substates which have common ℓ and m but different j values become a mixture of the two zero field components $\begin{matrix} j = \ell+\frac{1}{2},m \\ j = \ell-\frac{1}{2},m \end{matrix}$ and only those with the magnetic quantum number $m=|\ell+\frac{1}{2}|$ are unaffected. This mixing has to be taken into account when deriving the fine structure separations in zero field representation. For example, the positions of S-F signals depend on the zero field fine structure intervals $4S_{1/2}$-$4F_{5/2}$ and $4S_{1/2}$-$4F_{7/2}$ simultaneously. The intervals are identified as x and y axes of a rectangular co-ordinate system with the theoretical separations as the origin (see fig.33). Each anticrossing signal determines a straight line in the x,y-plane and at least two signals have to be combined to derive the two zero-field intervals.

As shown in fig.33, for the present results, three signals are used to get better defined values and uncertainties. The 3 lines form a triangle while in the ideal case they would cross at one point. The unweighted centre of gravity of the triangle and its uncertainty using the error propagation method has been calculated. The centre of gravity determines the measured values for the intervals.

The results for the derived fine structure intervals are summarised in table 4. These values are compared

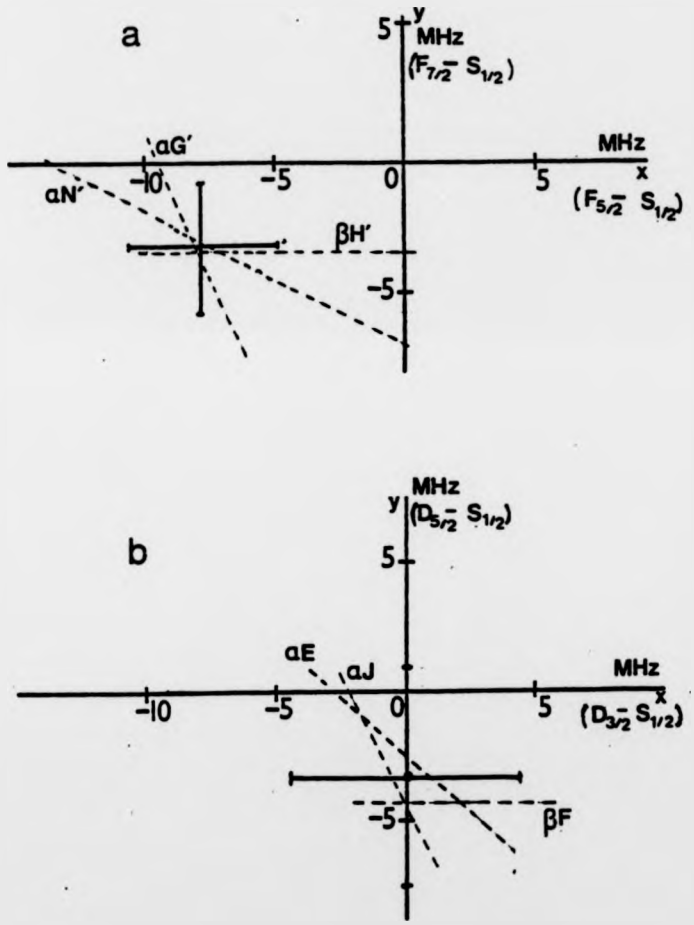

Fig. 33: The fine structure intervals, a) $F_{5/2}$-$S_{1/2}$ and $F_{7/2}$-$S_{1/2}$; b) $D_{3/2}$-$S_{1/2}$ and $D_{5/2}$-$S_{1/2}$, evaluated from the measured signals. The theoretical values of the intervals are taken as the origin of the coordinate system. The dashed lines which form a triangle, represent each of the three anticrossing signals. The centre of gravity of the triangle determines the measured values of the two intervals.

with the measurements of Beyer & Kleinpoppen, and Billy et al. and with the theoretical calculation of Erickson (1977)

Interval	Present Experiment	Other Measurements	Theory Erickson (1977)
$4F_{7/2} - 4S_{1/2}$	31100.7 ∓ 2.4	31098.2 ∓ 10.5* 31082. ∓ 24. **	31103.84 ∓ 0.04
$4F_{5/2} - 4S_{1/2}$	27438.1 ∓ 3.1	27435.7 ∓ 13.8* 27426. ∓ 21. **	27446.06 ∓ 0.04
$4D_{5/2} - 4S_{1/2}$	27455.8 ∓ 4.6	27455.4 ∓ 7.4* 27454.1 ∓ 3.9**	27459.02 ∓ 0.04
$4D_{3/2} - 4S_{1/2}$	20143.2 ∓ 3.9	20145.3 ∓ 7.8* 20137.7 ∓ 5.5**	20143.27 ∓ 0.04

Table 4: Fine structure separations derived from the crossing positions given in table 3.(MHz)

***Beyer & Kleinpoppen (1971, 1972)**

****Billy, Lhuillier & Faroux (1977)**

The present results are in agreement with the previous measurements (Beyer & Kleinpoppen and Billy et al). Billy et al also used anticrossing signals to derive the fine structure separations. They produced the excited helium ions by bombardment of the gas with a beam of neutral atoms directed perpendicular to the magnetic field. This provides a much lower signal to noise ratio than in our case, so that it is not surprising that most of their results for the anticrossing positions (see table 3) are considerably less accurate than the present results. Nevertheless the

accuracy quoted for the S-D separation is comparable to the present measurements.

The present results for the S-D separation agree with theory but the results for the S-F separations differ from theory by more than one standard deviation, σ. The difference is just a little over 1σ for the $^4F_{7/2}$-$^4S_{1/2}$ interval and about 2.5σ for the $^4F_{5/2}$-$^4S_{1/2}$ interval.

7.2. Stark Effect Results

The Stark constants of the anticrossings are listed in tables 5 & 6 and compared with the experimental work of Beyer et al (1973). The theoretical values in the table are based on the diagonalisation of the time independent energy matrix of n=4, He^+. As explained in sec.5.8.2, the signals having large Stark constants were influenced by the pressure change. This was particularly large for the αJ signal (see fig.31) so the Stark constant was extrapolated to zero pressure. A small pressure dependence was observed for the βH' signal, which had, however, negligible effect on the Stark constant.

With the exception of αN', the crossings have, in general, shown a quadratic Stark effect over the field range used, so that a fit based on a quadratic dependence could be employed to find the extrapolated crossings and the Stark constants. The αN' crossing, as described in sec.5.9, departs from the quadratic dependence even at low electric field. A three parameter function ($f(E) = AE^2 + BE^3 + c$) was found to be the best fitting function for the αN' crossings*.

Since the slopes of the crossings are not strictly constant as the electric field is varied, the experimental field range is used to derive the theoretical Stark constants. The values of the Stark constants are converted into $MHz/(V/cm)^2$.

---

*The function $f(E) = AE^2 + BE^4 + C$ used in the first place did not provide a good fit.

Anticrossing		Present Experiment mG/(V/cm)^2	Present Experiment kHz/(V/cm)^2	Beyer et al mG/(V/cm)^2	Beyer et al kHz/(V/cm)^2	Theory mG/(V/cm)^2	Theory kHz/(V/cm)^2	El.field Range V/cm
$^4F_{7/2}$-$^4S_{1/2}$	αG'	-0.114∓0.009	-0.484∓0.038	-0.092∓0.022	-0.386∓0.092	-0.131 -0.117*	-0.556 -0.496*	90-210
	βH'	0.757∓0.030	3.178∓0.126	0.80 ∓ 0.13	3.34 ∓ 0.54	0.786	3.300	10-210
$^4D_{5/2}$-$^4S_{1/2}$	αE	0.69 ∓0.30	2.04 ∓0.89	0.89 ∓ 0.27 (σ pol.)	2.6 ∓ 0.8	0.689	2.04	38-85
	βF	1.54 ∓0.16	4.31 ∓0.45	-	-	1.62	4.53	50-130
$^4D_{3/2}$-$^4S_{1/2}$	αJ	2.33 ∓0.060	9.04 ∓0.17	2.13 ∓ 0.36	8.3 + 1.4	2.36	9.15	70-140

Table 5 : Experimental and theoretical Stark constants for the observed anticrossing signals in n=4 of He^+. The quoted errors are overall uncertainties estimated according to sec. 6.2. The statistical uncertainties above representing 68% confidence limit. The theoretical Stark constant of the time independent calculation (Beyer et al 1973) and the present calculation (see sec. 3.2) are in agreement with the exception of the αG' signal.

*The Stark constant value for the present theoretical calculation.

	Stark constants of the αN'			
	A		B	
	$mG/(V/cm)^2$	$kHz/(V/cm)^2$	$mG/(V/cm)^3$	$kHz/(V/cm)^3$
Present experiment	-1.39 ∓ 0.03	7.68 ∓ 0.16	0.0020 ∓ 0.0002	0.011 ∓ 0.001
Theory	-1.44	7.95	0.0020	0.011

Table 6: **Experimental and theoretical Stark constant for the anticrossing αN'. The quoted errors are overall uncertainties estimated according to sec. 6.2. The statistical uncertainties representing 68% confidence limit. The theoretical Stark constant based on the true independent matrix diagonalisation (Beyer et al 1973) and the present calculation are in agreement.**

The present results and the previous ones (Beyer et al 1973) are in good agreement within their error limits. Observations at various pressure values made it possible to reduce the systematic uncertainty by a considerable amount as did the improvement of the Stark plate arrangement. Thus much more accurate values are obtained than those of Beyer et al.

The theoretical and the experimental results are also in good agreement. As explained in sec. 3.2.4., the Stark constant can be derived from the anticrossing signals which are calculated using the formula 3.16. The values found from these calculations agreed with the earlier calculation based on the diagonalisation of the time independent energy matrix of n=4, He^+. Only the Stark constant of the $\alpha G'$ signal as shown in table 6, differed slightly resulting in a better agreement with the present experiment.

7.3. Discussion

The present work provides the most accurate determination of the fine structure intervals S-D and S-F obtained so far for n=4 of He^+. The values are in agreement with the previous measurements (Beyer & Kleinpoppen 1971, 1972 and Billy et al. 1977), but there remain some discrepancies with the theory (Erickson 1977) for the S-F separations. All experimental investigations are based on the anticrossing method, with Billy et al. using an experimental set up completely different from the present one. It is therefore interesting to note that all fine structure results are below the theoretical values. This suggests that the apparent differences between theory and experiment, unless they are real, may have something to do with the fact that the anticrossing method was used for the investigations. Firstly, it is possible that some undiscovered systematic errors affecting all the experiments have remained uncorrected. Secondly, the fact that the measurements are taken in a strong magnetic field may play a role.

The present experiment included a careful investigation of the possible systematic effects in the pressure, the current and the excitation voltage. The analysis showed that all these effects are comparatively small. For example, the signals having large Stark constant were shifted by the pressure while their crossing centres are little affected (see fig.31). The pressure had also influence on the signal shape with a wider and weaker signal outside of the 4-10 mTorr pressure region, but there was no

observable effect on the crossing centres.

A possible systematic effect which may require further attention is the distortion of the line shape by the internal electric fields. Furthermore, the crossing positions are extrapolated to zero electric field without it being possible to observe a signal below a certain electric field strength. Therefore, the value found from the extrapolation may not specify the exact position of undisturbed crossing, although it should be small as the Stark constants are in good agreement with theory.

The differences between the theoretical and the experimental crossing centres seemed to be related to the strength of the magnetic field. A similar observation, reported by S.L. Kaufman in a paper by Narasimham & Strombotne 1971 for the measured intervals of n=2 of H (though not D), encouraged us to look more closely at the Zeeman effect. Tentatively, an attempt was made to derive a g_ℓ-value (sec. 3.2.1) from the zero electric field crossing centres instead of the fine structure intervals which are set to the theoretical values in this case. The g_ℓ values found from this derivation were very near to the value expected without nuclear mass correction. However as the nuclear mass correction is well established, we would not want to draw any conclusion from this result until the consequences for other fine structure experiments have been considered and all other sources of systematic uncertainties have been excluded.

The Stark effect measurements, on the other hand, are in good agreement with theory and with the earlier experi-

mental results of Beyer et al (1973). The new electron gun system with a better defined electric field resulted in an improved measurement accuracy of 2% compared with about 10-15% before. The accuracy of the quantum beat measurements made by Bourgey et al (1977) for the low field (300-900 V/cm) Stark effect in the level n=4 of He^+ was about 5%. Kollath & Kleinpoppen (1974) obtained 2% accuracy for the low field (0-250 kV/m) Stark effect in the level n=2 of hydrogen.

The theoretical results for the signal shape generally agreed with the experimental observation. The Stark constants and the crossing centres derived from the calculated signals are also in agreement with the calculated values based on the time independent diagonalisation of the energy matrix. However, the width of the calculated signals at low electric field did not agree with the present experiment nor with the previous calculation (Beyer 1973). This problem will require further attention.

A further improvement in the accuracy of the measurements can only be achieved by eliminating any systematic errors which might still have affected the present experiment in spite of thorough search for such effects. For example, introducing a more sophisticated fitting function could possibly reduce the uncertainty due to the line shape. The uncertainty due to the contact potential could also be eliminated if the measurements were performed in both ($\mp$ x) electric field direction. However this would double the data to be taken for the analysis.

REFERENCES

Altemose, V.O., 1961, J.Appl.Phys. 32, 1309-1316.

Anderson, R.J., Lee, T.P.E. & Lin, C.C., 1967, Phys. Rev. 160, 20-22.

Andrä, H.J., 1970, Phys. Rev.A. 2, 2200-2207.

Arzimovich, L.A., 1965, Elementary Plasma Physics (Trans Scripta Technica, Inc) Chap.7, New York: Blaisdell Publ. Comp.

Baird, J.C., Bradenberger, J., Gondaira, K.-I. & Metcalf, H., 1972, Phys.Rev.A. 5, 564-587.

Berry, H.G. & Roesler, F.L., 1970, Phys.Rev.A. 1, 1504-1507

Bethe, H.A. & Salpeter, E.E., 1977, Quantum Mechanics of One- and Two Electron Atoms, Chap.III, 205-246, Plenum Publishing Corporation, New York.

Beyer, H.J. & Kleinpoppen, H. 1967 Z.Physik 206, 177-183.

Beyer, H.-J., 1973, Ph.D Thesis, Stirling University.

Beyer, H.-J. & Kleinpoppen, H., 1971, J.Phys. B4, L129-L132.

Beyer, H.-J. & Kleinpoppen, H., 1972, J.Phys. B5, L12-L15.

Beyer, H.-J., Kleinpoppen, H. & Woolsey, J.M., 1972, Phys. Rev.Letts., 28, 263-265.

Beyer, H.-J., Kleinpoppen, H. & Woolsey, J.M., 1973, J.Phys.B. 6, 1849-1855.

Beyer, H.-J. & Kleinpoppen, H., 1975, J.Phys. B8, 2449-2455.

Beyer, H.-J. & Kleinpoppen, H., 1977, Int. J. Quantum Chem. Quantum Chemistry Symposium 11, 271-287.

Beyer, H.-J. & Kleinpoppen, H., 1978, in Progress in Atomic Spectroscopy, Ed. W. Hanle and H. Kleinpoppen), Vol.1. Chap.13, 607-637.

Billy, N., Lhuillier, C. & Faroux, J.P., 1977, J.Phys. (Paris), 28, L429-L434.

Bonch-Bruevich, A.M. & Kohodovoi, V.A., 1967, Sov. Fiz. Usp., 10, 637-657 (Usp. Fiz. Nauk 93, 71-110).

Bourgey, J., Denis, A. & Desesquelles, J., 1977, J.Phys. (Paris) 38, 1229-1235.

Brossel, J. & Bitter, F., 1952, Phys.Rev. 86, 308.

Cohen, E.R. & Taylor, B.N., 1973, J.Phys.Chem.Ref. Data 2 719.

Colegrove, F.D., Franken, P.A., Lewis, R.R. & Sands, R.H., 1959, Phys.Rev.Lettres 3, 420-422.

REFERENCES

Condon, E.V. & Shortley, G.H., 1970, The Theory of Atomic Spectra, Chap.5, 112-157, The University Press, Cambridge.

Eibofner, A. 1974 Phys.Lett 47A, 399.
Eibofner, A. 1976a Z.Physik A277, 225-231.
Eibofner, A. 1976b Phys.Lett 58A, 219

Eck, T.G., Foldy, L.L. & Wieder, E., 1963, Phys.Rev. Lett. 10, 239.

Eck, T.G. & Huff, R.J., 1968, in Beam-foil Spectroscopy (Ed. S. Bashkin) 193-202.

Erickson, G.E., 1977, J.Phys.Chem. Ref. Data 6, 831-869.

Gebauer, R. & Selhofer, H., 1970a, Acta.Phys.Austr. 31, 8-17.

Gebauer, R. & Selhofer, H., 1970b, Acta.Phys.Austr. 31, 108-116.

Glass-Maujen, M. & Descoubes, J.P., 1978, J.Phys.B. 11, 413-419.

Glass-Maujen, M., Julien, L. & Donhalik, T., 1978, J.Phys.B. 421-430.

Hatfield, L.L. & Hughes, H.H., 1967, Phys.Rev. 156, 102-108.

Isler, R.C., 1969, J.D.S.A., 59, 727-733.

Jacobs, R.R., Lea, K.R. & Lamb, W.E., 1971, Phys.Rev.A. 3, 884-905.

Kaufman, S.L., Lamb, W.E., Lea, K.R. & Leventhal, M., 1969, Phys.Rev.Lett. 11, 507-509.

Khadjavi, A., 1966, Ph.D Thesis, Colombia University.

Kollath, K.I. & Kleinpoppen, H., 1974, Phys.Rev.A. 10, 1519-1520.

Kollath, K.J. & Standage, M.C., 1978, in Progress in Atomic Spectroscopy (Ed. W. Hanle and H.Kleinpoppen) Vol.2, Chap.21, 955-997.

Lamb, W.E. & Retherford, R.C., 1947, Phys.Rev. 72, 241-243.

Lamb, W.E. & Retherford, R.C., 1950, Phys. Rev. 79, 549-572.

Lamb, W.E. & Retherford, R.C., 1951, Phys.Rev. 81, 222-232.

REFERENCES

Lamb, W.E., 1952, Phys.Rev. 85, 259-276.

Lamb, W.E. & Sanders, T.M., 1960, Phys.Rev. 119, 1901-1914.

Larson, H.P. & Stanley, R.W., 1967, J. Opt. Soc. Am. 57, 1439-1449.

Lea, K.R., Leventhal, M. & Lamb, W.E., 1966, Phys.Rev. Letters 16, 163-165.

Lo Surdo, A., 1913, Atti R. Accad. Naz. Lincei 22, Part 2, 664.

Mader, D.L., Leventhal, M. & Lamb, W.E., 1971, Phys. Rev.A. 3, 1832-1848.

Narasimham, M.N. & Strombotne, R.L. 1971. "Precision Measurement and Fundamental Constants", N.B.S. Special Publication No.343, p.401.

Pearse, R.W.B. & Gayden, A.G., 1965, The identification of molecular spectra, 3rd ed., p.121. London: Chapman & Hall Ltd.

Pokozan'ev, V.G. & Skrotskii, G.V., 1972, Usp. Fiz. Nauk 107, 623-656.

Roesler, F.L. & Mack, J.E., 1964, Phys.Rev. 135, A58-A71.

Rosebury, F., 1965, Handbook of electron tube and vacuum technique, ed., 11-19. Reading, Massachusetts: Addison-Wesley.

Series, G.W., 1964, Phys.Rev. 136, A684-A688.

Sutton, J.F. & Kay, R.B., 1974, Phys.Rev. A9, 697-703.

Wieder, H. & Eck, T.G., 1967, Phys.Rev. 153, 103-112.

Wilcox, L.R. & Lamb, W.E., 1960, Phys.Rev. 119, 1915-1933.

APPENDIX 1.

Physical constants used in the present work are those of Cohen & Taylor (1973)

Quantity	Symbol	Value	Units
Elementary charge	e	4.803242×10^{-10}	esu
Bohr radius	a_o	5.2917706×10^{-9}	cm
Planck constant	h	6.626176×10^{-27}	erg.s
Electron rest mass	m_e	9.109534×10^{-28}	g
Proton rest mass	m_p	$1.6726485 \times 10^{-24}$	g
Neutron rest mass	m_n	$1.6749543 \times 10^{-24}$	g
Bohr magneton $(eh/2M_eC)$	μ_B	1.3996124	MHz/G
Free electron g-factor	$ge/2 = \mu_e/\mu_B$	1.0011596567	-
g_ℓ-factor$(1 - \frac{m_e}{M_{He}})$	g_ℓ	0.99986394	-

APPENDIX 2

Crossing positions extrapolated to zero electric field and the Stark constants of the anticrossing signals at various pressure:

n=4, He^+ the anticrossing positions extrapolated to zero el. field, and Stark constants of the βH' signal					
Run Num.	Pressure (mTorr)	Specification	Crossing Centre (Gauss)	Stark Constant ($mG/V^2/cm^2$)	El.Field Range (V/cm)
35A*	13.8	I_A=300μA V_A=300V V_{g_2}=297V σ pol.	7407.49(0.24)†	0.755(0.007)†	100-210(8)✓
35B	13.8	σ pol. I_A=300μA V_A=300V Vg_2=Vg_3=297V	7407.36(0.25)	0.762(0.008)	100-210(8)
36A*	12.3	I_A=300μA σ pol.	7407.22(0.10)	0.761(0.003)	100-210(8)
36B	12.3	σ pol. I_A=150μA	7407.05(0.25)	0.769(0.008)	140-190(4)
36C	12.3	σ pol. I_A=500μA	7407.31(0.16)	0.754(0.005)	140-190(4)
37A*	11.5	σ pol. V_A=300v V_{g_2}=297V	7407.46(0.07)	0.751(0.002)	100-210(8)
37B	11.5	σ pol. V_A=250v V_{g_2}=247V	7407.23(0.03)	0.757(0.001)	140-190(4)
37C	11.5	σ pol. V_A=350v V_{g_2}=347V	7407.43(0.07)	0.757(0.008)	140-190(4)
38A*	11.2	σ pol.	7407.26(0.11)	0.760(0.003)	100-210(8)
38B	11.2	π pol	7407.73(0.42)	0.736(0.013)	130-210(6)
39*	1.7	σ pol.	7407.88(0.50)	0.746(0.015)	115-210(7)
40*	3.1	σ pol.	7407.67(0.16)	0.761(0.004)	115-210(7)
41*	4.3	σ pol.	7407.72(0.08)	0.755(0.002)	100-210(8)
42*	5.5	σ pol.	7407.64(0.22)	0.755(0.006)	100-210(8)
43*	7.2	σ pol.	7407.47(0.07)	0.756(0.002)	100-210(8)

Contd.

n=4, He^+ the anticrossing positions and the Stark constant of the $\beta H'$					
Run Num.	Pressure (mTorr)	Specification	Crossing Centre (Gauss)	Stark Constant ($mG/V^2/cm^2$)	El.Field Range (V/cm)
45A*	8.1	σ pol.	7407.30 (0.15)	0.761 (0.004)	100-210(8)
45B*	8.1	σ pol.	7407.36 (0.08)	0.762 (0.002)	100-210(8)
46A*	9.2	σ pol.	7407.42 (0.08)	0.758 (0.003)	100-210(8)
46B*	9.2	σ pol.	7407.42 (0.10)	0.758 (0.003)	100-210(8)

* The run numbers with asterik are used for the final analysis of the crossing positions.

† Statistical uncertainty

⁄ Number of signal

n=4, He^+ the anticrossing position and the Stark constant of the $\alpha G'$					
Run Num.	Pressure (mTorr)	Specification	Crossing Centre (Gauss)	Stark Constant ($mG/V^2/cm^2$)	El. Field Range (V/cm)
47A*	7.30	I_A=300 μA	6715.27(10.15)	-0.104(0.005)	90-210(8)
47B	7.30	I_A=150 μA	6715.02(0.07)	-0.102(0.002)	140-210(4)
47C	7.30	I_A=500 μA	6715.37(0.18)	-0.106(0.005)	140-210(4)
49A*	8.4	I_A=300 μA	6715.49(0.06)	-0.110(0.	90-210(8)
49B	8.4	I_A=150 μA	6715.63(0.09)	-0.116(0.002)	140-210(4)
49C	8.4	I_A=500 μA	6715.52(0.15)	-0.110(0.004)	140-210(4)
50A*	11.5	I_A=300 μA	6715.44(0.08)	-0.108(0.002)	90-210(8)
50B	11.5	I_A=150 μA	6715.53(0.23)	-0.107(0.008)	140-210(8)
50C	11.5	I_A=500 μA	6715.55(0.29)	-0.111(0.008)	140-210(8)
51*	15.0	I_A=300 μA	6715.37(0.21)	-0.104(0.008)	90-210(8)
52*	4.3	I_A=300 μA	6715.56(0.10)	-0.114(0.003)	90-210(8)
53A*	5.9	I_A=300 μA	6715.50(0.10)	-0.109(0.003)	90-210(8)
53B	5.9	I_A=150 μA	6715.18(0.36)	-0.100(0.011)	140-210(4)
53C	5.9	I_A=500 μA	6715.60(0.31)	-0.116(0.010)	140-210(4)

n=4, He^+ the anticrossing position and the Stark constant of the αN'						
Run Num.	Pressure (mTorr)	Specification	Crossing Centre (Gauss)	Stark Constant		El. Field Range V/cm
				$A(^{mG}/_{(V/cm)^2})$	$B(^{mG}/_{(V/cm)^3})$	
48	8.1	un pol.	5402.62(0.50)	-1.33 ∓ 0.05	0.0017 ∓ 0.0002	100-260(10)
54	6	un pol.	5403.09(0.23)	-1.38 ∓ 0.02	0.0018 ∓ 0.0001	100-260(10)
55	7.8	un pol.	5402.84(0.53)	-1.33 ∓ 0.05	0.0016 ∓ 0.0002	100-260(10)
56	11.2	un pol.	5402.64(0.31)	-1.31 ∓ 0.03	0.0016 ∓ 0.0001	100-260(10)
57	13.0	un pol.	5402.61(0.31)	-1.133 ∓ 0.03	0.0017 ∓ 0.0001	100-260(10)

n=4, He^+ the anticrossing positions and the Stark constant of the αJ					
Run Num.	Pressure (mTorr)	Specification	Crossing centre (Gauss)	Stark Constant ($mG/V^2/cm^2$)	El.field Range (V/cm
60	4.	σ pol.	5805.55(0.27)	2.233(0.022)	70-140(8)
61	7.07	σ pol.	5805.53(0.37)	2.226(0.029)	70-140(8)
62	9.61	σ pol.	5806.18(0.24)	2.152(0.018)	70-140(8)
63	12.3	σ pol.	5806.02(0.26)	2.089(0.020	70-140(8)
64	14.61	σ pol.	5805.33(0.36)	2.024(0.027)	70-140(8)

n=4, He^+ the anticrossing positions and the Stark constant of the αE					
Run Num.	Pressure (mTorr)	Specification	Crossing centre (Gauss)	Stark Constant $mG/(V/cm)^2$	El.field Range (V/cm)
66	3.23	unpol. light	8100.28(1.25)	0.616(0.382)	35-85(8)
67	6.30	unpol. light	8099.87(1.02)	0.758(0.278)	35-85(8)
68	8.07	unpol. light	8099.06(0.98)	0.871(0.267)	35-85(8)
69	10.61	unpol. light	8099.81(0.90)	0.502(0.239)	35-85(8)

n=4, He^+ the anticrossing positions and the Stark constants of the $\beta F'$					
Run Num.	Pressure (mTorr)	Specification	Crossing Centre (Gauss)	Stark Constant $mG/(V/cm)^2$	El.field Range (V/cm)
70	3.0	π pol.	9809.05(0.72)	1.507(0.09)	50-130(8)
72	7.4	π pol.	9808.45(0.56)	1.482(0.069)	50-130(8)
73	10.8	π pol.	9808.43(0.56)	1.606(0.069)	50-130(8)
74	12.4	π pol.	9808.19(0.91)	1.576(0.116)	50-130(8)

APPENDIX 3: Lamb's Notations (Appendix 2 of Beyer 1973)

m=	9/2	7/2	5/2	3/2	1/2	-1/2	-3/2	-5/2	-7/2	-9/2
$G_{9/2}$	A" 4/+	B" 3/+	C" 2/+	D" 1/+	E" 0/+	F" -1/+	G" -2/+	H" -3/+	I" -4/+	J" -4/-
$G_{7/2}$		K" 4/-	L" 3/-	M" 2/-	N" 1/-	O" 0/-	P" -1/-	Q" -2/-	R" -3/-	
$F_{7/2}$		A' 3/+	B' 2/+	C' 1/+	D' 0/+	E' -1/+	F' -2/+	G' -3/+	H' -3/-	
$F_{5/2}$			I' 3/-	J' 2/-	K' 1/-	L' 0/-	M' -1/-	N' -2/-		
$D_{5/2}$			A 2/+	B 1/+	C 0/+	D -1/+	E -2/+	F -2/-		
$D_{3/2}$				G 2/-	H 1/-	I 0/-	J -1/-			
$P_{3/2}$				a 1/+	b 0/+	c -1/+	d -1/-			
$P_{1/2}$					e 1/-	f 0/-				
$S_{1/2}$					α 0/+	β 0/-				

Notation used for the magnetic sublevels of hydrogenic fine structure systems following Lamb. The m-values are preserved at all magnetic fields. At low field they correspond to m_j, at high field (Paschen-Back effect) they are made up from m_l and m_s as noted below each sublevel, + and - denoting $m_s = +1/2$ and $m_s = -1/2$ respectively.